Notch-activated basophils support intestinal CD4^{+} T cell fate and function during helminth infection

Lindsey Marie Warner

A dissertation

submitted in partial fulfillment of the

requirements for the degree of

Doctor of Philosophy

University of Washington

2025

Reading Committee:

Elia Tait Wojno, Chair

Jessica Hamerman

Jakob von Moltke

Program Authorized to Offer Degree:

Immunology

University of Washington

Abstract

Notch Activated basophils support intestinal CD4$^+$ T cell fate and function during helminth infection

Lindsey Marie Warner

Chair of the Supervisory Committee:
Elia Tait Wojno
Department of Immunology

Parasitic helminth infections affect over 1 billion people worldwide, underscoring the need to study host-parasite interactions for therapeutic intervention. Helminth infection provokes a Type 2 inflammatory response orchestrated by CD4$^+$ T helper 2 (Th2) cells. In the intestine, Th2s elicit an interleukin-13 (IL-13)-dependent "weep and sweep" response from the epithelium to drive parasite clearance. Tissue-specific cues critically optimize intestinal CD4$^+$ T cell responses, but the exact mechanisms that regulate intestinal Th2 responses remain unclear. Basophils, a rare granulocyte, are associated with Th2 function. However, the basophil-dependent signals that support intestinal Th2s are incompletely defined. Previously, we identified the Notch signaling pathway in basophil activation during *Trichuris muris* infection, a mouse model of human whipworm. Here, we show that loss of Notch-activation in basophils results in defective parasite clearance and a blunted Th2 response. We found that basophil-intrinsic Notch was not only required for infection-elicited Th2 cytokine responses, but also for maintaining a broader IL-4 production program across a larger population of diverse intestinal CD4$^+$ T cells. Intestinal CD4$^+$ T cell cytokine production was basophil-dependent *in vitro* and *in*

vivo, but independent of basophil-secreted factors. Our findings highlight an IL-4 autocrine signaling module that mediates intestinal $CD4^+$ T cell fate and function via direct cell-cell interaction with basophils during helminth infection. These data improve our understanding of the tissue-specific mechanisms required for robust Type 2 immune responses and may inform the development of new therapeutic interventions for helminth infection.

TABLE OF CONTENTS

LIST OF FIGURES

LIST OF TABLES

ACKNOWLEDGEMENTS

First, I thank my advisor, Dr. Elia Tait Wojno, for her mentorship and consistent support throughout my time in her lab. Her commitment to my success through the peaks and troughs of graduate school was crucial to my success. Thank you for being patient with me and for always trying to push me to be a better scientist. Thank you for cultivating a work environment that is dynamic, collaborative, creative, scientifically rigorous, and fun.

To the members of the Tait Wojno lab, I am indebted to each one of you. Thank you to my fellow graduate students Alejandra Lopez Espinoza, Tighe Christopher, and Natalie Santillano for their comradery and positivity. A special thank you to Tighe, who kindly infected mice for me and kept my experiments alive during times of injury or illness. I also acknowledge Bridget Mooney, Pavithra Sundaravaradan, and Eric Helm not only for their scientific contributions, but for being wonderful colleagues. Many thanks to Dr. Lauren Webb, without who this work would not have been possible. It has been a privilege and great pleasure to be member of the Tait Wojno lab these last years.

I also thank Dr. Daniel Stetson and members of the Stetson lab for their support and guidance. A very special thank you to Stephanie Cambier and Dr. Hannah Volkman who have been my role models since my first year of graduate school. Your combined mentorship has had a measured impact on my development as a scientist, and I am incredibly lucky to have been mentored by such phenomenal women.

This work would also not have been possible without contributions from members of the von Moltke, Headley, and Ziegler labs, including. Thank you for your support.

A giant thank you to Sandy Turner. Without your support and gentle reminders, I would not have kept up with registration or paid student fees in a timely manner. Thank you for all that you do to support the immunology graduate student body.

Finally, my thesis committee, whose feedback and support have been instrumental in getting this work completed. So, thank you, Drs. Elia Tait Wojno, Jessica Hamerman, Jakob, von Moltke, Mark Headley, Jason Smith, Patrick Mitchell, and Wesley Van Voorhis.

DEDICATION

countless whiskered lives

carried my questions to rest—

thank you, gentle mice

Chapter 1. Introduction

1.1 Helminthiasis and the Type 2 inflammatory response

Soil-transmitted helminth (STH) infections effect over 1 billion people worldwide, underscoring an unmet need to study host-parasite interactions for therapeutic intervention[1]. STH infections are endemic to tropical and subtropical regions, and disproportionately impact countries where poor sanitation contributes to a high prevalence of helminthiasis, particularly in children, pregnant women, and adults in high-risk occupations[2–4]. Throughout the parasitic lifecycle, STHs impair the nutritional status of the host by feeding on tissues and competing for key nutrients, causing malnutrition, anemia, and significant morbidity[2,5]. Consequently, STH infections impose significant health and socioeconomic burdens on developing nations[5,6]. Current strategies to control STH burden involve periodic deworming and preventative chemotherapy in high-risk individuals[1,2,4]. However, limited access to drugs and lack of domestic financial support in endemic countries has made it difficult to implement preventative treatment and control rates of reinfection[7]. Thus, the demand for alternative therapeutic approaches to treat and prevent STH infection remains high.

The mammalian immune system has coevolved with STHs over millennia to generate an inflammatory response capable of sensing and responding to large non-replicating infections and noxious compounds in barrier tissues[8]. This “Type 2” immune response involves both innate and adaptive cellular players and cytokine mediators to remodel the tissue for effective parasite clearance[8,9]. The hallmarks of Type 2 inflammation include the release of epithelial-derived alarmins IL-25, IL-33, and thymic stromal lymphopoietin (TSLP), the production of the Type 2 cytokines IL-4, -5, -9, and -13, recruitment and expansion of ILC2s, induction of T helper 2

(Th2) $CD4^+$ T cells, increased mucous and fluid secretion, eosinophilia, and the expansion of class-switched IgE producing B cells—all mechanisms that aid in clearing parasites (Figure 1.1)[10–15].

During gastrointestinal helminth infection specifically, the Type 2 response is initiated by the sensing of helminths or helminth-derived products by tuft cells, a rare and highly specialized chemosensory cell of the intestinal epithelium[16,17]. Upon activation, tuft cells produce IL-25, which acts on various immune cells in the tissue lamina propria to trigger the production of Type 2 cytokines, specifically IL-13[16,18–20]. Critically, IL-13 acts directly on the stem cells of the intestinal epithelium to promote differentiation towards effector and secretory cell lineages, which elicit a classic "weep-and-sweep" response characterized by tuft and goblet cell hyperplasia for effective parasite clearance[20,21]. Hence, a complex interplay of immune- and epithelial-derived effectors of the Type 2 response must cooperate to mount a successful anthelminthic response. However, the exact cellular mechanisms that drive robust Type 2 immune responses are highly contextual and often demand a tissue-specific inflammatory milieu for optimal anti-helminth immunity. Therefore, understanding how Type 2 inflammation is initiated and maintained in distinct tissues is essential for improving upon current anti-helminth therapies and vaccines.

1.2 T helper 2 $CD4^+$ T cells and Type 2 immunity

The differentiation and expansion of T helper 2 (Th2) $CD4^+$ T cells is a hallmark of the adaptive Type 2 immune response and is indispensable for anti-helminth immunity[22,23]. During Type 2 inflammation, Th2 polarization is primarily driven by an IL-4 signaling circuit. Intrinsic IL-4/IL-4 receptor alpha (IL-4Ra) signaling results in phosphorylation of signal transducer and

activation of transcription (STAT6), which then dimerizes and translocates to the nucleus to promote the expression of the zinc finger transcription factor GATA-binding protein 3 (GATA3)[23–29]. GATA3, the Th2 defining transcription factor, cooperatively assembles with activated STAT5, which is induced by IL-2, IL-7, or TSLP signaling, at a shared *Il4-Il13* gene locus to drive Type 2 cytokine production[26,29–31]. Historically, IL-4 has been appreciated to be the major inducer of GATA3 expression for Th2 identity, but IL-4 independent mechanisms also upregulate and maintain GATA3. For example, T cell receptor (TCR) signaling strength associated with low-dose antigen and co-stimulation through CD28 or OX40 by antigen presenting cells (APCs) can upregulate GATA3 expression during T cell priming[32–34]. Regardless, the combination of these signals epigenetically modifies the *Il4-Il13* gene locus, primarily via sustained GATA3 expression, to maintain Th2 identify and promote a Th2 cytokine program required for robust Type 2 immunity. While the discreet molecular mechanisms required for supporting Th2 fate and function are well defined *in vitro,* the tissue-specific cues governing Th2 identity in the inflamed mucosa *in vivo* remain poorly understood.

The signals determining Th2 cell induction and activation during Type 2 inflammation in the tissue are diverse and occur in a context-dependent manner. In models of house dust mite (HDM) induced asthma, dendritic cells (DCs) respond to allergen by upregulating cysteinyl leukotriene production in the lung to activate Th2 cells[35]. Additionally, pathogen-derived materials from *Schistosoma mansoni* eggs, and even lipopolysaccharide (LPS), can modulate DC metabolism via mannose receptor internalization to induce Th2-promoting modules[36,37]. Indeed, many stimuli promote expression of Th2-activating signaling by DCs, including HDM, TSLP, IL-4, and FcγRIII, and are thought to largely converge on $CD11b^{+}CD301b^{+}PDL2^{+}$ DCs[35,38–41]. Type 2 conventional DCs produce C-C motif chemokine 17 to recruit Th2s to the inflamed lung during

hookworm infection[42]. However, no specific signal has been identified to be solely responsible for DC-dependent induction or maintenance of Th2 cells *in vivo.*

In addition to DCs, other cells can contribute to Th2 cell differentiation and function in the inflamed tissue, particularly in the lung. Epithelial-derived cytokines IL-25, IL-33, and TSLP can act directly or indirectly on Th2 cells to promote their differentiation and activation in the lung during HDM challenge or infection with the hookworm *Nippostrongylus brasiliensis*[22,43–46]. T cell exposure to these tissue-derived cytokines is required for optimal Th2 priming in the lung draining lymph node during *N. brasiliensis* infection; differentiated Th2 cells upregulate the receptors for IL-25, IL-33 and TSLP to facilitate their full acquisition of Type 2 effector functions[11]. Additionally, activation of group 2 innate lymphoid cells (ILC2s) by these alarmins, as well as common gamma-chain cytokines, is linked to the potentiation of Th2 function in the tissue. In the lung, ILC2s support antigen dependent $CD4^+$ T cell activation and provide co-stimulation to tissue resident Th2s to support survival and cytokine production during helminth infection[43,47,48]. Furthermore, ILC2s, while more commonly known to produce IL-5 and IL-13 during Type 2 immunity, can also serve as critical sources of IL-4 to support Th2 responses during *Heligmosomoides polygyrus* infection[49]. Thus, a complex inflammatory milieu incorporating various innate signals can impact Th2 differentiation and effector function in the tissue. However, many of these mechanisms of Th2 induction *in vivo* are specific to Type 2 inflammation in the lung and cannot necessarily be translated to mechanisms of intestinal Th2 induction and maintenance.

1.3 Basophils in Th2-dependent anti-helminth immunity

Basophils, a rare innate granulocyte, have been associated with both lung and intestinal Th2 fate and function during Type 2 inflammation. Historically, basophils were thought to be short-lived circulating granulocytes that functioned similarly to mast cells, but recent studies in mice and humans have established them as distinct effectors of Type 2 inflammation during helminth infection. Both basophils and mast cells arise from $CD34^+$ hematopoietic cells in the bone marrow, however, basophils typically enter circulation completely mature while mast cell progenitors migrate into specific tissues before full maturation[50]. Unlike mast cells, which are long-lived in the tissue, basophils have a half-life of about 30 hours at homeostasis[51,52] . Functionally, both cell types rapidly degranulate upon FcεRI-IgE crosslinking and release histamine, but the IgE independent stimuli activating these cells are markedly different and can elicit distinct inflammatory mediators, particularly cytokines[50,51,53]. For example, stem cell factor (SCF), IL-4, and IL-6 uniquely prime mast cells to produce heparin, chymases, prostaglandins, and many inflammatory cytokines, while basophils respond to IL-3 signaling to produce IL-4, chondroitin sulfate, basogranulin, and CCL5[50,53]. New mouse models allowing specific genetic targeting of mast cells and basophils have emphasized their phenotypic and functional differences, but the distinct biological roles basophils play in Type 2 inflammation requires clarification[52,54,55].

While mast cells and basophils share a common progenitor, basophils arise from a hematopoietic stem cell-derived granulocyte-monocyte progenitor (GMP) population in the bone marrow that gives rise to a common basophil-mast cell progenitor (BMCP)[51,54]. The induction of the transcription factors GATA2 and C/EBPa in BMCPs determines whether BMCPs differentiate into basophils or Mast cell precursors (MCPs), where the upregulation of GATA2 followed by C/EBPa expression commits a BMCP to the basophil lineage[52,54]. Basophil

precursors complete maturation through the upregulation of c-Kit, FcεR1a, mast cell protease 8 (Mcpt8) and CD34 prior to exiting the bone marrow into the periphery to respond to Type 2 inflammatory stimuli[51,52,54]. Alternatively, extramedullary hematopoiesis in the spleen can drive the differentiation of basophils in a TSLP-dependent fashion during *T. muris* infection, underscoring how unique inflammatory stimuli can elicit basophils from different hematopoietic origins[56–58]. Exactly how these differentially elicited basophils contribute to anti-helminth immunity remains unknown.

Canonically, hallmarks of basophil activation during Type 2 inflammation include FcεR1 crosslinking by IgE-antigen complexes that trigger degranulation to release inflammatory mediators, including leukotrienes and histamine[59,60]. However, recent studies have demonstrated basophils can be uniquely activated and recruited to employ diverse effector functions during helminth infection. For example, canonical IL-3 elicited basophils associated with leukotriene and histamine release are transcriptionally and functionally distinct from TSLP-elicited basophils that produce IL-4, IL-6, CCL3, and CCL4[61,62]; T cell derived IL-3 is required for basophil expansion during secondary infection with *Nippostrongylus brasiliensis*, while TSLP critically expands basophils during primary *Trichuris muris* and *Trichinella spiralis* infection[61,63,64].

The distinct induction of basophils and their effector functions have underscored the importance of basophil-mediated immunity for supporting Th2 cytokine responses. For example, basophils serve as a critical pool of IL-4 producers for Th2 dependent immunity against hookworm infection[65,66]. In addition to cytokine mediated effector functions, basophils can respond directly to helminth proteases and have been shown to present antigen to T cells via MHC class II to induce Th2 differentiation *in vitro*[67]. However, these direct peptide-MHC class II interactions have not been observed *in vivo*; inflammatory DCs, not basophils, are required for

priming Th2 cells in models of HDM allergic asthma and helminth infection[68]. Recent studies have demonstrated by two-photon microscopy that basophils do undergo prolonged interactions with $CD4^+$ T cells in the lung during helminth infection, but whether mechanisms of direct basophil-T cell interactions occur in the intestine during helminth infection is not clear[69].

The role of basophils in Th2-mediated immune responses to helminth infection often occurs in a helminth-species specific manner and depends on discrete tissue microenvironments. In contrast to primary infection with *N. brasiliensis* and *Schistosoma mansoni*[70,71], productive immunity against *Trichuris muris*, a murine model for human whip worm, requires basophils. *T. muris* infection elicits a TSLP-driven expansion of basophils that is required for supporting Th2 cell cytokine production and parasite clearance[72,73]. Depletion of basophils by treating mice with anti-FcεR1 abolishes Th2 cytokine responses required for effective immunity against *T. muris* infection, and the adoptive transfer of TSLP receptor (TSLPR) sufficient basophils into infected TSLPR deficient mice restores Th2 dependent anti-helminth immunity[63,72]. While these studies have uncovered a critical role for TSLP-elicited basophils in supporting Th2 cytokine responses in the intestine during *T. muris* infection, the specific molecular mechanisms that regulate basophil activation and effector function to augment Th2 cell fate and function in the inflamed mucosa remain incompletely defined.

1.4 Notch signaling in Type 2 inflammation

While the Type 2 inflammatory response is tightly regulated by various innate immune cells, their cytokines, and their production of bioactive lipids, recent studies have underscored a role for the Notch signaling pathway in governing Type 2 inflammation[74–76]. The Notch signaling pathway is a highly conserved ubiquitous receptor-ligand signaling pathway in

vertebrates that was originally described as a fundamental regulator in embryogenesis but has since been implicated in a variety of biological contexts[77–79]. Activation of the Notch signaling pathway requires direct cell-cell interaction, specifically the engagement of Notch ligand-receptor pairs, to mediate rapid changes in global gene expression programs[78]. Notch ligands Jagged 1/2 or Delta-like 1, 3, or 4 expressed on the signal-sending cell ligate directly with Notch receptor (Notch 1-4) on the signal-receiving cell, resulting in Notch extracellular truncation by the metalloprotease ADAM 10 followed by intramembrane proteolysis of the Notch receptor intracellular domain (NICD) by the key enzyme γ-secretase [77,78,80–82]. The cleaved form of the NICD translocates to the nucleus where it assembles with the DNA-binding protein CSL (CBF1/RBPjκ/Su(H)/Lag-1) and is recognized by transcriptional co-activator Mastermind-like protein (MAML), which critically assembles with additional coactivators (Co-A) and the transcription factor RPBJ to activate target Notch genes (figure 1.2)[78,83]. The molecular players of this signaling pathway intersect with many other pathways, meaning signaling occurs in a sensitive and dynamic manner in Notch-responsive cells that can integrate a variety of signals to dramatically reprogram gene expression in local tissue microenvironments[83–86]. This rapid transcriptional reprogramming is critical for generating host-protective anti-helminth immunity, where immune cells in the inflamed tissue are exposed to a variety of signals characteristic of Type 2 inflammation[74,76].

While the Notch signaling pathway is known to influence immune cell differentiation and function, particularly in Th2 cells and macrophages[76,87], its role in basophils is only now beginning to be understood. It was traditionally thought that because basophils – and other innate granulocytes – respond to IgE by degranulating and releasing large amounts of preformed inflammatory mediators, transcriptional reprogramming of basophils during inflammation did

not significantly impact their effector function. However, recent studies have shown that Notch signaling plays an essential role in basophil activation during Type 2 inflammation, where it modulates cytokine production and enhances their interaction with other immune cells[88,89]. For instance, pharmacological inhibition of Notch signaling in bone marrow-derived basophils results in failure to induce *Il4*, *Il6*, and *Il13* gene expression when basophils are stimulated *in vitro*[90]. In a murine model of allergic airway sensitization, transfer of *Rbpj* deficient basophils into OVA sensitized mice led to diminished mucus production and airway hyperresponsiveness relative to *Rbpj* sufficient basophils[91]. These data particularly underscore the importance of Notch signaling in promoting basophils responses during Type 2 inflammation.

Additionally, during *T. muris* infection mice harboring basophil specific deletion of Notch signaling (DNMAML F/F Mcpt8-Cre) failed to induce robust goblet cell hyperplasia and could not effectively clear worms relative to control mice[92]. This basophil-intrinsic loss of Notch signaling did not appear to impact basophil development, as the number of infection-induced splenic and intestinal basophils were comparable to control mice[92]. However, Notch activation in basophils was required for their proper orientation in the inflamed tissue: Notch deficient basophils were unable to localize to the crypts in the cecum lamina propria compared to Notch-sufficient basophils, which more frequently accumulate at the crypts[92]. In line with the role basophils play in supporting Th2 responses during helminth infection, these studies demonstrated that loss of Notch-activated basophils leads to a defect in the infection elicited expansions of GATA3^{+} Th2 cells and induction of *Il4* gene expression in the cecum lamina propria during *T. muris* infection[92]. Taken together, these previous studies define a critical role for Notch signaling in basophil activation and highlight the importance of this ancient

mechanism of cell-cell communication is shaping effective Th2 cellular responses for robust Type 2 immunity during helminth infection.

1.5 Premise of the thesis

Helminth infections are a global health challenge, affecting hundreds of millions worldwide. These infections trigger a Type 2 immune response characterized by the activation of Th2 cells, basophils, eosinophils, and ILC2s, all of which contribute to parasite expulsion, tissue repair, and restoration of intestinal homeostasis[93]. During helminth infections, basophils are recruited to the site of infection and interact with other immune cells, including T cells, to help shape an environment conducive to Th2 differentiation and function[69,72,94]. The Notch signaling pathway has been shown to critically activate basophils to support robust Type 2 immunity during *T. muris* infection[92]. These studies reinforce the idea that rapid transcriptional reprogramming of basophils is essential for supporting Type 2 inflammation during helminth infection, specifically Th2 cells and the expression of Th2-associated cytokines[63]. Understanding how Notch signaling influences basophil activation and their ability to promote Th2 responses will provide insights for developing targeted interventions for helminth infections and Type 2 inflammatory diseases.

The intestine presents unique challenges for immune responses due to its exposure to diverse antigens and the need to balance inflammation with tolerance. During helminth infections, Type 2 inflammation in the gut is adapted to clear parasites while minimizing tissue damage. For this reason, tissue-specific cues are essential for governing cell type specific responses and generating an inflammatory milieu that can drive goblet cell hyperplasia, mucus secretion, and epithelial cell turnover, all of which contribute to forming a protective barrier that

aids in parasite expulsion. Major unanswered questions in this field revolve around deciphering the discreet molecular and cellular players that generate and maintain Type 2 inflammation. Specifically, there is a gap in knowledge regarding the tissue specific mechanisms critical for optimizing Th2 cell fate and function in the inflamed intestine during helminth infection. Despite advances, the exact mechanisms of basophil-dependent support of Th2 cells are incompletely defined, and questions remain: How do tissue-specific signals influence Notch activation in basophils? What are the effects of Notch-activated basophils on Th2 cells during helminth infection? What is the significance of Notch signaling in driving basophil-$CD4^+$ T cell proximity in the tissue? How does Notch signaling in basophils affect downstream Th2 cell effector functions?

This thesis establishes a role for Notch-activated basophils in supporting intestinal Th2 cell fate and function during helminth infection and documents the complex heterogeneity of cytokine producing intestinal $CD4^+$ T cells that arise during helminth infection. We show that during *T. muris* infection, intestinal IL-4 production is not restricted to Th2 cells and occurs broadly across $CD4^+$ T cells. We demonstrate that Notch-activated basophils are required for Th2 cell expansion, proliferation, and Th2-dependent cytokine production. Additionally, Notch signaling in basophils was essential for promoting this previously unrecognized broader intestinal $CD4^+$ T cell IL-4 production program. These Th2-associacted effector functions depend on direct basophil- $CD4^+$ T cell interactions *in vitro,* where GATA3 and IL-4 expression was abolished when basophils and $CD4^+$ T cells were separated in culture. We highlight a potential IL-4 autocrine signaling module, where basophil support of Th2 cell -associated fate and function depended on IL-4 sufficient $CD4^+$ T cells *in vitro.* Finally, we show that Notch sufficient basophils are required for basophils to localize to $GATA3^+$ Th2 cells in the helminth

infected cecum, where basophil-Th2 proximity was lost in the absence of basophil specific Notch. Thus, this thesis demonstrates that Notch-activated basophils play an indispensable role in promoting large intestinal Th2 cell fate and function during helminth infection and provides a deeper understanding of the tissue specific cues that regulate Th2 cells to create new avenues of therapeutic intervention in Type 2 inflammatory diseases and disorders.

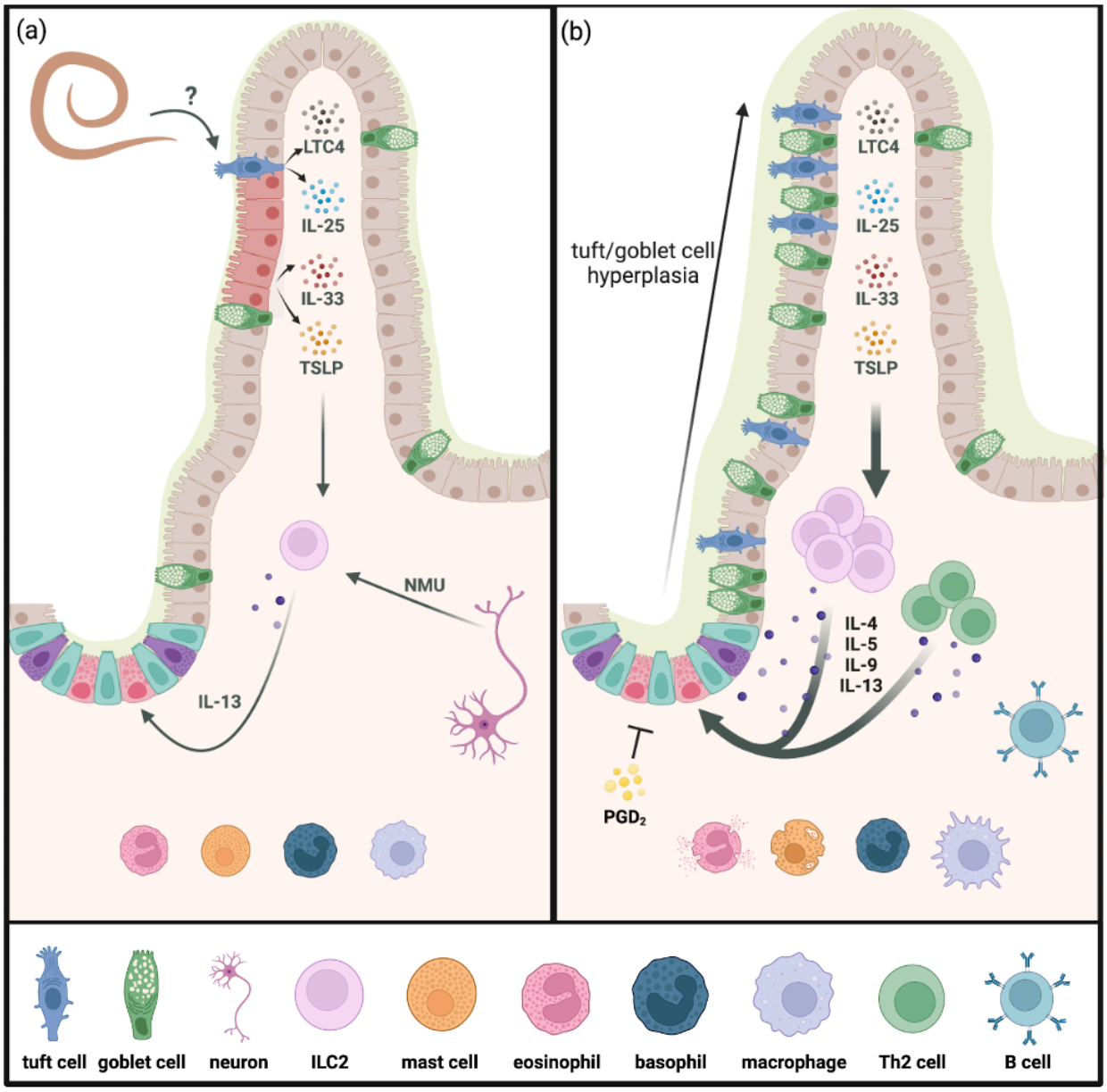

Figure 1.1. Type 2 response during gastrointestinal helminth infection

Overview of the Type 2 inflammatory response to soil-transmitted helminth (STH) infection. Tissue-specific sentinels of Type 2 immunity sense STHs and release primary signals (LTC4, IL-25, IL-33, TSLP) that activate downstream immune cells that can amplify the

response (a). These cells then release secondary signals that mobilize effector cells and remodel the intestinal epithelium into immune effectors. After mobilization and remodeling are complete, these effectors release signals that mediate the “weep and sweep” response to clear STH infection and repair damaged tissue (b).

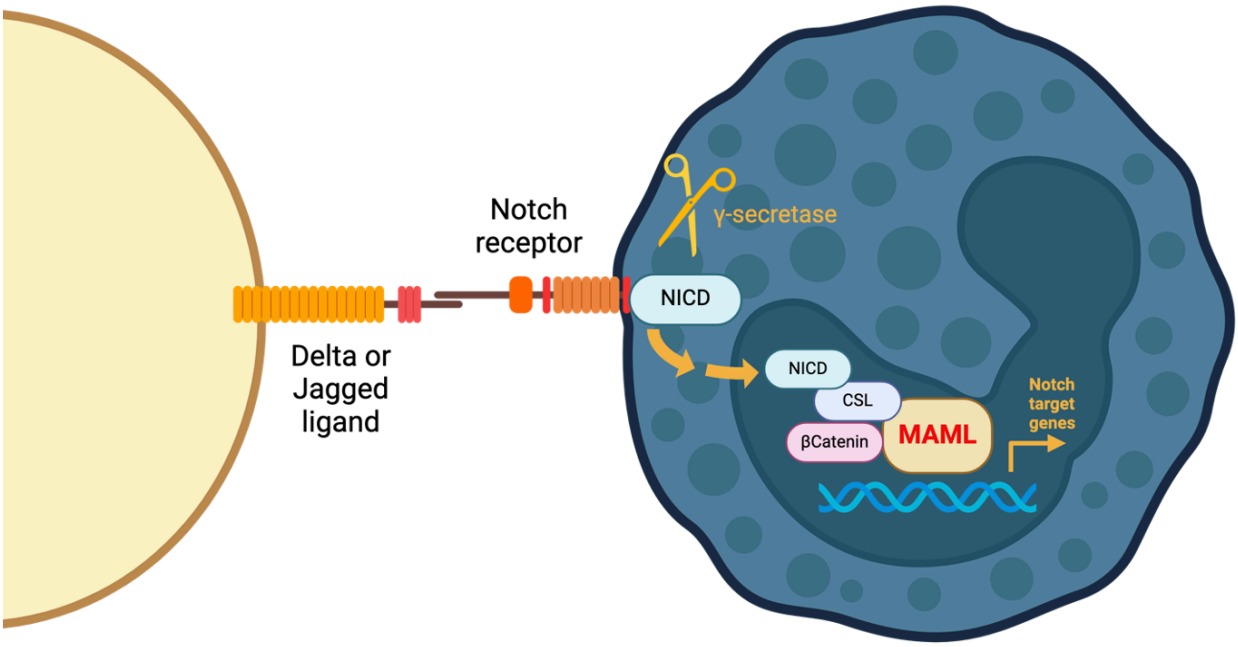

Figure 1.2. Cell-cell contact initiates the Notch singling pathway.

The Notch receptor is activated upon binding to Notch-ligand expressed by a neighbor cell. Truncation of the receptor ligand complex leads to the endocytosis of the Notch receptor and conformational changes in the receptor's intracellular domain to expose enzymatic cleavage sites. γ-Secretase cleaves the Notch transmembrane domain to release the Notch intracellular domain (NICD). NICD can then translocate to the nucleus where it interacts with the DNA-binding protein CSL and β-catenin. The transcriptional coactivator Mastermind-like (MAML) recognizes the NICD/CSL interface, and this complex can recruit additional coactivators (Co-A) to activate transcription.

Chapter 2. Notch-activated basophils support intestinal CD4$^+$ T cell fate and function during helminth infection

2.1 Introduction

Soil-transmitted helminths afflict billions worldwide, causing a significant global public health and socioeconomic burden[33]. Intestinal helminth infection provokes a Type 2 inflammatory response initiated by worm-induced damage to the epithelial barrier and subsequent release of IL-25, IL-33, and thymic-stromal lymphopoietin (TSLP). These alarmins activate group 2 innate lymphoid cells (ILC2s) and CD4$^+$ T helper Type 2 (Th2) cells to produce IL-4 and IL-13 in the intestine, orchestrating an epithelial remodeling "weep and sweep" response characterized by tuft and goblet cell hyperplasia, mucus production, and anti-helminth protein production to expel parasites[18–21,73]. The induction and maintenance of Th2 responses and Type 2 inflammation by various innate immune cells and their inflammatory mediators occurs in a context and tissue-specific manner. Thus, a better understanding of the mechanisms governing the regulation of Type 2 inflammation is required to improve anthelminthic therapies and vaccines[1,12].

CD4$^+$ T cells are essential for parasite expulsion in primary infection and protection against secondary challenge during infection with a murine model of human whipworm, *Trichuris muris*, which occupies the large intestinal cecum[63,95–97]. Th2s expressing the transcription factor GATA3 are a critical source of IL-4, IL-5, IL-9, and IL-13[24,26,30]. CD4$^+$ T cell activation and maintenance in other tissues depends upon tissue-specific signals from innate

immune and epithelial cells[26]. In the lung, ILC2s support $CD4^+$ T cell receptor (TCR) activation and provide co-stimulation to tissue resident Th2s to support survival and cytokine production. Type 2 conventional dendritic cells produce C-C motif chemokine 17 to recruit Th2s to the inflamed lung[42,47]. Other factors in the tissue microenvironment, including bioactive lipids and alarmins, act directly on Th2s to promote their function[97]. However, the tissue-specific cues that initiate and maintain Th2 responses in the inflamed intestinal mucosa remain unknown.

Basophils, rare innate granulocytes, drive Th2 responses during *T. muris* infection. During *T. muris* and *Trichinella spiralis* infection, TSLP is required for basophil expansion. Curtailment of TSLP activity inhibits basophilia and blocks anti-helminth responses essential for parasite expulsion[24,68], highlighting a role for basophils in orchestrating an adaptive Type 2 immune response. We have shown previously that basophil activation during *T. muris* infection depended on Notch signaling, where basophil-specific inhibition of Notch led to impaired parasite clearance and Type 2 inflammatory responses in the tissue[92]. This impairment was associated with a significant decrease in $GATA3^+$ Th2s in the inflamed intestine. While basophil recruitment to the intestine was unaffected in the absence of cell-intrinsic Notch signaling, basophil localization within the epithelium was dysregulated and basophil-$CD4^+$ T cell proximity was reduced. These observations suggest that basophils act within the tissue to promote Th2 activity, directly engaging with $CD4^+$ T cells in the intestine[69,92], in contrast to previous studies suggesting that basophils support $CD4^+$ T cell priming in the lymph node[13,68,69]. However, whether basophils directly impact intestinal $CD4^+$ T cell fate and function, including Th2s, is not known.

Here, we define a role for Notch-programmed basophils in augmenting $CD4^+$ T cell fate and function in the *T. muris*-infected large intestine in a contact-dependent manner. Single-cell

transcriptional analyses and Type 2 cytokine reporter mouse models revealed that Th2s exclusively produced IL-13 during infection, but diverse $CD4^+$ T cell subsets produced IL-4. *In vivo*, loss of Notch-activated basophils blunted Th2 and IL-4-producing intestinal $CD4^+$ T cell responses (both $GATA3^+$ and $GATA3^-$). In basophil-$CD4^+$ T cell co-cultures, basophils supported GATA3 expression and IL-4 production in $CD4^+$ T cells via a cell-contact dependent mechanism, independent of basophil IL-4 and MHC class II but dependent on IL-4-autocrine signaling in $CD4^+$ T cells. Finally, imaging studies revealed the importance of basophil-intrinsic Notch in driving basophil proximity to $GATA3^+$ Th2s in the *T. muris*-infected cecum. These findings highlight a novel, contact- and autocrine IL-4-dependent module by which Notch-programmed basophils support $CD4^+$ T cell IL-4 production and Th2-specific functions in the large intestine during helminth infection.

2.2 Results

2.2.1 $CD4^+$ T cells are the predominant source of IL-4 and IL-13 in the inflamed tissue during *T. muris* infection

$CD4^+$ T cells produce IL-4 and IL-13 to drive effector responses during *T. muris* infection[98–100]. However, innate immune cells also produce these cytokines during helminth infection[13,97,101]. To identify the primary source of Type 2 cytokines in the cecum during *T. muris* infection, we identified IL-4^+ ($huCD2^+$) and IL-13^+ ($huCD4^+$) cells in knock-in human CD2 KN2 IL-4 and knock-in human CD4 Smart13 IL-13 reporter mice at the peak of the $CD4^+$ T cell response at 14 days post-infection (p.i.), using infected C57BL/6 mice and fluorescence minus one (FMO) controls for huCD2 and huCD4 gating (Supplementary Fig. 2.1a A)[102,103]. There was an infection-driven increase in huCD2(IL-4) and huCD4(IL-13) expression by $CD45^+$

immune cells in the cecum lamina propria (LP) of mice on day (D)14 of infection with *T. muris* compared to naïve (D0) animals (Fig. 2.1 A, B). A small increase was seen in huCD2(IL-4) expression by $CD45^+$ cells in the mesenteric lymph nodes (MLN) at D14 p.i., but there was no appreciable increase in huCD4(IL-13) (Fig. 2.1 A, B). Consistent with previous studies[92,96], $CD4^+$ T cells expressed the majority of both IL-4 and IL-13 in naïve mice and animals on D14 p.i. (Fig. 2.1C, D, Supplementary Fig. 2.1a B), and the frequency of $CD4^+$ T cells that were huCD2(IL-4)$^+$ and huCD4(IL-13)$^+$ increased in the cecum LP, and to a lesser degree the MLN, during infection (Fig. 2.1E, F). We examined other cellular sources of IL-4 at D0, D7, and D14 p.i. and found the proportion of huCD2(IL-4)$^+$ basophils, ILC2s, and other cell subsets to be low at all timepoints, with $CD4^+$ T cells remaining the predominant source of IL-4 in the cecum LP (Supplementary Fig. 2.1a C).

While our data highlight that intestinal $CD4^+$ T cells are the major IL-13 producers during *T. muris* infection, prior studies show that ILC2-derived IL-13 is a critical driver of the "weep and sweep" response required for robust Type 2 immunity in several models of gastrointestinal helminth infection[18,19]. To determine if ILC2s were driving the Type 2 immune response during *T. muris* infection, we utilized Lcr1 (Locus control region 1) knock out (KO) mice. Lcr1 KO mice lack cis regulatory elements required for ILC2 development, effectively and specifically deleting ILC2s (Supplementary Fig. 2.1b A and B)[104]. We infected Lcr1 KO mice and wild type or heterozygous littermate controls (which are ILC2-sufficient) and assessed worm burden and the efficacy of the Type 2 immune response in the MLN at D21 p.i. Compared to littermate controls, Lcr1 KO mice similarly cleared parasites (Supplementary Fig. 2.1b C) and induced goblet cell hyperplasia and eosinophilia (Supplementary Fig. 2.1b D, E, and F). Importantly, the infection-induced increase in Th2 cell frequencies and the percentage of Th2

cells that produced IL-4 and IL-13 were intact in Lcr1 KO animals (Supplementary Fig. 2.1b G, H, and I). These data suggest that Lcr1-dependent ILC2s are not required for host protection or Type 2 immunity against *T. muris*. Taken together, our data suggest that $CD4^+$ T cells, not ILC2s, are the predominant functional source of IL-4 and IL-13 in the cecum LP during *T. muris* infection.

2.2.2 IL-13 production is restricted to Th2 cells during *T. muris* infection while heterogenous $CD4^+$ T cell subsets produce IL-4

Th2-derived IL-4 and IL-13 drive effective Type 2 immunity and parasite clearance during *T. muris* infection. However, helminth infection also expands IL-4- and IL-13-producing B-cell lymphoma 6 (BCL6)-expressing T follicular helper (Tfh) cells, while forkhead box protein 3 $(FOXP3)^+$ regulatory T cells (Tregs) produce IL-13 in an IL-33-dependent fashion during lung inflammation[105–108]. To identify critical $CD4^+$ T cell subsets producing IL-4 and IL-13 in the cecum during *T. muris* infection, we performed single-cell RNA-sequencing (scRNA-seq) of $TCR\beta^+CD4^+$ T cells sort-purified from the cecum LP of naïve mice or mice on D14 p.i.. Using a previously published gene list to identify $CD4^+$ T cell subsets[109], we observed clusters representing Tfh-like, Th1 cells, highly activated Th1 cells (Th1 hi), Th17 cells, Tregs (including a distinct cluster of GATA binding protein 3 $(GATA3)^+$ Tregs), early activated cells, IFN-responsive cells, and Th2 cells (Fig. 2.2 A). While the distribution of $CD4^+$ T cell subsets was largely unchanged between D0 and D14 p.i., there was enrichment in the frequency of Th2 cells and early activated cells in infected mice compared to controls (Supplementary Fig. 2.2a A).

We next investigated the distribution of *GATA3*, *Il4*, and *Il13* expression across clusters between naïve and infected animals (Fig. 2.2 B, C, and D). Expression of *GATA3* was not unique

to the Th2 cell cluster, but highly enriched in this population in naïve and infected mice (Fig. 2.2 A, B, and E). At steady state and in infection, expression of *Il4* was not restricted to Th2 cells and was found in other T cell subsets, including Tfh, Th1 cells, Tregs, early activated cell, and in the IFN-responsive clusters (Fig. 2.2 A, C, and F). *Il13* was largely undetectable in naïve mice, and specifically induced in the Th2 cell cluster during infection (Fig. 2.2 A, D, and G). Interestingly, *Il4* transcript expression was not statistically significantly correlated with *GATA3* expression across various T cell subsets (Fig. 2.2 H), suggesting that non-Th2 cells could be a source of IL-4.

To explore this concept further, we re-analyzed the scRNA-seq data to curate specific "bins" of Th cell subsets as defined by differential expression of lineage-defining transcription factors *GATA3*, *Foxp3*, *Rorc*, *Bcl6*, and/or *Tbx21* cells (Supplementary Fig. 2.2a B) and examined *Il4* gene expression across these subsets. The majority of $CD4^+$ T cells were negative for any lineage-defining transcription factor, or transcription factor "negative" (TF^-) (Supplementary Fig. 2.2a C). During infection, a proportion of *Bcl6* single-positive, *Bcl6*/*GATA3* double-positive, *Foxp3*/*Tbx21* double-positive, *GATA3* single-positive, *GATA3*/*Tbx21* double-positive, and TF- cells expressed *Il4* (Supplementary Fig. 2.2a D). The total number of sequenced, *Il4*-expressing cells was highest in the TF- subset (edit to main Fig. 2.2 I). A very low frequency of *Il4*-expressing cells across all bins co-expressed *Ifnγ* (Supplementary Fig. 2.2a E). Some *Il4*-expressing cells also expressed *Il13*, predominantly in the *Gata3* single-positive bin (Supplementary Fig. 2.2a F). Differential gene expression and Uni-manifold approximation (UMAP) analysis showed that *Il4*-expressing TF^- cells clustered distinctly from *Il4*-expressing, *GATA3* single-positive $CD4^+$ T cells and had a unique transcriptional program (Supplementary Fig. 2.2 a I and J). Together, these transcriptional analyses revealed that in the cecum LP during

T. muris infection, *Il13* transcript was induced by an infection-dependent Th2 cell-restricted program, while *Il4* expression was produced across more heterogenous $CD4^+$ T cell populations.

We next asked how these transcriptional programs relate to T helper subset production of IL-4 and IL-13 protein, employing flow cytometric analysis of cytokine production from cecum LP $CD3\varepsilon^+TCR\beta^+CD4^+$ T cells (defined as single-positive for FOXP3 (Tregs), GATA3 (Th2 cells), T-box expressed in T cells (T-bet) (Th1 cells), retinoic acid receptor-related orphan nuclear receptor yt (RORyt) (Th17 cells), or BCL6 (Tfh) (Supplementary Fig. 2.2b A and B). As expected, there was a five-fold increase in IL-4-producing $huCD2(IL\text{-}4)^+GATA3^+$ Th2s in the cecum of KN2 mice at D14-post *T. muris* infection (Fig. 2.2b I and J). However, as in our scRNA-seq analysis, we identified a population of TF^- $CD4^+$ T cells with undetectable levels of lineage-defining TFs as dominant IL-4 producers in both naïve and *T. muris*-infected KN2 mice in the cecum LP, with IL-4 production in other defined subsets as well, including Th1 and Th17 cells, and Tregs (Fig. 2I and J). In contrast, 80-100% of $huCD4(IL\text{-}13)^+$ $CD4^+$ T cells were $GATA3^+$ in both naïve and D14 p.i. *T. muris*-infected Smart13 mice (Supplementary Fig. 2.2b B and C). TF^- $IL\text{-}4^+$ cells were defined as $BCL6^-$ (Supplementary Fig. 2.2b A), and while there was an infection-driven increase in IL-4-producing $BCL6^+$ Tfh-like cells, this population did not substantially contribute to total IL-4-producing $CD4^+$ T cells (Fig. 2.2 I and J; Table 1). Thus, while IL-4-producing Th2 cells expand in the cecum during *T. muris* infection, the majority of $IL\text{-}4^+$ $CD4^+$ T cells at steady state and at D14 of infection comprise a previously unappreciated pool of $GATA3^-$ IL-4-producing intestinal $CD4^+$ T cells.

2.2.3 Basophil-intrinsic Notch signaling shapes cecum CD4$^+$ T cell transcriptomes during *T. muris* infection.

We next hypothesized that Notch-programmed basophils, which are required for intestinal *Il4* gene expression and parasite clearance in *T. muris* infection[92], shape infection-induced transcriptional activation of CD4$^+$ T cells. To this end, we isolated cecum CD4$^+$ T cells from naïve (N) or D14 p.i. *T. muris*-infected Mcpt8Cre$^-$ DNMAML F/F or Mcpt8Cre$^+$ DNMAML F/F mice that lack functional Notch signaling in basophils and performed bulk RNA-seq. Samples from naïve mice clustered together regardless of genotype (Fig. 2.3 A), with few differentially expressed genes (DEGs) (Supplementary Fig. 2.3 A). Broadly, naïve and infected samples clustered separately (Fig. 2.3 A), with 251 DEGs between samples from infected vs. naïve Mcpt8-Cre$^-$ DNMAML F/F mice (Fig. 2.3 B). Notably, intestinal CD4$^+$ T cells from infected basophil-Notch-deficient compared to -sufficient mice clustered separately (Fig. 2.3 A) and were transcriptionally distinct, with 166 upregulated and 415 downregulated DEGs (Fig. 3C). These data indicate that Notch-programmed basophils influence cecum CD4$^+$ transcriptional programs during *T. muris* infection but not in the steady state.

We next employed Ingenuity pathway analysis (IPA) to characterize functional pathways engaged in CD4$^+$ T cells from mice with or without basophil-intrinsic Notch signaling. IPA predicted that in the presence of Notch-competent basophils, cecum CD4$^+$ T cells showed evidence of alterations of pathways and molecules associated with Type 2 responses, including increased activity of IL-4, IL-2, BCL11B and decreased activity of RORyt (Fig. 2.3 D). A list of the top 10 pathways significantly induced in cecum CD4$^+$ T cells from infected mice that were dependent on the presence of basophil-intrinsic Notch signaling included the Leukocyte extravasation pathway (Fig. 2.3 E). Transcripts associated with accumulation of cells in the

tissue, including *Vcam 1*, *Itgb1*, and *Itgam*, were significantly upregulated in $CD4^+$ T cells from infected basophil-Notch-sufficient vs. -deficient mice (Fig. 2.3 F), highlighting a potential role for Notch-activated basophils in promoting $CD4^+$ T cell accumulation or distribution in the inflamed intestine.

Finally, we observed a downward trend in normalized gene counts for *Il4* and *Il5* in $CD4^+$ T cells from infected Mcpt-Cre^+ DNMAML F/F mice compared to controls and significantly reduced *Il13* counts, suggesting a defect in the induction of Th2 cytokine expression in the absence of Notch-activated basophils during *T. muris* infection (Fig. 2.3 G, H, and I). In agreement, IPA curated differential networks of genes downstream of IL-25 between $CD4^+$ T cells from infected basophil-Notch-sufficient and -deficient mice, with richer activation of Type 2-associated genes in $CD4^+$ T cells from infected mice with Notch-competent basophils (Supplementary Fig. 2.3 B and C). Overall, these data show that basophil-intrinsic Notch signaling is required for Type 2 inflammatory and *T. muris*-induced gene expression programs in cecum $CD4^+$ T cells.

2.2.4 Notch-programmed basophils are required for intestinal $CD4^+$ T cell IL-4 and IL-13 production during *T. muris* infection.

Based on our sequencing data, we hypothesized that Notch-programmed basophils critically regulate cecum $CD4^+$ T cell (including Th2 and TF^- cell) IL-4 and IL-13 production during infection. In Mcpt8-Cre^+ DNMAML F/F mice lacking functional Notch signaling in basophils, there was a decrease in the frequency of $GATA3^+FOXP3^-CD4^+$ T cells in the cecum LP (Fig. 2.4 A, B) but not MLN on D14 p.i. (Supplementary Fig. 2.4a A, B), consistent with our previous findings[92]. There were no changes in the frequencies of Tregs, Th1 cells, or Th17 cells;

alarmin-responsive (IL-17RB$^+$ or ST2$^+$) CD4$^+$ T cells; or activated (CD44$^+$CD127$^-$) versus memory (CD44$^+$CD127$^+$) T cells (Supplementary Fig. 2.4a C-I). Among GATA3$^+$CD4$^+$ T cells in the cecum LP, but not MLN (Supplementary Fig. 2.4b A-D), the infection-induced increase in IL-4 and IL-13 production was ablated in basophil-Notch-deficient vs. -sufficient mice, as detected by intracellular cytokine staining (Fig. 2.4 C, D and E) and high sensitivity cytometric bead array of supernatants from *ex vivo* stimulated, cecum CD4$^+$ T cells (Fig. 2.4 F and G). This loss of IL-4 and IL-13 production capacity in Th2s coincided with a defect in infection-induced Th2 proliferation as measured by Ki67 in the cecum LP, but not in the MLN (Fig. 2.4 H and Supplementary Fig. 2.4b E). IL-4 and IL-13 production were not significantly altered in other lineage-committed CD4$^+$ T cell populations, including Tfh-like cells, in the absence of Notch-programmed basophils during infection (Fig. 2.4 I and J and Supplementary Fig. 2.4c A-F). We next asked whether the decrease in Th2 proliferation and cytokine production in CD4$^+$ T cells from Mcpt8-Cre$^+$ mice coincided with defects in TCR activation. Using Nur77 as an indicator of TCR signaling, we found that both MLN and cecum LP GATA3$^+$ Th2 cells from mice with Notch-deficient basophils failed to upregulate Nur77 in an infection dependent manner compared to mice with Notch-sufficient basophils (Supplementary Figure 2.4d), suggesting Notch-activated basophils may support TCR signaling in in Th2 cells in addition to cytokine production.

Given the observed TF$^-$ IL-4-producing population of CD4$^+$ T cells we observed in the *T. muris*-infected cecum (Fig. 2.2 J), we also assessed whether Notch-programmed basophils were critical in promoting IL-4 production from this population. The frequency of IL-4$^+$ and IL-13$^+$ cells out of total, bulk FOXP3$^-$ intestinal CD4$^+$ T cells was significantly diminished in mice lacking Notch-activated basophils at D14 p.i. (Supplementary Fig. 2.4e A and B), while IL-10

and IFNγ production were unaffected (Supplementary Fig. 2.4e C and D). However, TF^- intestinal $CD4^+$ T cells, the predominant cecum IL-4 producers (Fig. 2.4 J), did depend on Notch-activated basophils for optimal IL-4 but not IL-13 production on day 14 p.i. (Fig. 2.4 K and L). Together, these data suggest that basophil-intrinsic Notch signaling is required not only for infection-elicited Th2 cytokine responses but for maintaining a broader IL-4-production program in $GATA3^-CD4^+$ T cells in the intestine during *T. muris* infection.

2.2.5 Notch-activated basophils are required for the accumulation of migratory dendritic cells in the mesenteric lymph node.

Interestingly, Th2 cells derived from the gut-draining lymph node in mice lacking Notch-activated basophils failed to induce Nur77 (Supplementary Figure 2.4d) but had no defects in IL-4 and IL-13 production (Figure 2.4). Because of this, we hypothesized that Notch-activated basophils may indirectly impact early TCR activation and/or priming in the lymph node during *T. muris* infection, resulting in Th2s that fail to proliferate and produce Type 2 cytokines upon entering the inflamed tissue. To begin testing this, we infected Mcpt8Cre^- and Cre^+ mice with *T. muris* and measured the proportion of resident ($CD11c^{hi}$MHC II^{lo}) and migratory ($CD11c^{lo}$MHC II^{hi}) dendritic cells (DCs) in the MLN at day 14 p.i.. The frequency of resident and migratory DCs remained comparable between Cre^- and Cre^+ animals at steady state (Figure 2.5). However, during infection we observed a striking reduction in the percentage of migratory DCs in the MLN in mice with Notch-deficient basophils compared to mice with Notch-sufficient basophils Figure 2.5), suggesting that Notch-activated basophils are important for the infection dependent increase of migratory DCs in the MLN during *T. muris* infection. Thus, these preliminary data

highlight a potential route by which Notch-activated basophils indirectly support Th2 cell activation via the accumulation of migratory DCs in the lymph node during helminth infection.

2.2.6 Direct basophil-T cell interactions mediate intestinal CD4$^+$ T cell fate and function via an IL-4 autocrine module

To elucidate mechanisms by which basophils support CD4$^+$ T cell IL-4 production and Th2 fate, we established an *in vitro* co-culture assay with CD4$^+$ T cells and splenic basophils isolated from C57BL/6J mice on D14 of *T. muris* infection. Infection-experienced T cells were provided with weak TCR stimulation and no exogenous antigen[72]. After 3 days of co-culture, in the presence or absence of exogenous recombinant murine (rm)IL-4, CD4$^+$ T cells were analyzed for GATA3 expression, IL-4 production, and proliferation. In the presence of splenic basophils, MLN- and cecum-derived CD4$^+$ T cells exhibited increased retention or induction of GATA3 compared to CD4$^+$ T cells cultured alone, accompanied by an increase in total CD4$^+$ T cell IL-4 production and proliferation (Ki67$^+$), regardless of supplementation with exogenous rmIL-4 (Fig. 2.6 A-F). During *T. muris* infection, there is an influx of eosinophils into inflamed tissue[73,110,]. Unlike basophils, however, eosinophils did not support the GATA3$^+$CD4$^+$ T cell population *in vitro* (Supplementary Fig. 2.6 A). Consistent with our finding that IL-4 production by intestinal Th2 and TF$^-$ CD4$^+$ T cells depended on Notch-activated basophils during *T. muris* infection *in vivo* (Fig. 2.4 D and K), basophils similarly supported IL-4 production by both GATA3$^+$ and GATA3$^-$ CD4$^+$ T cells *in vitro* (Fig. 2.6 G and H). Together, these data demonstrate that basophils preferentially maintain CD4$^+$ T cell Th2 fate and IL-4 production in the context of *T. muris* infection.

We next utilized this co-culture system to dissect mechanisms by which basophils optimize Th2 fate and function. Because basophils can produce IL-4[66,111], we tested whether IL-4-deficient basophils support MLN $CD4^+$ T cell GATA3 expression and observed that IL-4-sufficient and -deficient basophils similarly maintained $CD4^+$ T cell GATA3 expression (Fig. 2.6 I). Likewise, soluble factors in concentrated, basophil-conditioned media from overnight cultures of infection-experienced basophils did not support Th2 fate and function in $CD4^+$ T cells (Supplementary Fig. 2.6 B), suggesting that basophil-derived soluble factors, including IL-4, do not support Th2 cell fate and function *in vitro*. We next hypothesized that a cell-cell contact-dependent mechanism might be required for basophil-mediated support of Th2 cell fate and function. To test this, $CD4^+$ T cells and basophils were separated in co-culture assays using a transwell insert. When basophils and $CD4^+$ T cells were separated, basophil support of $CD4^+$ T cell GATA3 expression was abolished (Fig. 5J). Importantly, this contact-dependent mechanism is most likely independent of MHC class II, as an MHC class II blocking antibody did not disrupt basophil support of Th2 cell accumulation (Supplementary Fig. 2.6 C).

The identification of contact-dependent basophil support of $CD4^+$ T cell GATA3 and IL-4 production does not preclude participation of other factors in this interplay. Considering that Notch-activated basophils maintained IL-4 production in both Th2 and TF^- intestinal $CD4^+$ T cells *in vivo* (Fig. 2.4 D and K), and the defined role of T cell-derived, autocrine IL-4 signaling in maintaining Th2 fate[112–114], we hypothesized that direct basophil-$CD4^+$ T cell contact serves to maintain an autocrine IL-4 signaling program in $CD4^+$ T cells. To test this idea, we performed co-culture assays as described above, but with IL-$4^{-/-}$ basophils co-cultured with either WT or IL-$4^{-/-}$ $CD4^+$ T cells, in the presence or absence of exogenous rmIL-4. While GATA3 expression was increased by basophil contact in WT $CD4^+$ T cells, IL-$4^{-/-}$ $CD4^+$ T cells failed to induce

GATA3 in the presence of basophils, with or without rmIL-4 (Fig. 2.6 K and L). Since bioactive exogenous IL-4 (Supplementary Fig. 2.6 D) did not significantly rescue Th2 induction in IL-4-deficient $CD4^+$ T cells, we assessed responsiveness to the IL-4 in IL-4-sufficient vs. -deficient cells and found that IL-4Rα expression on MLN-derived $CD4^+$ T cells at D14 p.i. was reduced on IL-4-deficient compared to -sufficient controls during *T. muris* infection (Supplementary Fig. 2.6 E and F). Overall, these data indicate that $CD4^+$ T cells must be IL-4-sufficient to benefit from basophil-dependent induction of GATA3 expression, revealing an IL-4 autocrine signaling program that maintains $CD4^+$ T cell identity and function through a direct basophil-T cell contact-dependent mechanism.

2.2.7 Proximity between $GATA3^+$ Th2 cells and basophils in the cecum during *T. muris* infection is dependent on basophil-intrinsic Notch

Basophil-$CD4^+$ T cell proximity in the inflamed intestinal epithelium at D19 of *T. muris* infection depended on Notch-intrinsic programming of basophils[18]. Our finding of a contact-dependent mechanism by which basophils support cecum LP Th2 fate and function (Fig. 2.4) led us to hypothesize that basophil-intrinsic Notch signaling is required to bring basophils and Th2 cells into the proximity required for cell contact-dependent support *in vivo.* To test this hypothesis, mice with Notch-deficient or -sufficient basophils were infected with *T. muris* and immunofluorescence staining analysis of basophil ($Mcpt8^+$; red), $CD4^+$ cells ($CD4^+$; green) and Th2 cell ($CD4^+$; $green^{+\ +}$ $GATA3^+$; magenta) positioning and proximity at D14 p.i. was performed. At this earlier timepoint of infection, loss of basophil-intrinsic Notch did not disrupt normal basophil localization in the cecum LP (Supplementary Fig. 2.7 A and B), in contrast to D19, a timepoint associated with *T. muris* expulsion in WT mice. In agreement with our flow

cytometry data (Fig. 2.7 A and B), there was an infection-induced increase in the number of $GATA3^+CD4^+$ Th2s per crypt-unit in the cecum in basophil-Notch-sufficient mice, which was diminished in basophil-Notch-deficient mice (Fig. 2.6 A-C). Quantification of basophil-Th2 proximity highlighted that Notch-activation of basophils was required to optimally co-localize basophils with $GATA3^+$ but not $GATA3^-$ $CD4^+$ T cells during infection (Fig. 2.7 D-G). Overall, these data implicate basophil-intrinsic Notch signaling in positioning basophils to promote contact-dependent, basophil-$CD4^+$ T cell interactions that support GATA3 and IL-4 expression in intestinal $CD4^+$ T cells during intestinal helminth infection, potentially via $CD4^+$ T cell-intrinsic, autocrine IL-4 signaling.

2.3 Discussion

This study highlights a novel role for Notch-activated basophils in orchestrating $CD4^+$ T cell fate and function within the large intestine during *T. muris* infection. Notch-programmed basophils augment intestinal $CD4^+$ T cell responses by inducing or maintaining GATA3 expression and the ability of $GATA3^+$ and $GATA3^-$ cells to produce IL-4 (Fig. 2.4D and K, Fig. 2.6 G and H). Thus, basophils both promote and sustain large intestinal Th2 responses via Notch-dependent mechanisms during *T. muris* infection[115,116]. We show Notch-activated basophils do not merely facilitate Th2 expansion and function but are pivotal for a broader IL-4 production program across various intestinal $CD4^+$ T cell subsets.

KN2 and Smart13 reporter mice revealed that $CD4^+$ T cells were the predominant sources of IL-4 and IL-13 in the cecum at D14 p.i. with *T. muris*, the peak of the $CD4^+$ T cell response, in agreement with published findings (Fig. 2.1 C and D)[24,92,96]. While previous studies have shown that ILC2-derived IL-13 drives the tissue remodeling required for robust Type 2

immunity in several models of helminth infection[20,21], our studies using Lcr1 KO mice revealed that Lcr1-dependent ILC2s are not required for productive immunity against *Trichuris muris* (Supplementary Fig. 2.1b). These data underscore that the potent proinflammatory role that ILC2s play in other models of helminth infection cannot be generalized across all species of helminths and, taken with our cytokine reporters, suggest that $CD4^+$ T cells are a crucial source of Type 2 cytokines in the inflamed large intestine during *T. muris* infection.

Intriguingly, IL-4 production was not restricted to $GATA3^+$ Th2 cells in the cecum during *T. muris* infection (Fig. 2.2 C, F, H, and J, Supplementary Fig. 2.2a D-J); rather, TF^- $CD4^+$ T cells were the predominant IL-4 source in both naïve and infected mice (Fig. 2.2 I and J). In addition, Notch-activated basophils promoted a Type 2 inflammation-associated transcriptional program in cecum $CD4^+$ T cells (Fig. 2.3). While Th2-associated cytokine transcript levels cannot be directly correlated with cytokine production, we confirmed that Notch-activated basophils are required for IL-4 production by both TF^- $CD4^+$ T cells and Th2 cells (Fig. 2.4 D and K). These findings challenge prevailing models where IL-4 production is isolated to Th2 cells and Tfh-like cells during Type 2 inflammation. Recent studies have highlighted similar situations where diverse immune cells, including unconventional sources, can produce Type 2 cytokines independently of GATA3[49,65,117]. It is possible that TF^- $CD4^+$ T cells arise from transcriptionally transient and heterogenous naïve $CD4^+$ T cells induced early in helminth infection and establish a critical initial source of IL-4[112]. The importance of IL-4 in promoting worm expulsion and antibody responses during *T. muris* is documented, but it will be important to understand which aspects of anti-helminth immunity are distinctly regulated by TF^- $IL\text{-}4^+$ $CD4^+$ T cells[20,30,118]. Additionally, whether TF^- $IL\text{-}4^+$ $CD4^+$ T cells arise during gastrointestinal helminth infection in a GATA3-independent but STAT6-dependent fashion will

be critical to improve our understanding of how Th2-associated functions are programmed outside of the lymph node. Future experiments will also be needed to clarify the importance of basophils in activating these cells and in maintaining the overall Type 2 inflammatory milieu in the large intestine.

We found that Notch-activated basophils supported IL-4 and IL-13 production specifically by intestinal $CD4^+$ T cells *in vivo*, but not MLN-resident T cells (Fig. 2.4 C-E, Supplementary Fig. 2.4b A-C). Basophils largely do not accumulate in lymph nodes during helminth infection, but are robustly recruited to peripheral tissues, indicating that there may be a tissue-specific large intestinal niche for optimal basophil-$CD4^+$ T cell interactions[69,92]. This could be attributed to localized signals or microenvironmental factors present in the intestine that are not replicated in lymph nodes[119]. Indeed, tissue-specific immune responses are highly contextual and differ significantly based on helminth species-specific effects in distinct tissue microenvironments[120,121]. Our data reinforce this idea, highlighting that Notch-activated basophils are programmed to migrate to the correct tissue microenvironment to tailor their support to local $CD4^+$ T cell populations, suggesting that intestinal basophils have specialized functions other cells cannot fulfill. Future studies will be required to determine the specific and unique roles that basophils play in this regard, compared to those of other innate cells.

Basophils require intact Notch signaling to correctly position themselves in the cecum at D19 post-*T. muris* infection, where basophil-$CD4^+$ T cell proximity depends on Notch-activated basophils[92]. The mechanisms of Notch activation in basophils, including the sources of basophil-activating Notch ligands, remain unclear. However, our data suggest that basophils interact directly with effector T cells in the inflamed intestine. Basophils localized near $GATA3^+$ $CD4^+$ T cells, and this association was dependent on basophil-intrinsic Notch signaling at D14 post-*T.*

muris infection (Fig. 2.7 D-H). In parallel, basophils supported GATA3 expression and IL-4 production in intestinal $CD4^+$ T cells via a cell-contact dependent mechanism *in vitro* (Fig. 2.44).

Notably, MHC class II, IL-4, and basophil-secreted factors (Fig. 2.6 I and Supplementary Fig. 2.6 B and C) were not required for basophil support of $CD4^+$ T cells; thus, the precise molecular nature of the basophil-$CD4^+$ T cell interaction remains unclear. Although basophil-derived IL-4 was inconsequential, intact $CD4^+$ T cell autocrine IL-4 production was required for upregulating GATA3 expression in a basophil-dependent manner (Fig. 2.6 K and L), potentially via reduced IL-4Rα in IL-4-deficient $CD4^+$ T cells (Supplementary Fig. 2.6 E and F). In agreement with this, IL-4Rα expression induces a feedback loop critical for initiating and/or maintaining Th2 responses[28,113,114]. Additionally, recent work has highlighted the importance of $CD4^+$ T cell clustering to promote localized IL-4-sensing to maintain Th2 fate and function[122]. Our data further provoke the notion that basophils may deploy similar strategies to promote IL-4 sensing in inflamed tissue microenvironments by helping to cluster key sources of IL-4. Basophils can undergo prolonged direct contact with $CD4^+$ T cells in helminth-infected lung tissue, but whether this occurs in the intestine during *T. muris* infection has remained unclear until now[69]. Future studies will elucidate the molecular mechanisms by which basophils mediate contact-dependent augmentation of $CD4^+$ T cell fate and function.

Our study expands a growing body of evidence suggesting that basophils do not merely enter inflamed tissues and degranulate but are transcriptionally active players that deploy several effector functions during Type 2 inflammation[63,69,92,123,124]. Our identification of a major non-Th2, IL-4-producing intestinal $CD4^+$ T cell population dependent on Notch-programmed basophils also provides new insight into how optimal Th2 responses are orchestrated in tissues during helminth infection. Collectively, our findings suggest that basophils serve as a critical

bridge between the innate and adaptive Type 2 inflammatory response, with Notch-activated basophils amplifying or maintaining Th2 responses necessary for a full effector Th2 program at the site of infection. Taken together, our studies have the potential to inform efforts to modulate tissue-specific $CD4^+$ T cell responses in the tissue that dictate the outcome of helminth infection as well as other inflammatory diseases.

2.4 Materials and methods

Mice

Male and female C57BL/6 wildtype mice were purchased from Jackson Laboratories or bred in-house. Male and female C57BL/6 KN2$^{+/+}$ (*Il4*$^{-/-}$)[72], KN2$^{+/-}$ (*Il4*$^{+/-}$), Mcpt8Cre^{+} DNMAML F/F[31,107,108], and Smart13[110] mice were bred in-house. KN2$^{+/+}$, Smart13, and Lcr1 knock out (KO) mice were kindly provided by Dr. Marion Pepper (University of Washington) and Dr. Jakob von Moltke (University of Washington). Mice were randomly assigned to experimental groups, but were between 6-16 weeks of age, age- and sex-matched, and housed in specific pathogen-free conditions at the University of Washington, in accordance with the Institutional Animal Care and Use Committee (IACUC 4478-01). Animals undergoing helminth infection do not display overt signs of morbidity. No unexpected adverse events or mortality occurred in the study. Animals were monitored daily by animal care and laboratory staff.

In vivo treatments and *ex vivo* tissue preparation

T. muris eggs were generated in-house by infecting *Rag2*$^{-/-}$ mice with 300 eggs by oral gavage. Adult worms were collected from ceca between 6-10 weeks post-infection and cultured overnight at 37°C and 5% CO_2. Eggs were collected and stored in ultra-pure water at 30°C until embryonation. Experimental mice were infected with 300 eggs *T. muris* by oral gavage and euthanized on D14 p.i.

Spleen and MLN single-cell suspensions were prepared by mashing tissue through a 70 μm strainer, and red blood cells were lysed with ACK lysis buffer (Lonza). For cecum single-cell suspensions, ceca were harvested into ice-cold PBS, with the cecum patch removed, cut

longitudinally, washed, and washed an additional two times in ice-cold PBS with 10% FBS (Denville Scientific). Tissue was sectioned and placed in ice-cold HBSS (ThermoFisher) with 10% FBS (Denville Scientific), stored on ice, then strained and incubated in warm HBSS with 2 mM EDTA (ThermoFisher) for 15 min at 37°C in a shaking incubator at 160 rpm. Samples were strained and incubated for 20 min in fresh HBSS/ EDTA at 37°C at 160 rpm and incubated in 1 U/mL Liberase TL and 20 μg/mL DNase for 30 min at 37°C in a shaking incubator at 160 rpm. Samples were washed and mashed through 70 μm strainers to obtain single-cell suspensions.

Flow cytometry and cell sorting

Single-cell suspensions from MLN or cecum were cultured *in vitro* for 4 h in complete RPMI (VWR) (10% FBS, 1% L-glutamine, 1% Penicillin/Streptomycin, 55 μm beta-mercaptoethanol, 25 mM HEPES) with 10 μg/mL brefeldin-A (Sigma-Aldrich) and 10μg/mL monensin-A (Sigma-Aldrich) at 37 °C, 5% CO_2. For all staining approaches, single cell suspensions were incubated with Aqua Live/Dead Fixable Dye (Life Technologies) and fluorochrome-conjugated monoclonal antibodies against mouse CD3ε (145-2C11, BV650), CD4 (GK1.5, BV711), CD5 (53-7.3, PerCpCy5.5), CD8 (53-6.7, PerCp-eF710), CD11c (N418, PerCpCy5.5), CD19 (eBio1D3, PerCpCy5.5), CD44 (1M7, APC), CD45 (30-F11, BUV805), CD45.1 (A20, APC), CD45.2 (104, eF780), CD117 (2B8, PerCpCy5.5), CD123 (5B11, PE), (CD200R (OX-110, APC), IL-4Rα (LEW, biotin), IL-17RB (MMUNC33, APC), NK1.1 (PK136, PerCpCy5.5), ST2 (RMST2-2, PE), Streptavidin (APC), TCRβ (H57-597, ACP-Cy7) or TCRγδ (eBioGL3, PerCpCy5.5). Surface staining was performed in 10% rat serum (Jackson ImmunoResearch), 1 μg/mL FcR block (anti-CD16/32, 2.4G2, BioXCell) and 10% SuperBright/Brilliant staining buffer (ThermoFisher/BD Biosciences). For transcription factor

intracellular staining, cells were fixed with 2% paraformaldehyde (only for cytokine staining) after surface staining and/or Foxp3 fixation/permeabilization buffer and permeabilized with the accompanying permeabilization buffer (ThermoFisher). Cells were stained with monoclonal antibodies against BCL6 (K112-91, CF594), FOXP3 (FJK-16s, eF450), GATA3 (TWAJ, AF488), RORyt (B2D, PE-Cy7), T-bet (4B10, BV421), Ki67 (B56, AF700), IL-2 (JES6-5H4, PE-CF594), IL-4 (11B11, APC), IL-5 (TRFK5, BV421), IL-10 (JES5-16E3, BV650), IL-13 (eBio13A, PE) and/or IFNγ (XMG1.2, BV786). For analysis of KN2 and Smart13, reporter cells were surface-stained with antibodies against human CD2 (RPA-2.10, APC) (KN2) or human CD4 (RPA-T4, APC) (Smart13), and transcription factor staining panel included BCL6, FOXP3, GATA3, RORyt, and T-bet for KN2 cells, and FOXP3, GATA3, T-bet for Smart13. For analysis of Lcr1 knock out mice, cells were stained with monoclonal antibodies against CD3e (BV421), CD4 (GK1.5, AF700), CD5 (53-7.3, PerCpCy5.5), CD11b (BUV395), CD11c (N418, PerCpCy5.5), CD19 (eBio1D3, PerCpCy5.5), CD45 (30-F11, BUV805), CD90.2 (BUV496), CD127 (PE-Cy7), IL-17RB (MMUNC33, APC), KLRG1 (APC eF780), NK1.1 (PK136, PerCpCy5.5), SiglecF (PECF594), ST2 (RMST2-2, PE). All antibodies were obtained from BD Biosciences, BioLegend or ThermoFisher. Samples were run on a 5-laser LSR II (BD Biosciences), 5-laser FACSymphony A3 (BD Biosciences) flow cytometer, and/or Cytek Aurora Spectral Flow cytometer, and FlowJo 10 (Tree Star) was used to analyze data. Gates were set using C57BL/6J mice and fluorescence minus one (FMO) controls. For cell sorting, single cell suspensions were sorted using a 3 or 4-laser Aria II (BD Biosciences) with a 70 or 85 μm nozzle. All leukocyte populations were first gated as singlet, live (Live/Dead$^-$), leukocytes (by FSC-A/SSC-A). Basophils were sorted as CD45$^+$Lin$^-$CD200R$^+$CD123$^+$. The basophil lineage gate (Lin) included CD3, CD5, CD11c, CD19, CD117 and NK1.1. For scRNA-seq analysis and CD4$^+$

T cell co-cultures, $CD4^+$ T cells were gated as $CD45^+$Lin (CD11c/CD19/NK1.1/TCRγδ)$^-$ $TCR\beta^+CD8^-CD4^+$.

Enhanced sensitivity cytometric bead array

Cecum LP $CD4^+$ T cells were sort-purified from Naïve Mcpt8-Cre^-, Naïve Mcpt8-Cre^+, Tm Mcpt8-Cre^-, and Tm Mcpt8-Cre^+ mice D14 p.i. *Trichuris muris* and plated at 25,000 cells per well in a 96 well plate precoated with anti-CD3e (1 μg/mL) and anti-CD28 (1μg/ml) and cultured *in vitro* for 48 hrs. Cells were then spun down at 1500 rpm for 5 min, and the cell-free supernatant was collected and frozen at -80 C until ready for use. For the detection of IL-4 and IL-13 in cell free supernatants, we used BD Cytometric Bead Array (CBA) Mouse IL-13 and IL-4 Enhanced Sensitivity Flex Set (BD biosciences) and BD Cytometric Bead Array (CBA) Mouse Enhanced Sensitivity Master buffer kit (BD biosciences). Standards for IL-4 and IL-13 were prepared according to the kit instructions. Samples were incubated with capture beads for 2 hrs at RT shaking at 400 rpm, washed with kit wash buffer twice, and then incubated with detection beads for 2 hrs at RT shaking at 400 rpm. Samples were washed twice more, and then incubated with the enhanced sensitivity detection reagent for 1 hr at RT shaking at 400 rpm. Samples were washed twice and then resuspended in wash buffer prior to sample acquisition by flow cytometry. Standard curves and data analysis were done in FlowJo using the CBA plug-in (BD biosciences).

Th2 polarization assay

Naïve $CD4^+$ T cells were isolated from the mesenteric lymph node of naïve C57J/B6 mice using a naïve $CD4^+$ T cell isolation kit (Miltenyi). Naïve $CD4^+$ T cells were plated at a

density of 100,000 cells per well in an anti-CD3e (5 ug/mL) and anti-CD28 (2 ug/mL) precoated 24 well plate in Th0 (10 ug/mL anti-IFNγ, 10 ug/mL anti-IL-4, 10 ng/mL recombinant murine IL-2) or Th2 (10 ug/mL anti-IFNγ, 10 ng/mL recombinant murine IL-2, 50 ng/ml recombinant murine IL-4) polarizing conditions. Cells were cultured under these conditions for 48 hrs, then the media was replenished, and cells were cultured for an additional 48 hrs to complete the polarization assay. At the end time point (~4 days total), cells were washed twice with 1 XPBS and then treated with PMA and ionomycin for 3 hrs. Cells were then washed with PBS twice and proceeded to staining for flow cytometric analysis.

$CD4^+$ T cell: basophil co-cultures

Splenic basophils were sort-purified, and MLN or cecum $CD4^+$ T cells were sort-purified and/or purified using the MACS $CD4^+$ T cell isolation kit (Miltenyi) from mice on D14 of *T. muris* infection. >95% purity was confirmed, and then T cells were cultured ± splenic basophils in complete RPMI with 1 μg/mL soluble anti-CD3 (ThermoFisher) and anti-CD28 (ThermoFisher), ± 20 ng/mL rmIL-4 (R&D) at 37°C, 5% CO_2 for 72 h. For MLN $CD4^+$ T cell cultures, $3x10^4$ $CD4^+$ T cells were cultured alone or with $5x10^3$ basophils/ well. For cecum $CD4^+$ T cell cultures, $1.5x10^4$ $CD4^+$ T cells were cultured alone or with $2.5x10^3$ basophils/ well. For transwell assays, $1x10^4$ MLN $CD4^+$ T cells were cultured for 72 h on a transwell insert with 0.4 μm pores (Corning), alone, with $1x10^3$ splenic basophils ± transwell separation with soluble anti-CD3/CD28 ± rmIL-4. For supernatant assays, $5x10^3$ sort-purified splenic basophils/well were cultured in complete RPMI overnight and supernatants were collected and pooled. Cell-free complete RPMI was collected as a negative control. Media was centrifuged to remove cell debris, filter-concentrated in a 100K centrifugal filter (Amicon) and dialyzed in a 20K MW

Slide-A-Lyzer MINI dialysis device (ThermoFisher) at 4°C. Concentrated media was added at 1:20 with complete RPMI to MLN $CD4^+$ T cells in the presence of plate-bound anti-CD3 and soluble anti-CD28 ± rmIL-4. At 72 hrs, $CD4^+$ T cells were harvested for flow cytometry analysis.

Immunofluorescence staining

Cecal samples were washed in PBS and fixed in 2% PFA (Sigma-Aldrich) at 4°C for 1-2 hours, incubated in 15% and 30% sucrose (Sigma- Aldrich) solutions overnight, mounted in optimal cutting temperature (OCT) embedding medium (Sakura), frozen, and sectioned. Seven μm cryosections were permeabilized with 0.4% Triton-X 100 (Sigma-Aldrich) for 10 min at room temperature (RT) then 90% ice cold methanol for 5 min on ice and blocked in 5% normal donkey serum (Jackson ImmunoResearch) plus 5% BSA (Sigma-Aldrich) for 1-2 hrs at RT. Sections were incubated with primary antibodies against Mcpt8 (TUG8; BioLegend) and CD4 (EPR19514; Abcam) or isotype controls overnight at 4°C, washed, and incubated with Alexa Fluor 647 Mouse anti–GATA3 (L50-823; BD Biosciences), Alexa Fluor 488–conjugated donkey anti–rat IgG, and Alexa Fluor 547–conjugated donkey anti–rabbit IgG (Jackson ImmunoResearch) for 2 hrs at RT. Slides were washed with PBS, mounted in mounting medium containing DAPI (Vector Laboratories) and imaged on a Nikon A1R confocal microscope with laser emission wavelengths of 488, 547, 633, and 405 (DAPI) under the 20X objective lens.

For cellular proximity, cell X, Y coordinates were measured in a 512 X 512 μm grid using the FIJI multi-point tool. Distance matrices were generated in Python, and the percentage of basophils <10 μm of $GATA3^+CD4^+$ T cells or $GATA3^-CD4^+$ T cells was determined. Four to seven images were captured per mouse and averaged for one biological replicate. Quantification of the number of Th2 cells/crypt was done manually, counting $GATA3^+CD4^+$ T cells in a single-

crypt unit. Four to seven images were captured per mouse and averaged for one biological replicate. Quantifications were performed by an investigator blinded to sample identity.

Single-cell RNA sequencing and bulk RNA sequencing

Cecum $CD4^+$ T cells were sort-purified from single cell suspensions from 1-2 Mcpt8Cre$^-$ DNMAML F/F female mice on D0 or D14 p.i. with *T. muris*. For single-cell, cells were loaded onto the 10x Chromium Controller (10X Genomics) according to the manufacturer's protocol, with a target capture of $3x10^3$ cells per channel. Sequencing libraries were generated using the NextGEM Single Cell 5' Kit v1.1 kit. Gene expression and mouse TCR libraries were pooled in groups of 4 samples at a ratio of 6:1 (GEX:TCR) and treated with the Illumina Free Adapter Blocking Reagent (Illumina) to reduce index-hopping. Sequencing of pooled libraries was carried out on a NextSeq 2000 sequencer (Illumina), using three NextSeq P2 flowcells (Illumina) with a target depth of $3x10^4$ raw reads per cell. Kallisto was used to associate the reads with cells of origin and tie reads to unique molecular identifiers (UMIs)[111] and create a cell x gene matrix by quantifying the abundance of annotated target transcripts with reference to GRCm38 (mm10) release 79 from RNAseq data, with the estimated fragment length (-l = 300), SD (-s = 100), and 100 bootstrap iterations. We also specified strand-specific reads with the first read on the reverse strand (--rf-stranded). Differentially expressed transcripts were identified by using a non-parametric Wilcoxon rank sum test in Seurat and filtered for a false discovery rate of 10%[36,37]. Visualizations were generated in R, after centering transcript abundance estimates by the mean and scaling to the SD.

For bulk RNAseq, total RNA was purified from sort-purified cecum LP $CD4^+$ T cells using Norgen Biotek Total RNA Purification Plus Micro Kit (Norgen Biotek). Total RNA was

added to reaction buffer from the SMART-Seq v4 Ultra Low Input RNA Kit for Sequencing (Takara), and reverse transcription was performed followed by PCR amplification to generate full length amplified cDNA. Sequencing libraries were constructed using the NexteraXT DNA sample preparation kit with unique dual indexes (Illumina) to generate Illumina-compatible barcoded libraries. Libraries were pooled and quantified using a Qubit® Fluorometer (Life Technologies). Sequencing of pooled libraries was carried out on a NextSeq 2000 sequencer (Illumina) with paired-end 59-base reads, using a NextSeq P3 XLEAP sequencing kit (Illumina) with a target depth of 5 million reads per sample. Base calls were processed to FASTQs on BaseSpace (Illumina), and a base call quality-trimming step was applied to remove low-confidence base calls from the ends of reads. The FASTQs were aligned to the GRCm38 mouse reference genome, using STAR v.2.4.2a and gene counts were generated using htseq-count. QC and metrics analysis was performed using the Picard family of tools (v1.134). Differential expression testing was conducted using DESeq2. VST count values were used for principal component analysis. Genes were considered statistically significant if p value < 0.05 and fold change > 1.5. For binned analyses, cells were assigned bins based on detection of *Gata3, Foxp3, Rorc, Bcl6,* and/or *Tbx21.* Bins with greater than 75 cells were included for subsequent analysis. RNAseq data are available in GEO with accession # (TBD).

Statistics

To determine the group sizes necessary to account for variability associated with ex vivo and in vivo experiments, power and sample size estimation analysis was used, using the JMP statistical package, based on preliminary data. Groups sizes that meet or exceed those calculated to reject the null hypothesis (power>0.8, $\alpha=0.05$) are indicated in figure legends. To account for

cage effects, mice were co-housed and animals were age- and sex-matched across groups. No other confounders were controlled for. Statistical analysis of all non-sequencing data was done in JMP (SAS), analyzed using linear mixed effects models with a fixed effect of experimental group and a random effect of experiment day. Model assumptions of normality and homogeneous variance were assessed by a visual analysis of the distribution of the raw data and model residuals. Skewed data was log (x+1), or square root transformed. Experimental group was considered a random effect and statistically significant if the fixed effect F test *p*-value was less than or equal to 0.05. Post-hoc pairwise comparisons between experimental groups were made using Tukey's HSD multiple-comparison test, one way ANOVA, or unpaired student's t-test. Statistical outliers were identified using the extreme studentized deviate method and omitted prior to the model analysis. Graphs of results were shown as mean ± SEM of untransformed data using Prism version 9 (GraphPad). For IHC analysis, quantifications were performed by an investigator blinded to sample identity. No other samples were blinded.

Limitations of study.

Biological findings from *in vitro* and *in vivo* experiments do not necessarily relate to each other or translate to human studies. Evidence suggest mouse models are relevant to human studies, but no human studies were performed. There is potential for bias in unblinded samples.

2.5 Acknowledgements

We thank members of the Tait Wojno lab for their contributions and feedback during manuscript development; Thane Mittelstaedt and Delphina Walker-Phelan at the University of Washington School of Medicine Cell Analysis Facility for assistance with flow cytometric analysis and FACS-based cell sorting; Dr. Dale Hailey and the Garvey Imaging Core at the Institute for Cell & Regenerative Medicine at the University of Washington for assistance with imaging studies; Dr. Vivian Gersuk and the Genomics Core at the Benaroya Research Institute for their assistance with RNA sequencing services; Dr. Kazushige Ninomiya and the Ziegler lab at the Benaroya Research Institute for sharing critical reagents; and Ashley N. Warner, for writing and running a Python script for the generation of distance matrices for immunofluorescence analyses.

This body of work was supported by the National Institutes of Health National Institute of Allergy and Infectious Diseases (R01 AI132708 to E.D. Tait Wojno), University of Washington start-up funds (to E.D. Tait Wojno), and T32 training grant (GM007270 to L.M. Warner). The authors of this manuscript are responsible for its content and do not necessarily represent the official views of the National Institutes of Health.

Author contributions.

Lauren M. Webb, Lindsey M. Warner, and Elia D. Tait Wojno designed the project, executed experiments, performed data analysis and curation, and wrote the manuscript, with feedback provided by all other authors. Bridget Mooney performed experiments and data curation. Pavithra Sundaravaradan curated and analyzed single-cell RNAseq data. Macy K.

Matheson, Tighe Christopher, and Alejandra Lopez Espinoza executed experiments. Elia D. Tait Wojno conceived the project and supervised the research.

2.6 Figures

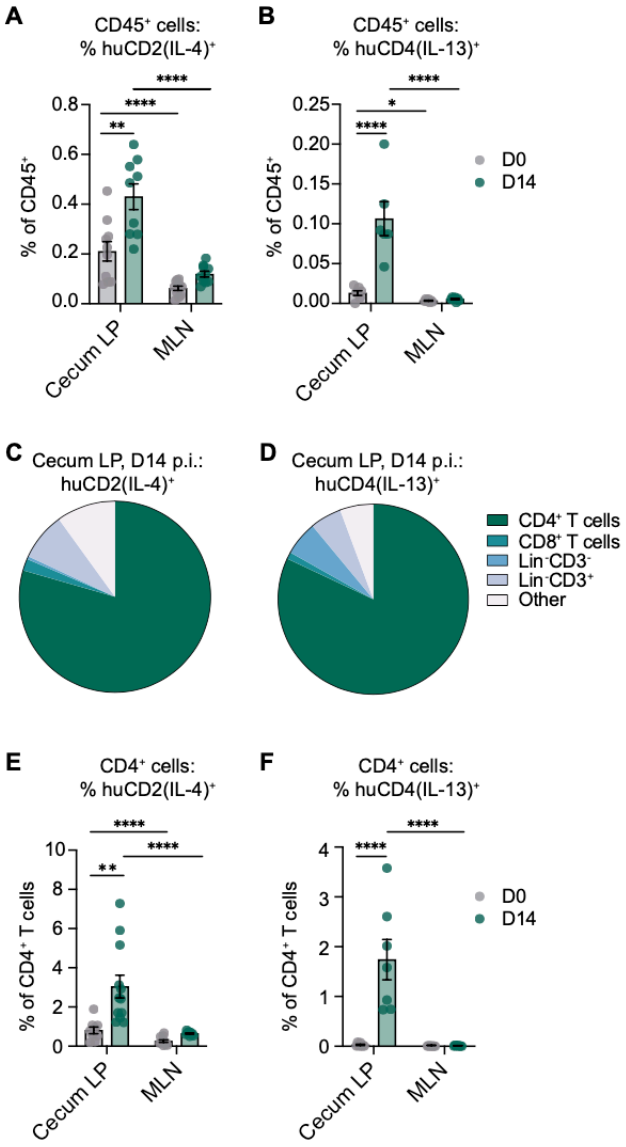

Figure 2.1. CD4$^+$ T cells are the predominant source of IL-4 and IL-13 in the inflamed cecum during *T. muris* infection.

KN2 mice **(A, C, and E)** and SMART13 mice **(B, D, and F)** at day 0 (D0) or day 14 (D14) post-infection (p.i). with *T. muris* were analyzed by flow cytometry for the frequency of huCD2(IL-4)$^+$ or huCD4(IL-13)$^+$ cells in the cecum lamina propria (LP) and mesenteric lymph

nodes (MLN). Frequency of **(A)** huCD2(IL-4)$^+$ and **(B)** huCD4(IL-13)$^+$ cells in total CD45$^+$ cells at D0 and D14 p.i.. Distribution of **(C)** huCD2(IL-4) and **(D)** huCD4(IL-13) expression among CD45$^+$ immune cell subsets, including CD4$^+$ T cells (dark green), CD8$^+$ T cells (teal), Lin(CD11c/CD19/NK1.1/TCRγδ)$^-$ cells (blue), Lin$^-$CD3e$^+$ (lavender), and other (light pink) immune cells at D14 p.i. Frequency of **(E)** huCD2(IL-4)$^+$ and (**F)** huCD4(IL-13)$^+$ cells in total CD4$^+$ T cells in the cecum LP and MLN at D0 and D14 p.i.. Mean ± SEM; *, $P < 0.05$; **, $P < 0.01$; ****, $P < 0.0001$. **(A-F)** Data were analyzed using linear mixed effects models and post-hoc pairwise comparisons between groups using Tukey's HSD-multiple-comparison test. (**A, C, and E)** 3-4 independent experiments pooled together (MLN D0, n = 11; MLN D14, n = 9; Cecum LP D0, n = 9; cecum LP D14, n = 12). **(B, D, and F)** 3 independent experiments pooled together (MLN D0, n = 7, MLN D14, n = 7, Cecum LP D0, n = 7; Cecum LP D14, n = 6-7). N is total across all experiments.

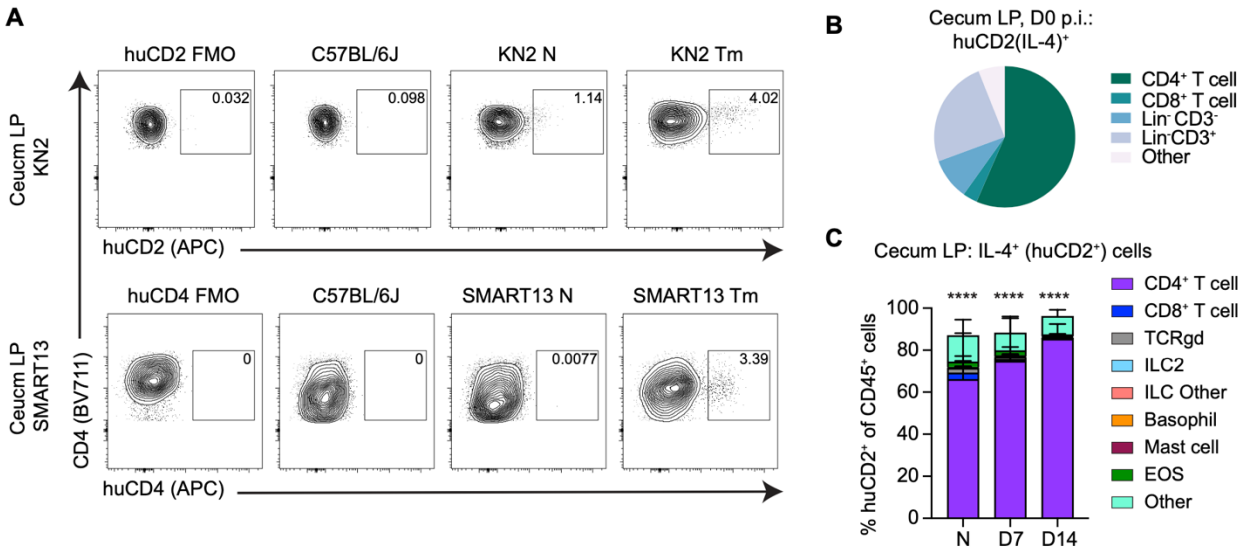

Supplementary Figure 2.1a (related to figure 2.1) IL-4 production by immune cells in the cecum of naive mice.

Pie chart of the frequency of huCD2(IL-4$^+$) cells of total CD45$^+$ immune cells isolated from the cecum lamina propria (LP) of naive KN2 mice. Data were analyzed using linear mixed effects models, and post-hoc pairwise comparisons between groups were made using Tukey's HSD-multiple-comparison test. Four independent experiments were pooled together (n = 9 total across all experiments).

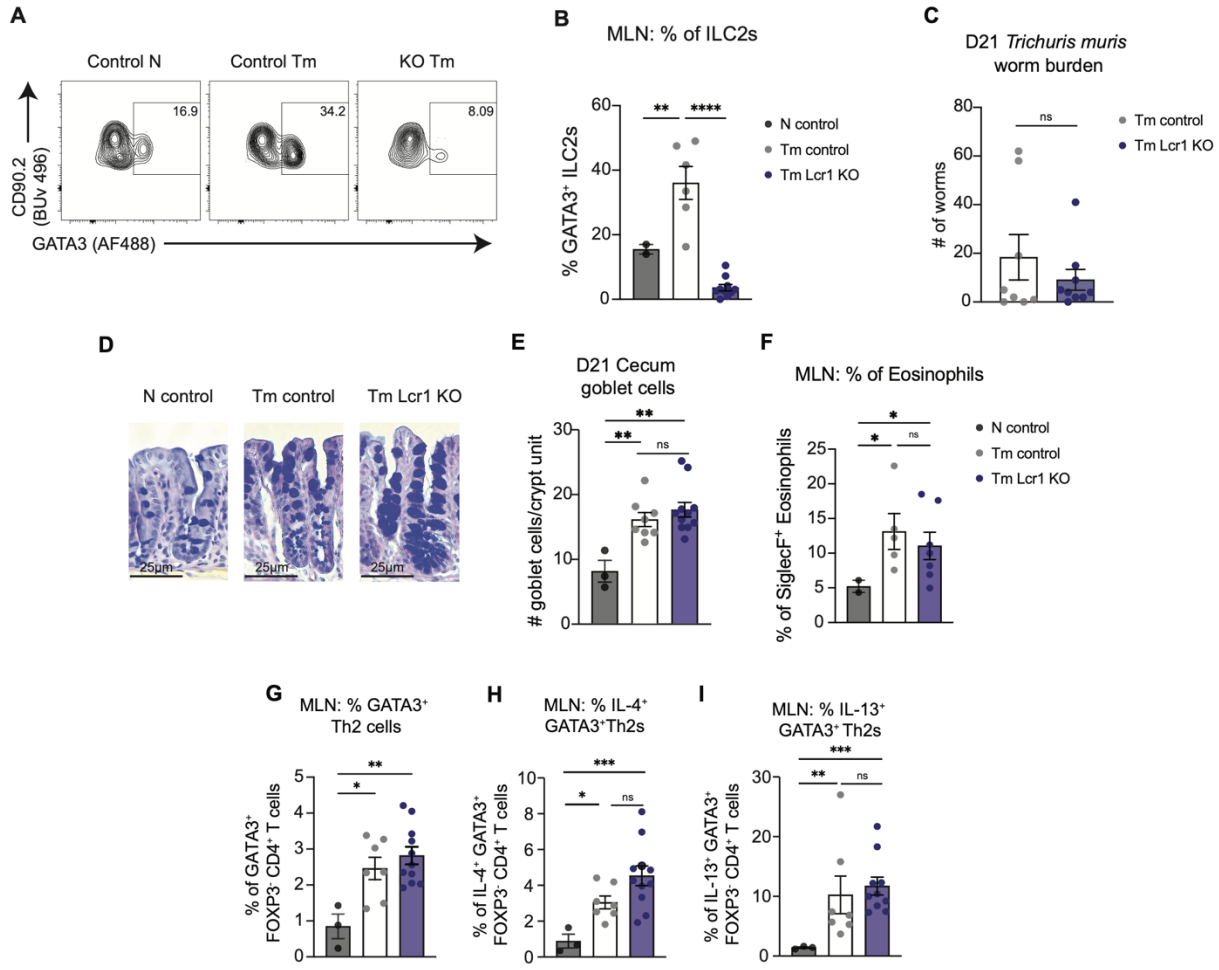

Supplementary Figure 2.1b (related to Figure 2.1) Characterization of the Type 2 immune response against *Trichuris muris* (*Tm*) in Lcr1 Knock out mice.

(A-I) Wild type or heterozygous control mice (control) and Lcr1 KO mice were infected with 300 eggs Tm and at D21 post-infection (p.i.) characterized for worm burden, goblet cell hyperplasia, mesenteric lymph node (MLN) eosinophilia, and MLN $CD4^+$ T cell responses. **(A)** Representative flow plots of MLN-$GATA3^+$ ILC2s and **(B)** respective quantification of the percentage of $GATA3^+$ ILC2s (gated as $CD45^+Lin^-CD3e^-CD11b^-CD127^+CD90.2^+$) in the MLN. **(C)** Worm counts from the cecum/proximal colon of Tm control or Tm Lcr1 KO mice at D21 p.i. **(D)** Representative PAS/Alcian blue staining of cecum goblet cells (dark purple)

(scale bar = 25μm) and **(E)** quantification of the number of goblet cells per cecum crypt unit. **(F)** Quantification of the percentage of eosinophils (gated as $CD45^{+}Lin^{-}CD3e^{-}CD11b^{+}SiglecF^{+}$) in the MLN at D21 p.i. Frequency of **(G)** $GATA3^{+}$ $FOXP3^{-}CD4^{+}$, **(H)** $IL\text{-}4^{+}GATA3^{+}FOXP3^{-}CD4^{+}$, and **(I)** $IL\text{-}13^{+}GATA3^{+}FOXP3^{-}CD4^{+}$T cells isolated from the MLN at D21 p.i**.** Mean ± SEM; *, $P < 0.05$; **, $P < 0.01$; ***, $P < 0.001$; ****, $P < 0.0001$. **(A-F)** Data were analyzed using linear mixed effects models, and post-hoc pairwise comparisons between groups were made using **(A, B, D-F)** Tukey's HSD-multiple-comparison test or **(C)** unpaired student's t-test. **(A-F)** Three independent experiments were pooled together (N control, n = 2-3; Tm control, n = 7-8; Tm Lcr1 KO, n = 7-9).

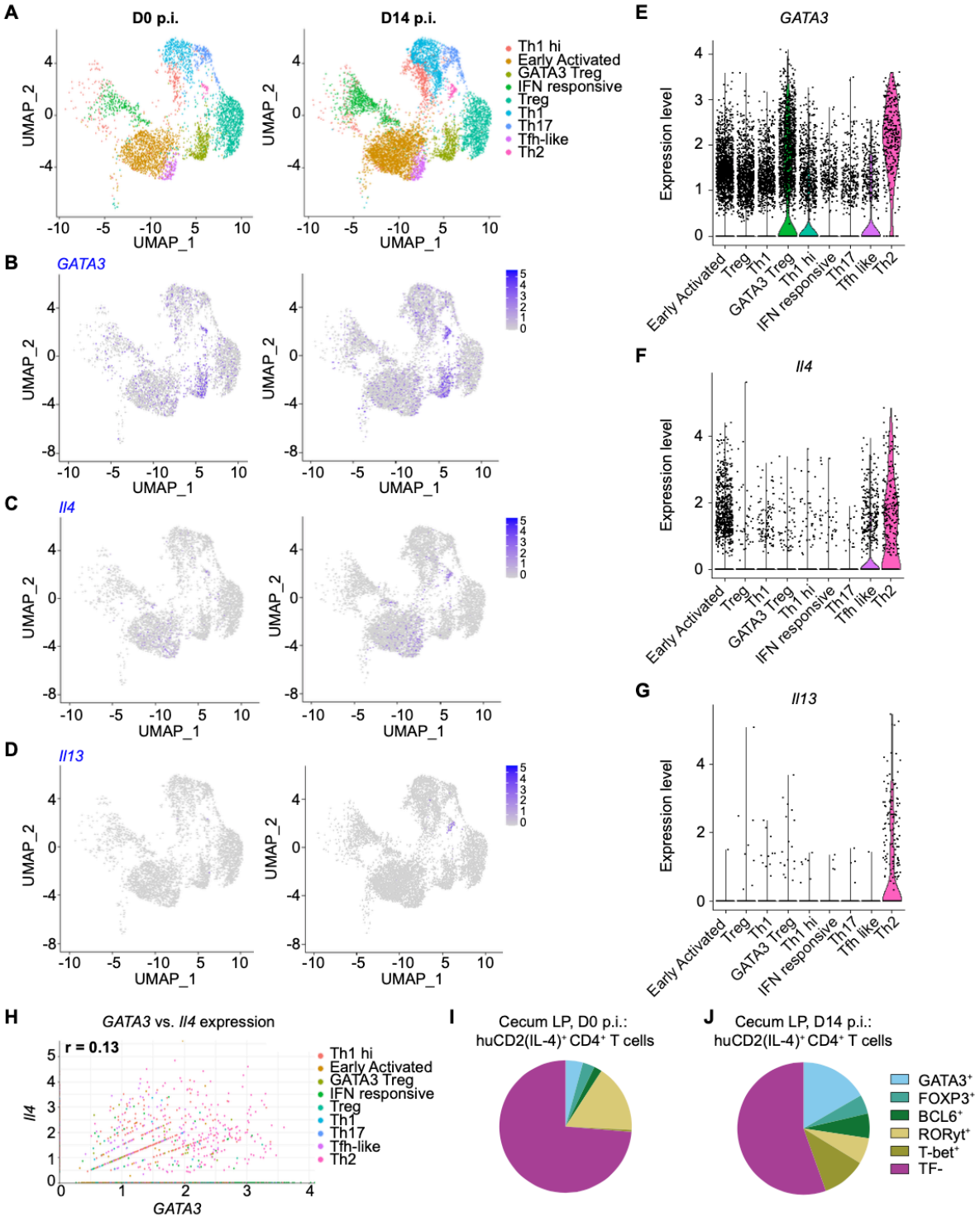

Figure 2.2. Heterogenous CD4$^+$ T cell subsets produce IL-4 during *T. muris* infection while IL-13 production is restricted to Th2 cells.

Singe-cell RNA sequencing of sort-purified $CD4^+$ T cells isolated from the cecum LP of naïve, D0 post-infection (p.i.) **(A-D, left column)** and D14 *T. muris* infected **(A-D, right column) (E-G represents both D0 and D14 pooled)** $McptCre^-$ DNMAML F/F mice. Uniform Manifold Approximation and Projection (UMAP) analysis of **(A)** cecum lamina propria (LP) $CD4^+$ T cell populations and the distribution of **(B)** *GATA3*, **(C)** *Il4*, and **(D)** *Il13* gene expression in naïve, D0 **(A-D, left column)** and D14 *T. muris* infected **(A-D, right column)** $McptCre^-$ DNMAML F/F mice. Violin plots of the combined distribution of gene expression levels for **(E)** *GATA3*, **(F)** *Il4*, and **(G)** *Il13* transcript in combined naïve, D0 and D14 *T. muris* infected $McptCre^-$ DNMAML F/F mice. **(H)** Scatter plot correlation between *GATA3* and *Il4* gene expression across cecum LP $CD4^+$ T cell populations (r = 0.13). Distribution of huCD2(IL-4)$^+$ T cells in $CD4^+$ T cell lineages in KN2 mice at **(I)** D0 and **(J)** D14 post-*T. muris* infection ($GATA3^+$ = blue; $FOXP3^+$ = teal; $BCL6^+$ = dark green; $RORyt^+$ = yellow; T-bet^+ = olive; TF^- = magenta). **(A-H)** Differentially expressed transcripts were identified using a non-parametric Wilcoxon rank sum test in Seurat and filtered for a false discovery rate of 10%, and **(H)** linear association between *GATA3* and *Il4* gene expression was determined by Pearson's Correlation Coefficient. **(I and J)** Data were analyzed using linear mixed effects models and post-hoc pairwise comparisons between groups were made using Tukey's HSD-multiple-comparison test**.** **(A-H)** one experiment (D0, n = 3; D14, n = 3). **(I and J)** 3 independent experiments were pooled together (D0, n = 9; D14, n = 12). N is total across all experiments.

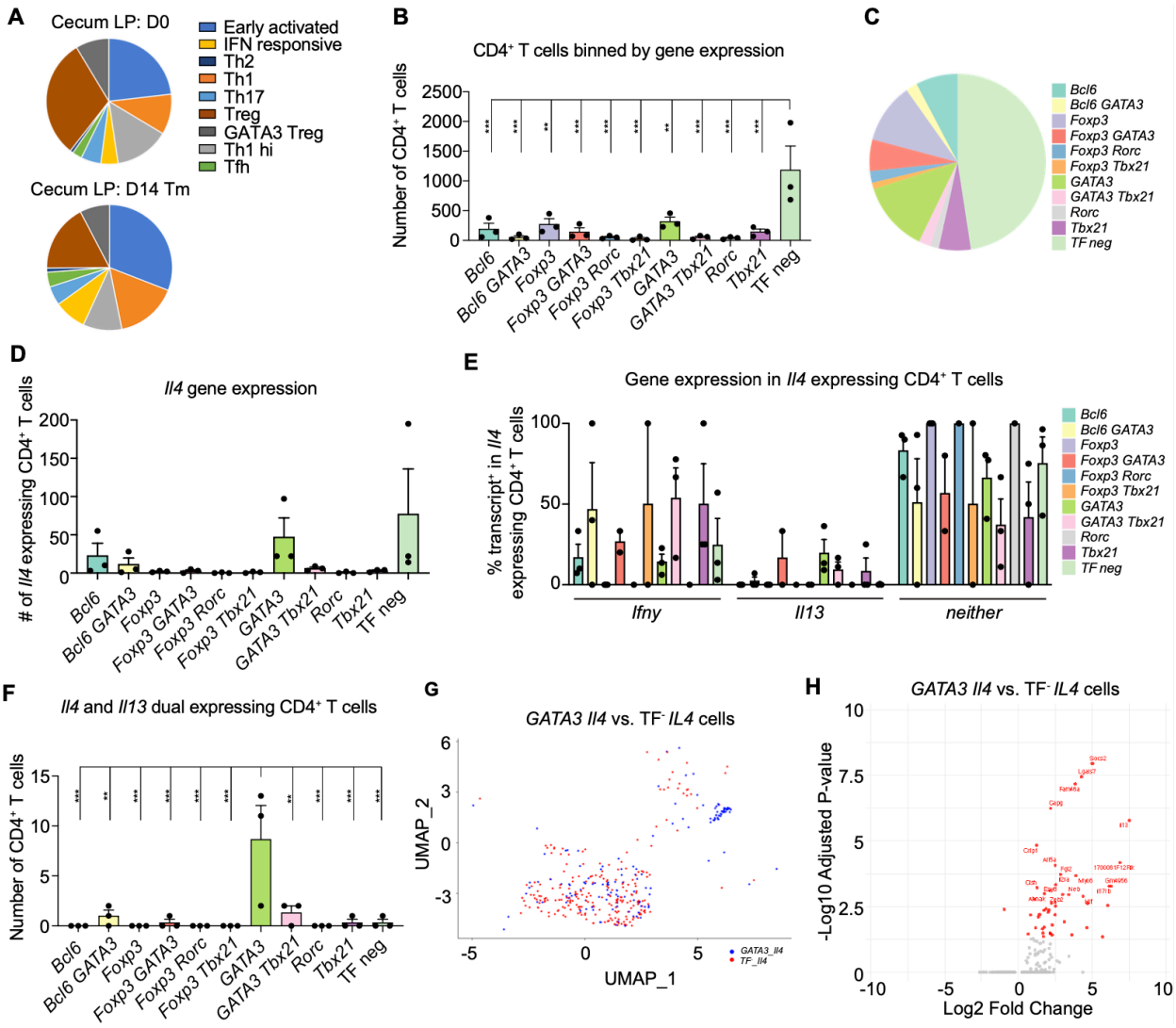

Supplementary Figure 2.2a (related to figure 2.2) Single-cell RNA sequencing analysis of intestinal CD4⁺ T cells at day 14 post-infection *Trichuris muris.*

Single-cell RNA sequencing of sort-purified CD4+ T cells isolated from the cecum lamina propria (LP) of D14 *T. muris* infected McptCre- DNMAML F/F mice. **(A)** Pie chart of the frequency of CD4+ T cell subsets defined by unbiased cluster of total cecum lamina propria (LP) CD4+ T cells from single-cell RNA sequencing at D0 (top) and D14 (bottom) post-infection with *T. muris*. **(B)** Number of cells per bin, where cells were assigned bins based on detection of *GATA3, Foxp3, Rorc, Bcl6*, and/or *Tbx21,* or defined as Transcription factor

"negative" (TF-). Bins with greater than 75 cells were included for subsequent analysis. **(C)** Pie chart of data in **(B)**. **(D)** Number of *Il4* expressors across all binned CD4+ T cell subsets. **(E)** Percentage of gene expression in *Ifny*, *Il13,* or neither of total *Il4* expressing CD4+ T cells. **(F)** Number of *Il4* and *Il13* expressing CD4+ T cells among total CD4+ T cells by binned subsets. **(G)** Uniform Manifold Approximation and Projection (UMAP) analysis of cecum LP CD4+ T cell populations and the distribution of *GATA3 Il4* cells by TF- *Il4* cells. **(H)** Volcano plot of differential gene expression comparing *GATA3 Il4* expressing cells by TF- *Il4* expressing CD4+ T cells (GATA3 excluded) (not significant = gray; significant = red). **(B, D-F)** Mean ± SEM; *, $P < 0.05$; **, $P < 0.01$; ***, $P < 0.001$. **(A-H)** Differentially expressed transcripts were identified using a non-parametric Wilcoxon rank sum test in Seurat and filtered for a false discovery rate of 10%. Data were analyzed using linear mixed effects models and post-hoc pairwise comparisons between groups were made using **(B, D-F)** one way ANOVA. Mean ± SEM; $P < 0.05$. Three independent experiments were pooled together (n = 3; n is total across all experiments).

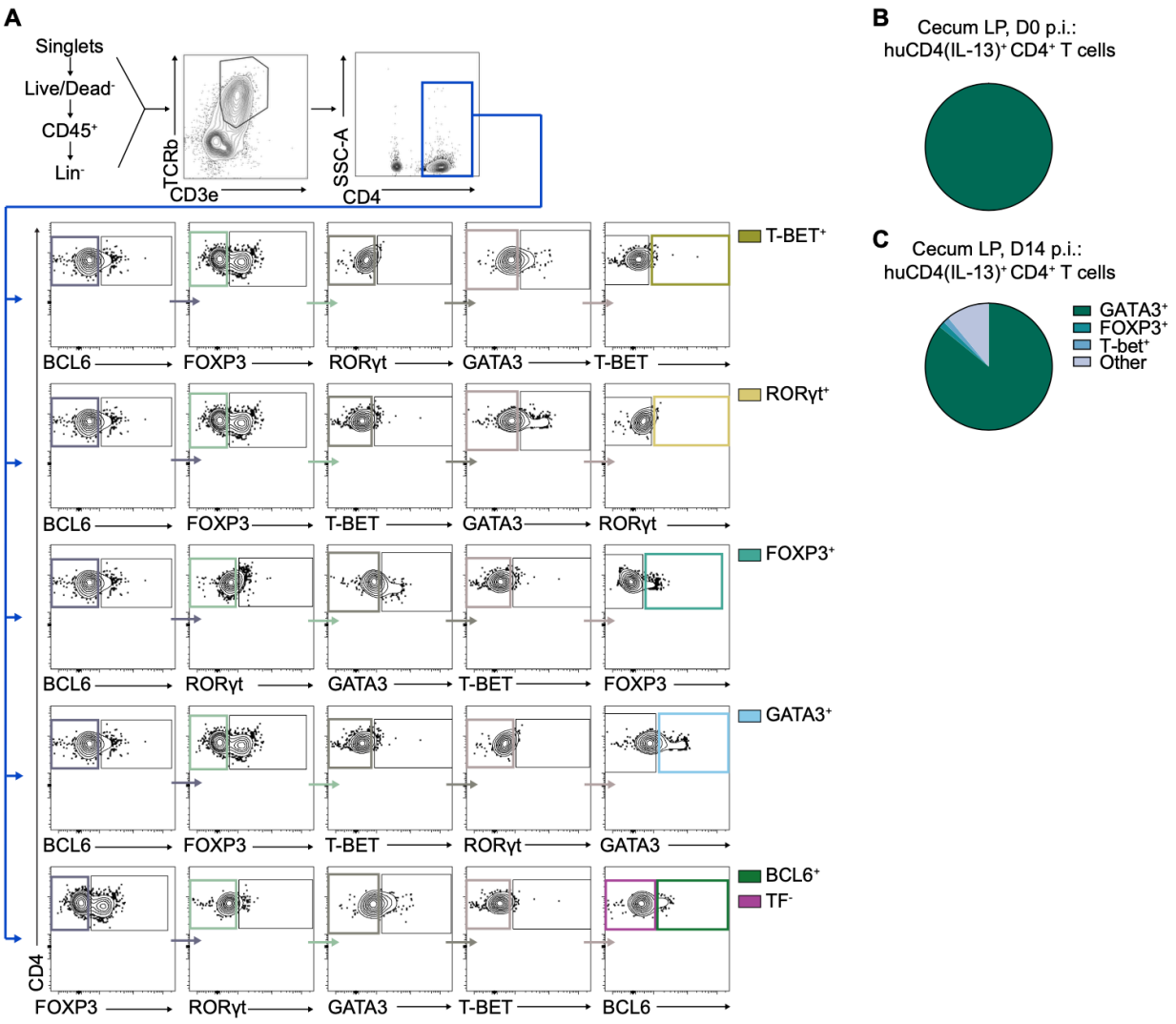

Supplementary Figure 2.2b (related to figure 2.2) Characterization of intestinal CD4$^+$ T cells subsets and cytokine production in naive and *T. muris*-infected mice.

(A) Gating strategy for CD4+ T cell subsets single-positive for lineage-defining transcription factors isolated from the cecum LP of KN2 mice at D14 p.i.. Fluorophores used in representative flow plots: GATA3 (AF488), FOXP3 (AF700), TBET (BV421), RORγt (PE-Cy7), BCL6 (CF594), CD4 (BV711), huCD2 (APC), CD3e (BV650), TCRb (APC-Cy7), CD45 (BUV805). **(B and C)** Pie chart of huCD4(IL-13)+ CD4+ T cell subsets in the cecum LP in SMART13 mice at **(B)** D0 and **(C)** D14 post-*T. muris* infection (flow staining panel was limited

to GATA3, FOXP3, and T-BET for SMART13 transcription factor characterization). **(C and D)** Data were analyzed using linear mixed effects models and post-hoc pairwise comparisons between groups were made using Tukey's HSD-multiple-comparison test. Three independent experiments were pooled together (n = 6-7 total across all experiments).

Tukey's HSD multiple comparison	p-Value
D0 TF^- vs. D0 $Tbet^+$	**<.0001**
D0 TF^- vs. D0 $Bcl6^+$	**0.0004**
D0 TF^- vs. D0 $Foxp3^+$	**0.0008**
D0 TF^- vs. D0 $GATA3^+$	**0.0015**
D0 TF^- vs. D0 $RORyt^+$	0.1406
D14 TF^- vs. D14 $Tbet^+$	0.0984
D14 TF^- vs. D14 $Bcl6^+$	0.0946
D14 TF^- vs. D14 $Foxp3^+$	**0.0174**
D14 TF^- vs. D14 $GATA3^+$	0.8348
D14 TF^- vs. D14 $RORyt^+$	0.1723
D0 TF^- vs. D14 TF^-	1.0000
D0 $Bcl6^+$ vs. D14 $Bcl6^+$	0.6612
D0 $GATA3^+$ vs. D14 $GATA3^+$	0.1569

Table 2.1 Table 1. Statistical comparisons between Cecum LP $CD4^+$ T cell subsets

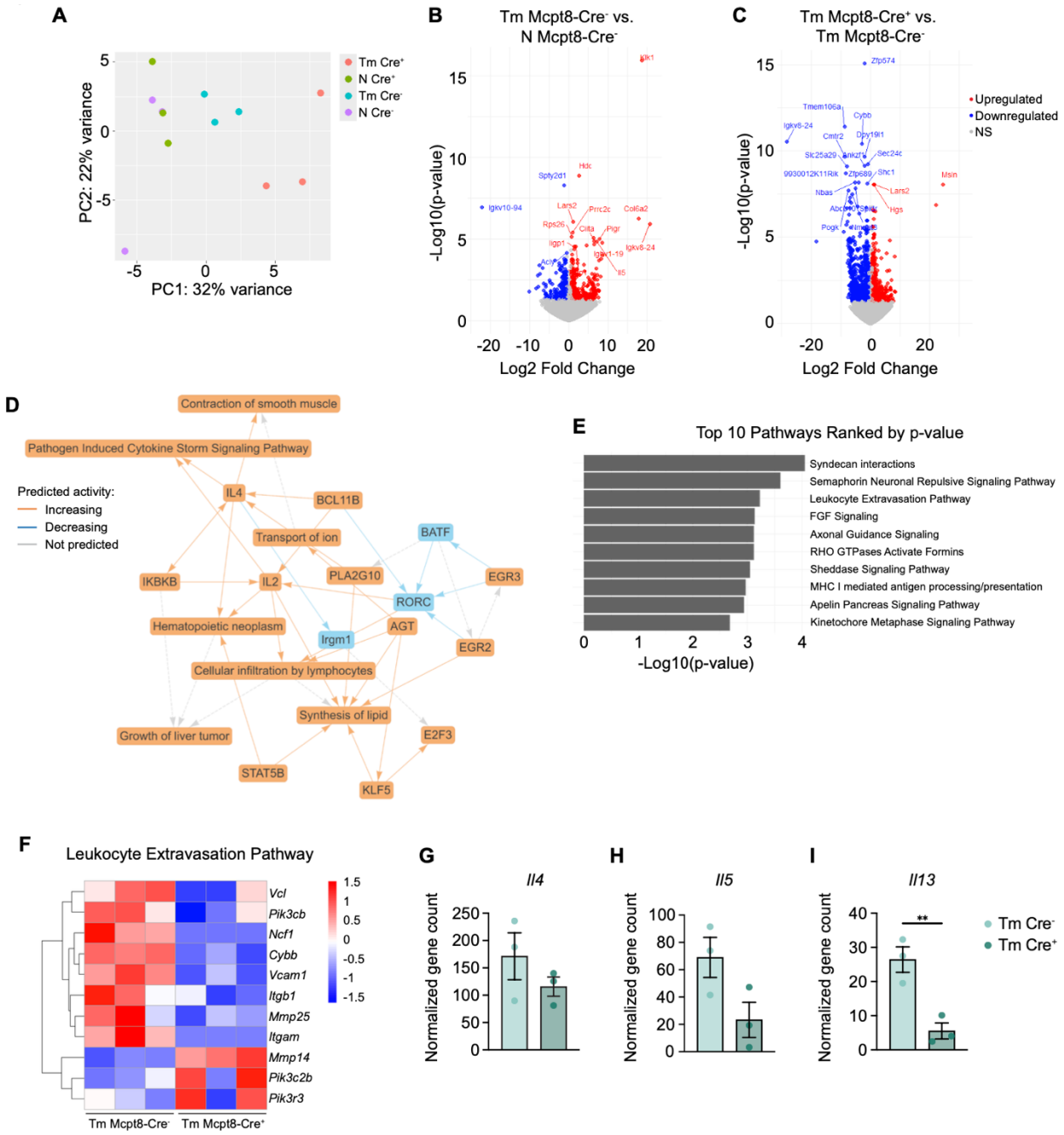

Figure 2.3. Basophil-intrinsic Notch signaling shapes cecum CD4$^+$ T cell transcriptomes during *T. muris* infection.

Bulk RNA sequencing of intestinal CD4$^+$ T cells sort-purified from the cecum lamina propria (LP) of naïve or D14 p.i. Mcpt8Cre$^-$ DNMAML F/F and Mcpt8Cre$^+$ DNMAML F/F

mice. **(A)** Principal component analysis (PCA) of differentially expressed genes in cecum-derived $CD4^+$ cells from naïve (N) Mcpt8Cre^- DNMAML F/F (N Cre^-; purple), N Mcpt8Cre^+ DNMAML F/F (N Cre^+; green), D14 *T. muris* (Tm)-infected Mcpt8Cre^- DNMAML F/F (Tm Cre^-; blue), and D14 Tm-infected Mcpt8Cre^- DNMAML F/F (Tm Cre^+; coral). **(B and C)** Volcano plots highlighting differentially expressed genes in $CD4^+$ T cells from **(B)** Tm Cre^- versus N Cre^- and **(C)** Tm Cre^- versus Tm Cre^+, with -log10(P value) >~1.5 shown in red (significantly upregulated), blue (significantly downregulated), or gray (not significant (NS)). **(D)** Ingenuity pathway analysis (IPA) curated summary of genes and biological functions significantly upregulated (orange) or downregulated (blue) in $CD4^+$ T cells from Tm Cre^- versus N Cre^- mice. **(E)** Top 10 canonical pathways significantly upregulated in cecum LP $CD4^+$ T cells from Tm Cre^- versus Tm Cre^+ mice. **(F)** Heat map showing differential expression of transcripts associated with leukocyte extravasation in cecum LP $CD4^+$ T cells isolated from infected Mcpt8-Cre^- and Mcpt8-Cre^+ mice. **(G, H, and I)** Normalized gene counts of **(G)** *Il4*, **(H)** *Il5*, and **(I)** *Il13* in Mcpt8-Cre^- (aqua) and Mcpt8-Cre^+ (dark green) at D14 p.i.. **(A-I)** Three independent experiments pooled together (N Cre^-, n = 3; N Cre^+, n = 3; Tm Cre^- = 3; Tm Cre^+, n = 3).

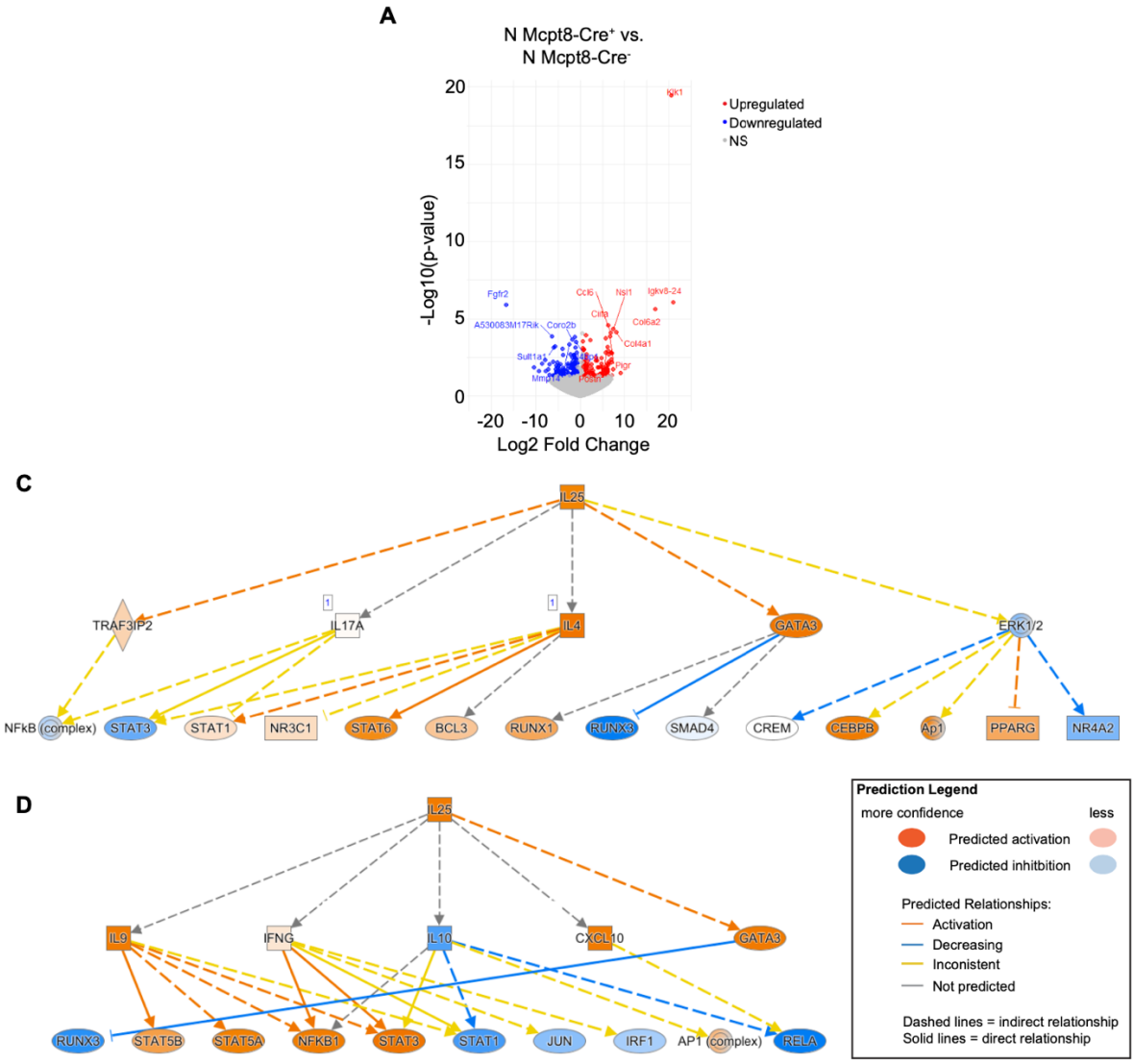

Supplementary Figure 2.3 (related to Figure 2.3) Differential gene expression and Ingenuity pathway analysis (IPA).

Bulk RNA sequencing of intestinal CD4$^+$ T cells sort-purified from the cecum lamina propria of naïve or D14 p.i. Mcpt8Cre- DNMAML F/F and Mcpt8Cre$^+$ DNMAML F/F mice. **(A)** Volcano plot highlighting differentially expression genes in CD4$^+$ T cells from Naive (N) Cre$^-$ versus N Cre$^+$. Differentially expressed genes with −log10(q value) > ~1.5 shown in red (upregulated) or blue (downregulated) with gene names labeled when –log10(q value) > ~8. **(C and D)** Ingenuity Pathway Analysis (IPA) of the IL-25 signaling network depicting genes

downstream of IL-25 in **(C)** Tm Cre^{-} mice and **(D)** Tm Cre^{+} mice. Predicted upstream regulators are shown as activating (orange) or inhibiting (blue) of target genes. **(A-C)** Three independent experiments pooled together (N Cre-, n = 3; N Cre^{+}, n = 3; Tm Cre- = 3; Tm Cre^{+}, n = 3).

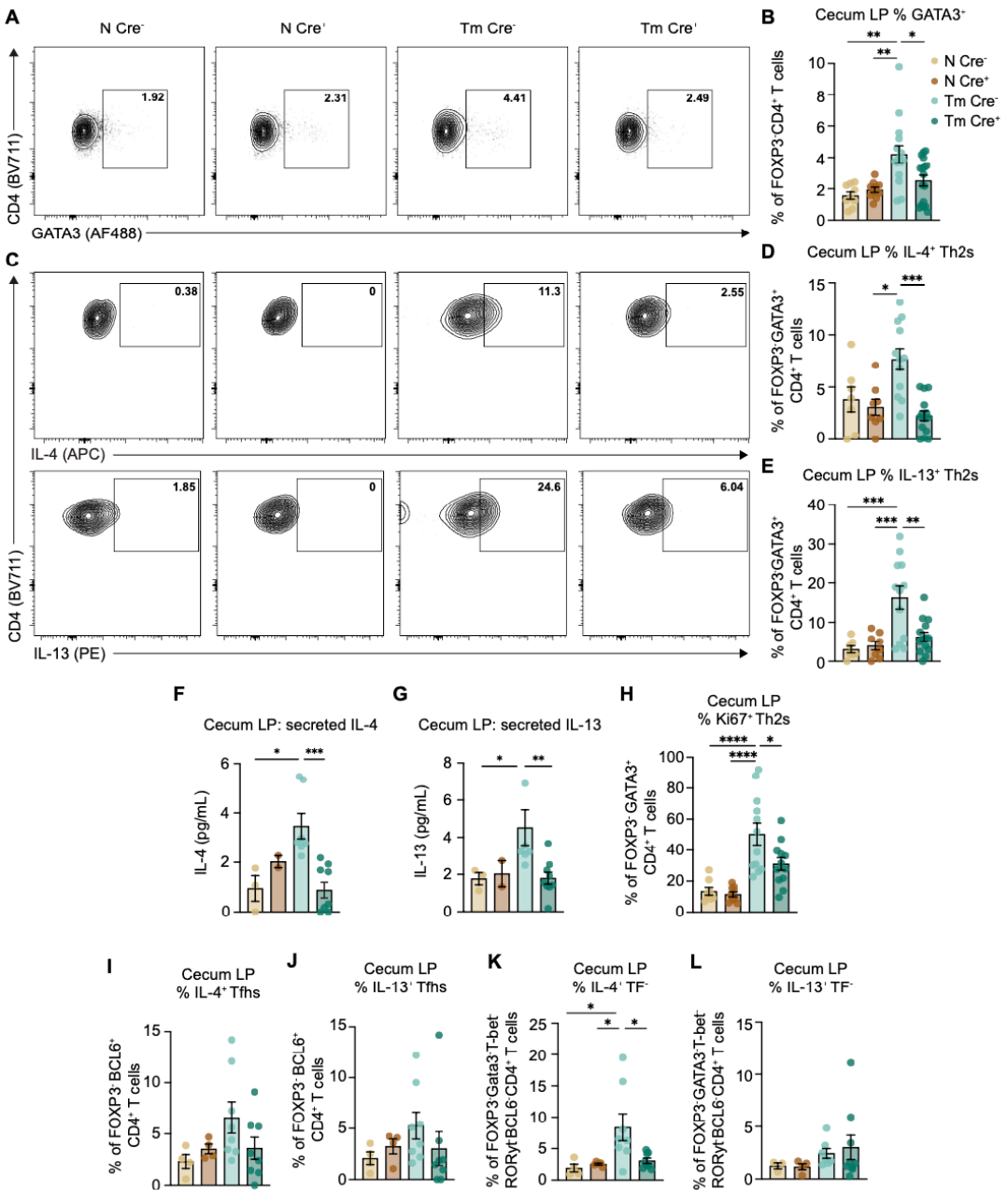

Figure 2.4. Intestinal CD4$^+$ T cell production of IL-4 and IL-13 is curtailed in mice lacking Notch-programmed basophils.

(A-E, H-L) Flow cytometric analysis of CD4$^+$ T cells isolated from the cecum lamina propria (LP) of naïve (N) Mcpt8Cre$^-$ DNMAML F/F (N Cre$^-$; yellow), N Mcpt8Cre$^+$ DNMAML F/F (N Cre$^+$; sienna), D14 *T. muris* (Tm)-infected Mcpt8Cre$^-$ DNMAML F/F (Tm Cre$^-$; aqua),

and D14 Tm-infected Mcpt8Cre$^-$ DNMAML F/F (Tm Cre$^+$; dark green). **(F and G)** Cytometric bead array measuring IL-4 and IL-13 concentrations from the supernatant of CD4$^+$ T cells harvested form the cecum LP of naïve (N) Mcpt8Cre$^-$ DNMAML F/F (N Cre$^-$; yellow), N Mcpt8Cre$^+$ DNMAML F/F (N Cre$^+$; sienna), D14 *T. muris* (Tm)-infected Mcpt8Cre$^-$ DNMAML F/F (Tm Cre$^-$; aqua), and D14 Tm-infected Mcpt8Cre$^-$ DNMAML F/F (Tm Cre$^+$; dark green) and stimulated by anti-CD3e (1 ug/mL) and antiCD28 (1 ug/mL) *in vitro* for 48 hrs. **(A)** Representative flow plots and quantification of % **(B)** GATA3$^+$ of total FOXP3$^-$CD4$^+$ T cells. **(C)** Representative flow plots and quantification of % **(D)** IL-4$^+$ and **(E)** IL-13$^+$ of total GATA3$^+$FOXP3$^-$CD4$^+$ cells. **(F)** IL-4 protein and **(G)** IL-13 protein concentrations in the supernatant of *ex vivo* stimulated CD4$^+$ T cells sort-purified from the cecum LP, measured by enhanced sensitivity cytometric bead array. **(H)** Quantification of % Ki67$^+$ of total GATA3$^+$FOXP3$^-$CD4$^+$ cells. Quantification of % **(I)** IL-4$^+$ and **(J)** IL-13$^+$ cells of total FOXP3$^-$ Bcl6$^+$CD4$^+$ T cells. Quantification of % **(K)** IL-4$^+$ and **(L)** IL-13$^+$ of total FOXP3$^-$GATA3$^-$T-bet$^-$ RORγt$^-$BCL6$^-$CD4$^+$ factor negative (TF$^-$) cells. Mean ± SEM; *, $P < 0.05$; **, $P < 0.01$; ***, $P < 0.001$; ****, $P < 0.0001$. **(A-L)** Data were analyzed using linear mixed effects model and post-hoc pairwise comparisons using Tukey's HSD-multiple-comparison test. **(A-E, H)** 5 independent experiments pooled together (N Cre$^-$, n = 7-8; N Cre$^+$, n = 8; Tm Cre-, n = 12; Tm Cre$^+$, n = 12-14). **(I-L)** 3 independent experiments pooled together (N Cre$^-$, n = 4; N Cre$^+$, n = 4; Tm Cre-, n = 8; Tm Cre$^+$, n = 8). N is total across all experiments. (F and G) Three independent experiments pooled together (N Cre$^-$, n = 3; N Cre$^+$, n = 2; Tm Cre-, n = 6-7; Tm Cre$^+$, n = 8-9).

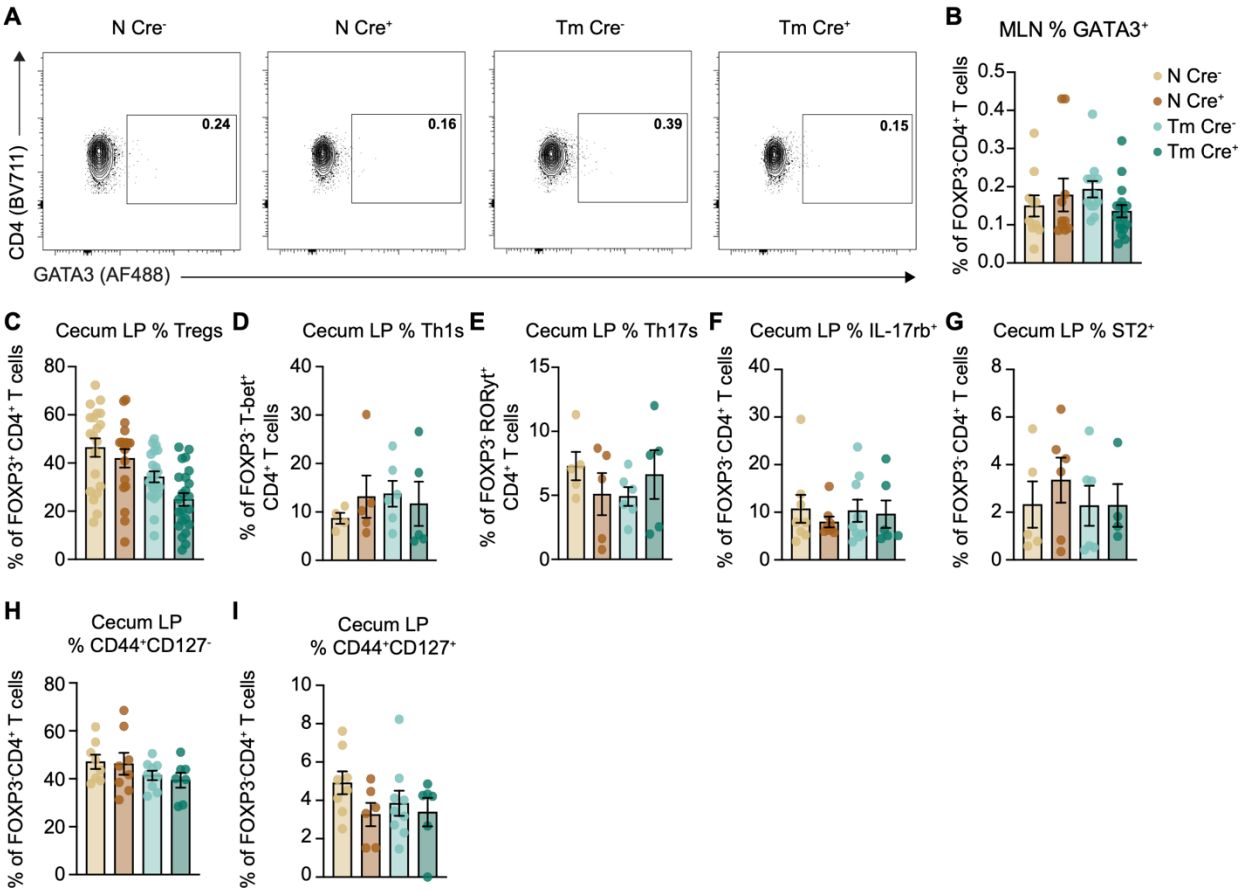

Supplementary Figure 2.4a (related to figure 2.4). Phenotypic characterization of CD4$^+$ T cells from the MLN and cecum LP of *T. muris*-infected Mcpt8-Cre$^-$ or Cre$^+$ DNMAML F/F animals.

(A) Representative flow plots and **(B)** quantification of % GATA3$^+$ of FOXP3$^-$CD4$^+$ T cells isolated from the mesenteric lymph node (MLN) of naive (N) Mcpt8-Cre$^-$ DNMAML F/F (N Cre-; yellow), N Mcpt8-Cre$^+$ DNMAML F/F (N Cre$^+$; sienna), D14 *T. muris* (Tm)-infected Mcpt8-Cre$^-$ DNMAML F/F (Tm Cre$^-$; aqua), and D14 Tm-infected Mcpt8-Cre$^-$ DNMAML F/F (Tm Cre$^+$; dark green) mice. Quantification of % of **(C)** FOXP3$^+$ Tregs, **(D)** T-bet$^+$ Th1 cells, **(E)** RORγt$^+$ Th17 cells, **(F)** IL-17RB$^+$ cells, **(G)** ST2$^+$ cells, **(H)** CD44$^+$CD127$^-$ activated cells, and **(I)** CD44$^+$CD127$^+$ memory cells, of total FOXP3$^-$CD4$^+$ T cells isolated from the cecum lamina propria (LP) from the same groups described in **(A)**. **(B-I)** Data were analyzed using linear

mixed effects models and post-hoc pairwise comparisons between groups were made using Tukey's HSD-multiple-comparison test. Mean ± SEM. Three-5 independent experiments were pooled together (N Cre-, n = 8-15; N Cre^{+}, n = 8-13; Tm Cre-, n = 6-17; Tm Cre^{+}, n = 6-22; n is total across all experiments).

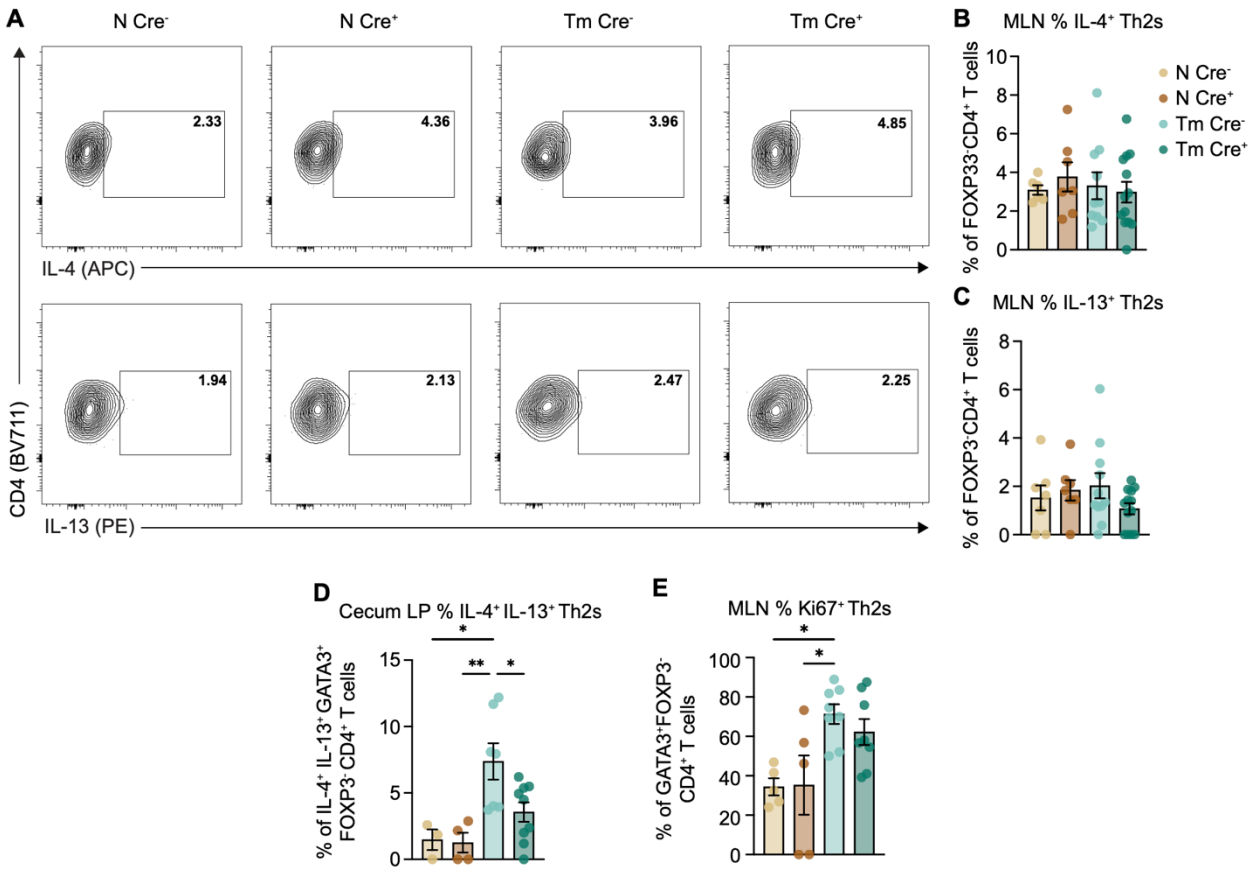

Supplementary Figure 2.4b (related to figure 2.4). Cytokine production and cellular proliferation in MLN-derived CD4$^+$ T cells in Mcpt8-Cre$^-$ or Cre$^+$ DNMAML F/F mice during *T. muris* infection.

(A) Representative flow plots and quantification of % **(B)** IL-4$^+$ and **(C)** IL-13$^+$ of GATA3$^+$FOXP3$^-$CD4$^+$ T cells isolated from the mesenteric lymph node (MLN) of naïve (N) Mcpt8-Cre- DNMAML F/F (N Cre$^-$; yellow), N Mcpt8-Cre$^+$ DNMAML F/F (N Cre$^+$; sienna), D14 *T. muris* (Tm)-infected Mcpt8-Cre$^-$ DNMAML F/F (Tm Cre$^-$; aqua), and D14 Tm-infected Mcpt8-Cre$^-$ DNMAML F/F (Tm Cre$^+$; dark green) mice. **(D)** Quantification of % IL-4$^+$ IL-13$^+$ double positive Th2 cells of GATA3$^+$FOXP3$^-$CD4$^+$ T cells in the cecum LP from the same groups described in **(A). (E)** Quantification of % Ki67$^+$ of GATA3$^+$FOXP3$^-$CD4$^+$ T cells in the MLN from the same groups described in **(A)**. **(B-E)** Data were analyzed using linear mixed

effects models and post-hoc pairwise comparisons between groups were made using Tukey's HSD-multiple-comparison test. Mean ± SEM; $P < 0.05$. Three independent experiments were pooled together (N Cre^-, n = 3-7; N Cre^+, n = 4-7; Tm Cre^-, n = 7-11; Tm Cre^+, n = 8-13; n is total across all experiments).

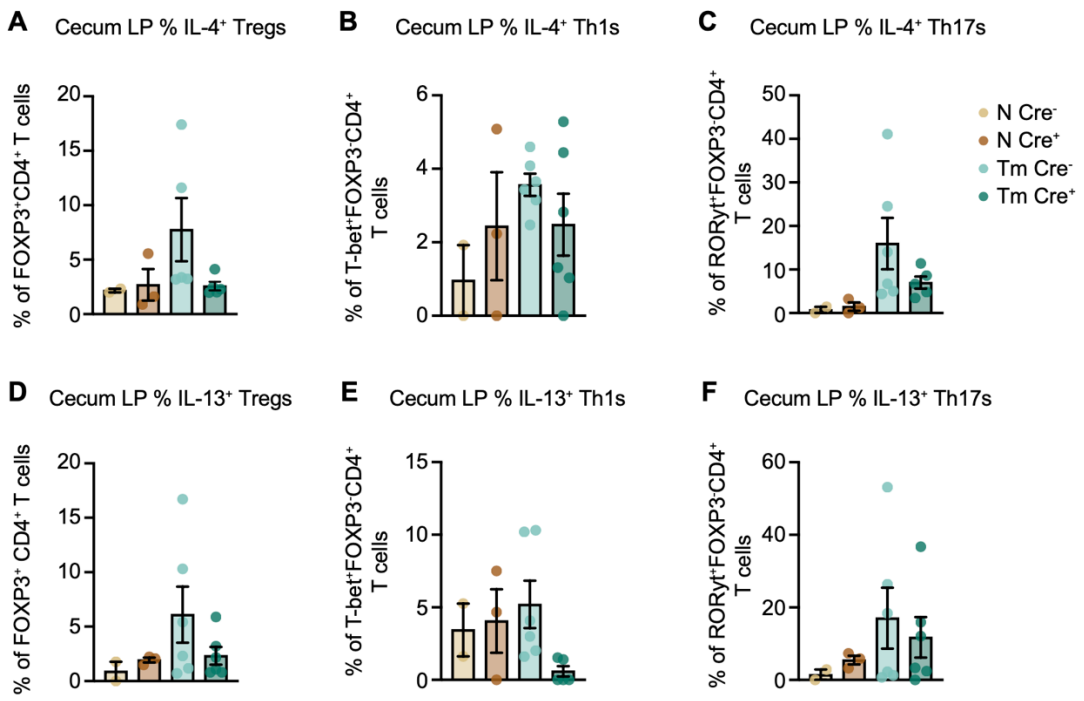

Supplementary Figure 2.4c (related to figure 2.4) IL-4 and IL-13 production by Treg, Th1, and Th17 cells in the cecum lamina propria of Mcpt8-Cre- or Cre$^+$ DNMAML mice during *T. muris* infection.

Quantification of % **(A)** IL-4$^+$ of Tregs, **(B)** IL-4$^+$ of Th1s, **(C)** IL-4$^+$ of Th17s, **(D)** IL-13$^+$ of Tregs, **(E)** IL-13$^+$ of Th1s, and **(F)** IL-13$^+$ of Th17s, of CD4$^+$ T cells gated as indicated, isolated from the cecum lamina propria (LP) of naïve (N) Mcpt8-Cre- DNMAML F/F (N Cre-; yellow), N Mcpt8-Cre$^+$ DNMAML F/F (N Cre$^+$; sienna), D14 *T. muris* (Tm)-infected Mcpt8-Cre- DNMAML F/F (Tm Cre-; aqua), and D14 Tm-infected Mcpt8-Cre- DNMAML F/F (Tm Cre$^+$; dark green) mice. **(A-F)** Data were analyzed using linear mixed effects models and post-hoc pairwise comparisons between groups were made using Tukey's HSD-multiple-comparison test. **(A-F)** Two independent experiments were pooled together (N Cre-, n = 2; N Cre$^+$, n = 3; Tm Cre-, n = 6; Tm Cre$^+$, n = 5-6; n is total across all experiments).

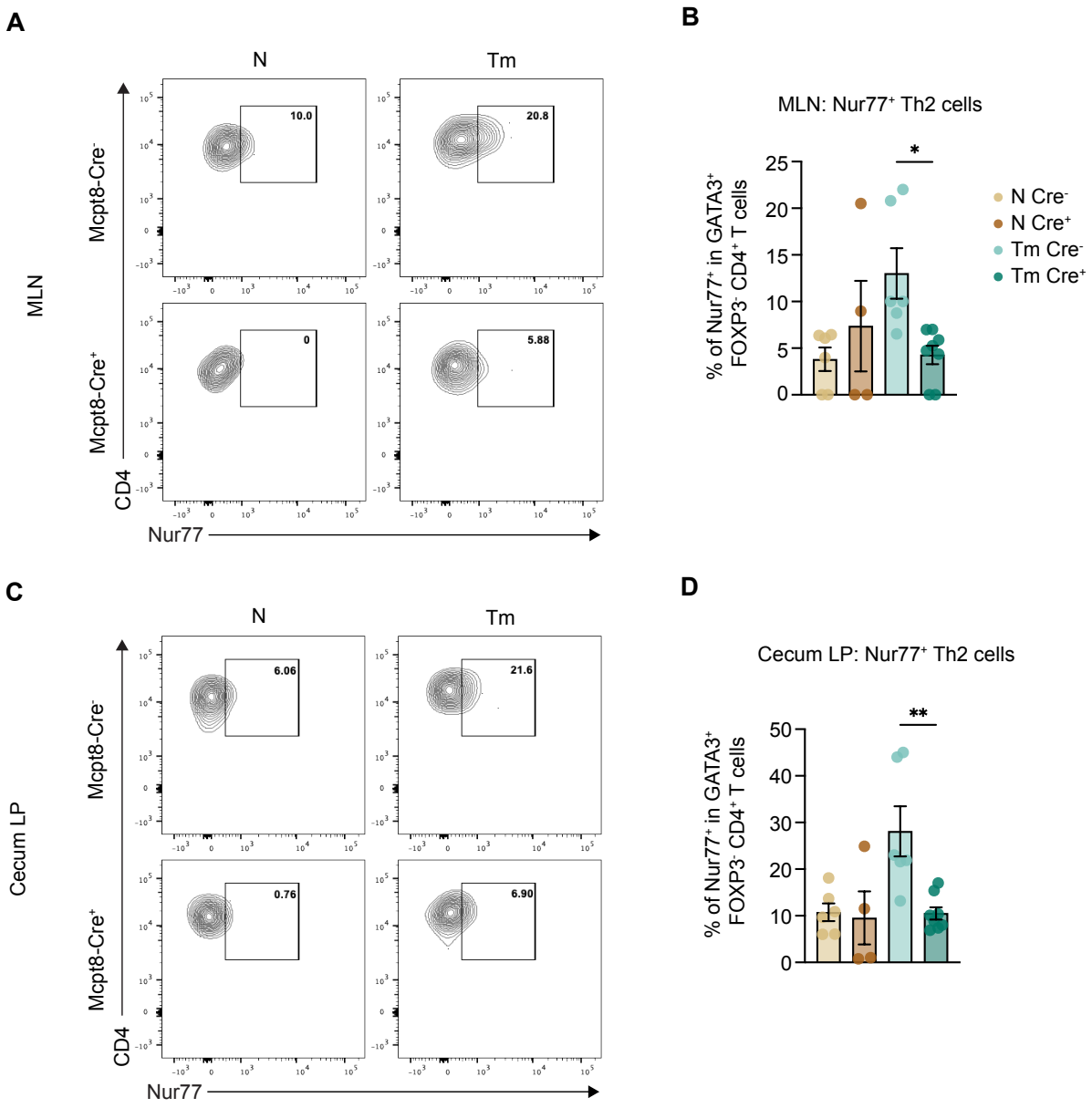

Supplementary Figure 2.4d (related to Figure 2.4) Nur77 expression is reduced in intestinal Th2 cells in mice lacking Notch-activated basophils.

(A-D) Flow cytometric analysis of CD4$^+$ T cells isolated from **(A and B)** the mesenteric lymph node or **(C and D)** the cecum lamina propria (LP) of naïve (N) McptCre$^-$ DNMAML F/F (N Cre$^-$; yellow), N McptCre$^+$ DNMAML F/F (N Cre$^+$; sienna), D14 *T. muris* (Tm)-infected McptCre$^-$ DNMAML F/F (Tm Cre$^-$; aqua), and D14 Tm-infected McptCre$^-$ DNMAML F/F (Tm Cre$^+$; dark

green**). (A)** Representative flow plots and quantification of % **(B)** $Nur77^{+}GATA3^{+}$ of total $FOXP3^{-}CD4^{+}$ T cells isolated from the MLN. (**C)** Representative flow plots and quantification of % **(D)** $Nur77^{+}GATA3^{+}FOXP3^{-}CD4^{+}$ cells isolated from the cecum LP. Mean ± SEM; *, $P < 0.05$; **, $P < 0.01$. **(A-D)** Data were analyzed using linear mixed effects model and post-hoc pairwise comparisons using Tukey's HSD-multiple-comparison test. **(A-D)** Three independent experiments pooled together (N Cre^{-}, n = 6; N Cre^{+}, n = 4; Tm Cre-, n = 12; Tm Cre^{+}, n = 12-14). **(G-J)** 3 independent experiments pooled together (N Cre^{-}, n = 4; N Cre^{+}, n = 4; Tm Cre-, n = 6; Tm Cre^{+}, n = 8). N is total across all experiments.

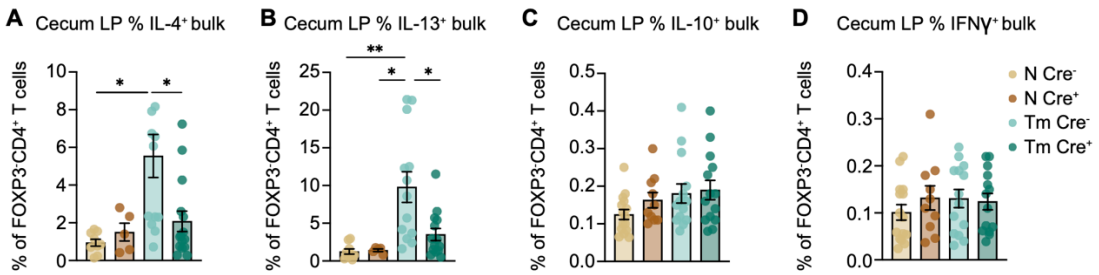

Supplementary Figure 2.4e (related to Figure 2.4) Cytokine production by cecum LP bulk CD4$^+$ T cells in Mcpt8-Cre$^-$ or Cre$^+$ DNMAML F/F mice during *T. muris* infection.

Quantification of % **(A)** IL-4$^+$, **(B)** IL-13$^+$, **(C)** IL-10$^+$, and **(D)** IFNγ$^+$ of bulk FOXP3-CD4$^+$ T cells isolated from the cecum lamina propria (LP) of naïve (N) Mcpt8-Cre- DNMAML F/F (N Cre$^-$; yellow), N Mcpt8-Cre$^+$ DNMAML F/F (N Cre$^+$; sienna), D14 *T. muris* (Tm)-infected Mcpt8-Cre$^-$ DNMAML F/F (Tm Cre$^-$; aqua), and D14 Tm-infected Mcpt8-Cre$^-$ DNMAML F/F (Tm Cre$^+$; dark green) mice. **(A-D)** Data were analyzed using linear mixed effects models and post-hoc pairwise comparisons between groups were made using Tukey's HSD-multiple-comparison test. Mean ± SEM; *, $P < 0.05$; **, $P < 0.01$. Four-5 independent experiments were pooled together (N Cre$^-$, n = 9-15; N Cre$^+$, n = 5-13; Tm Cre$^-$, n = 10-14; Tm Cre$^+$, n = 12-14; n is total across all experiments).

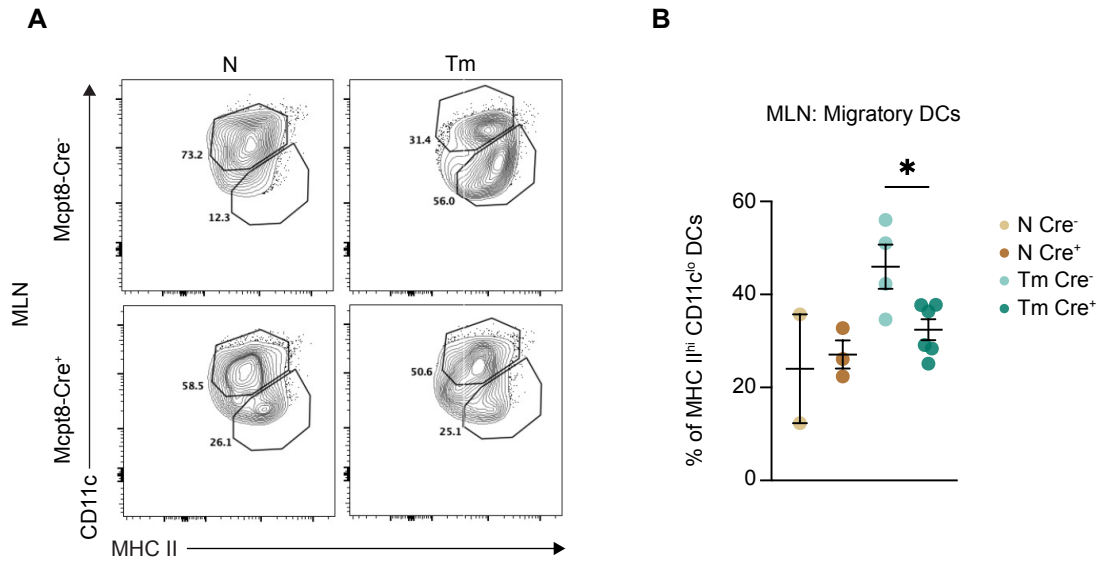

Figure 2.5 Notch-activated basophils are required for the accumulation of migratory dendritic cells in the mesenteric lymph node.

(A and B) Flow cytometric analysis of CD19$^-$B220$^-$CD3e$^-$NK1.1$^-$Ly6G$^-$CD64$^-$ dendritic cells (DCs) isolated from the mesenteric lymph node (MLN) of naïve (N) Mcpt8Cre$^-$ DNMAML F/F (N Cre$^-$; yellow), N Mcpt8Cre$^+$ DNMAML F/F (N Cre$^+$; sienna), D14 *T. muris* (Tm)-infected Mcpt8Cre$^-$ DNMAML F/F (Tm Cre$^-$; aqua), and D14 Tm-infected Mcpt8Cre$^-$ DNMAML F/F (Tm Cre$^+$; dark green**). (A)** Representative flow plots and quantification of % **(B)** MHCII^{hi}CD11c^{lo} DCs isolated from the MLN. Mean ± SEM; *. **(A and B)** Data were analyzed using linear mixed effects model and post-hoc pairwise comparisons using Tukey's HSD-multiple-comparison test. **(A and B)** Two independent experiments pooled together (N Cre$^-$, n = 2; N Cre$^+$, n = 3; Tm Cre-, n = 4; Tm Cre$^+$, n = 6). N is total across all experiments.

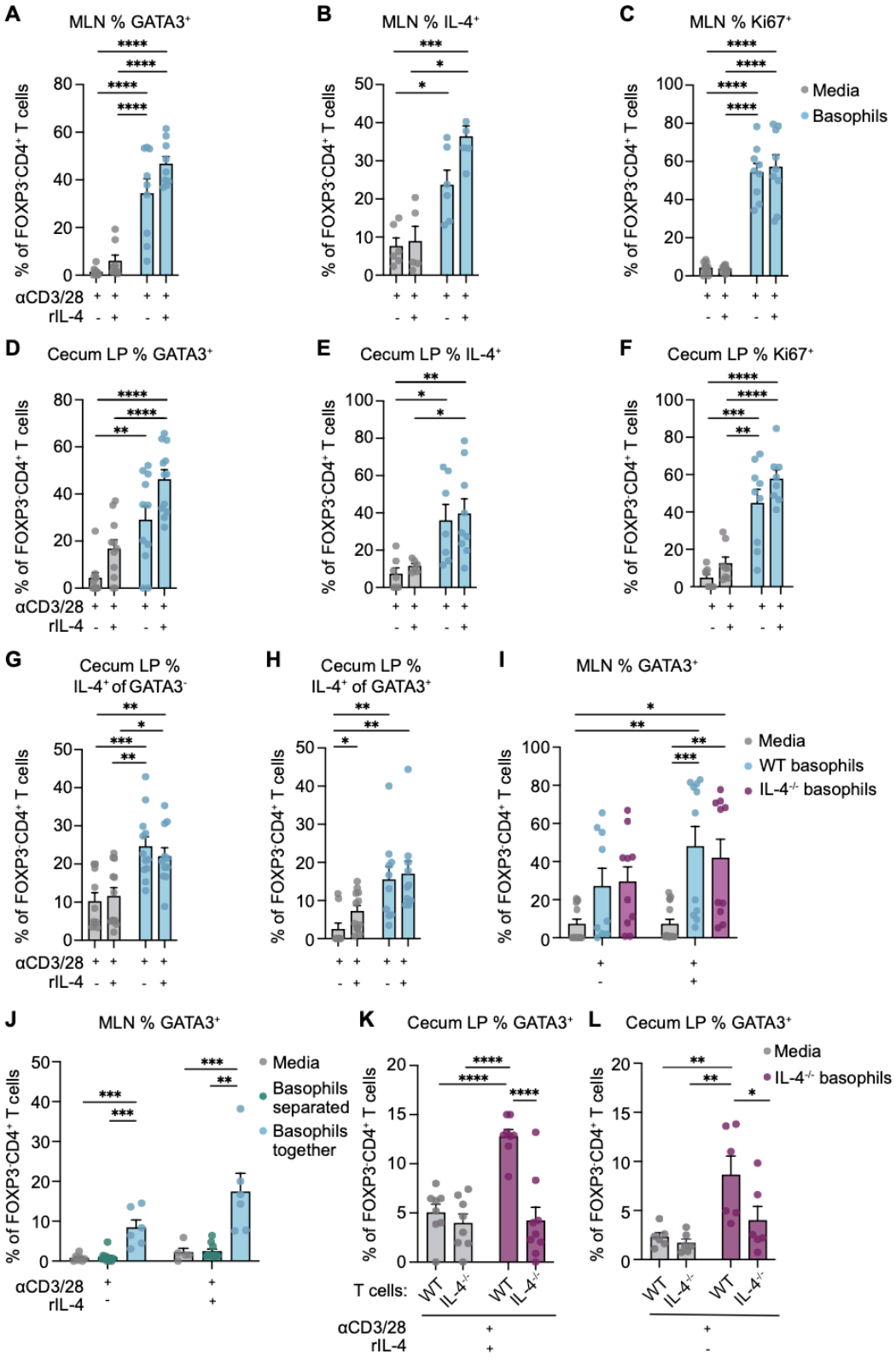
A
MLN % GATA3+
% of FOXP3-CD4+ T cells
αCD3/28
rIL-4
B
MLN % IL-4+
C
MLN % Ki67+
Media
Basophils
D
Cecum LP % GATA3+
E
Cecum LP % IL-4+
F
Cecum LP % Ki67+
G
Cecum LP % IL-4+ of GATA3-
H
Cecum LP % IL-4+ of GATA3+
I
MLN % GATA3+
Media
WT basophils
IL-4-/- basophils
J
MLN % GATA3+
Media
Basophils separated
Basophils together
K
Cecum LP % GATA3+
T cells:
WT
IL-4-/-
L
Cecum LP % GATA3+
Media
IL-4-/- basophils

Figure 2.6 Basophils support GATA3 expression in CD4$^+$ T cells in a contact- and IL-4 autocrine signaling-dependent manner *in vitro*.

Splenic basophils were sort-purified from mice of the indicated genotypes (C57BL/6 unless otherwise specified) on D14 of *T. muris* infection and cocultured with **(A-C, I, and J)** mesenteric lymph node (MLN)- or **(D-H, K, and L)** cecum lamina propria (LP)-derived CD4$^+$ T cells from mice of the indicated genotypes (C57BL/6 unless otherwise specified) on D14 of *T. muris* infection. Cells were cultured for 72 hours with or without recombinant murine (rm)IL-4 and analyzed by flow cytometry. Quantification of % **(A)** GATA3$^+$, **(B)** IL-4$^+$, and **(C)** Ki67$^+$ of total MLN FOXP3$^-$CD4$^+$ T cells; % **(D)** GATA3$^+$, **(E)** IL-4$^+$, and **(F)** Ki67$^+$ of total cecum LP FOXP3$^-$CD4$^+$ T cells; and % IL-4$^+$ of cecum LP **(G)** GATA3$^-$FOXP3$^-$CD4$^+$ or **(H)** GATA3$^+$FOXP3$^-$CD4$^+$ T cells (gray = T cells alone; blue = T cells $^+$ basophils). (**I**) Quantification of % GATA3$^+$ T cells of total MLN FOXP3$^-$CD4$^+$ T cells when co-cultured with wild-type (WT) or IL-4$^{-/-}$ basophils (gray = T cells alone; blue = T cells + WT basophils; magenta = T cells $^+$ IL-4$^{-/-}$ basophils). **(J)** Quantification of % GATA3$^+$ T cells of total MLN FOXP3$^-$CD4$^+$ T cells when co-cultured with basophils together or separated by a transwell insert (gray = T cells alone; green = T cells $^+$ basophils separated; blue = T cells $^+$ basophils together). Quantification of % GATA3$^+$ of WT or IL-4$^{-/-}$ cecum LP FOXP3$^-$CD4$^+$ T cells (K) with or (L) without rmIL-4 when co-cultured with IL-4$^{-/-}$ basophils (gray = T cells alone; magenta = T cells $^+$ IL-4$^{-/-}$ basophils). Mean ± SEM; *, $P < 0.05$; **, $P < 0.01$; ***, $P < 0.001$; ****, $P < 0.0001$. **(A-L)** Data were analyzed using linear mixed effects models and post-hoc pairwise comparisons between groups were made using Tukey's HSD-multiple-comparison test. **(A and B)** 2 independent experiments with technical replicates pooled together (T cells alone, n = 6; T cells + basophils, n = 6). **(C)** 3 independent experiments with technical replicates pooled together (T

cells alone, n = 10; T cells + basophils, n = 9). **(D-H)** 3 independent experiments with technical replicates pooled together (T cells alone, n = 10-12; T cells + basophils, n = 7-12). **(I)** 5 independent experiments with technical replicates pooled together (T cells alone; n = 13-15; T cells + WT basophils, n = 9-11; T cells + IL-4$^{-/-}$ basophils, n = 10). **(J)** 4 independent experiments with technical replicates pooled together (T cells alone, n = 5-7; T cells + basophils separated, n = 10-12; T cells + basophils together, n = 5-6). **(K and L)** 2-3 independent experiments with technical replicates pooled together (T cells alone, n = 6-8; T cells + IL-4$^{-/-}$ basophils, n = 6-9). N is total across all experiments.

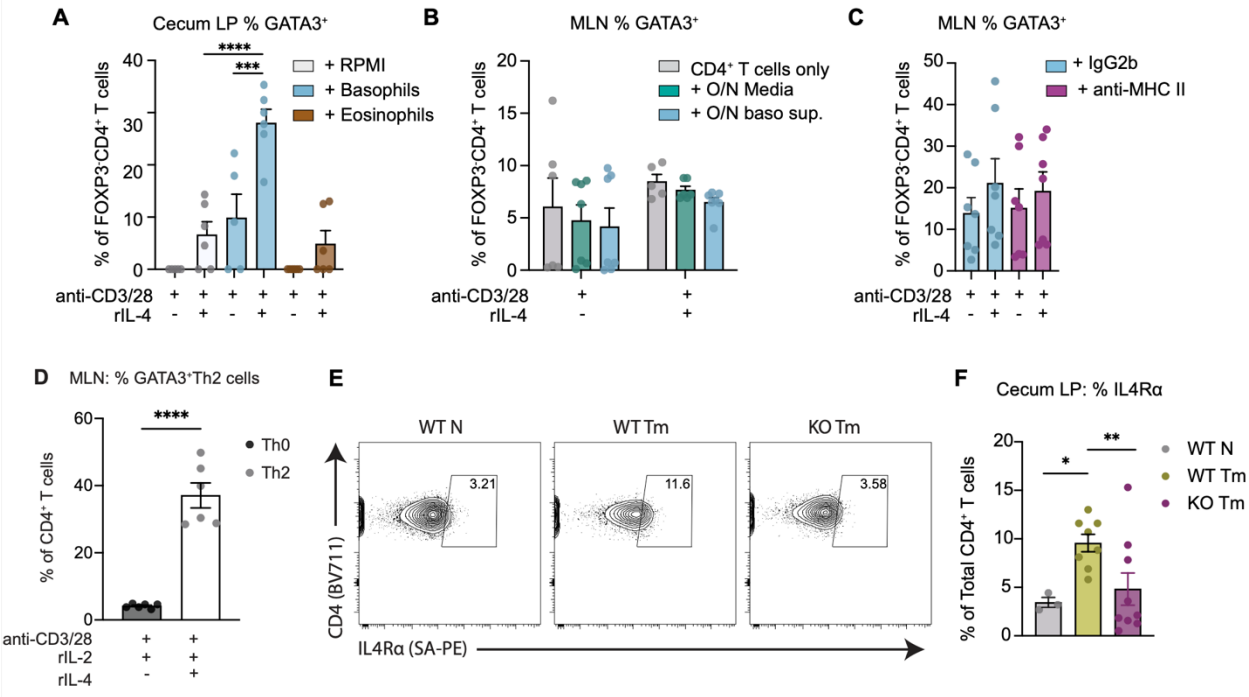

Supplementary Figure 2.6 (related to Figure 2.6) Basophil-CD4$^+$ T cell coculture assays and IL-4 KO in *Trichuris muris* infection.

Splenic basophils or eosinophils were sort-purified from C57BL/6 mice and co-cultured with cecum lamina propria (LP) or mesenteric lymph node (MLN)-derived CD4$^+$ T cells sort-purified from C57BL/6 mice at D14 p.i. with *T. muris* for 72 hours under the indicated conditions. **(A)** % of GATA3$^+$ of cecum LP CD4$^+$ T cells co-cultured with or without basophils, with or without eosinophils, and with or without rmIL-4. **(B)** % of GATA3$^+$ of MLN CD4$^+$ T cells co-cultured with or without basophils or basophil-conditioned media (O/N baso. sup) or a media control (O/N Media) (basophils cultured or 24 hours prior to supernatant collection), and with or without rmIL-4. **(C)** % of GATA3$^+$ of MLN CD4$^+$ T cells co-cultured with or without anti-MHC II and rIL-4. **(D)** MLN CD4$^+$ T cells were column enriched from naive C57BL/6 mice and cultured under Th0 (10ug/mL anti-IFNγ, 10 ug/mL anti-IL-4, 10ng/mL rIL-2) and Th2 (10ug/mL anti-

IFNγ, 10ug/mL IL-2, 50ng/mL rIL-4), polarizing conditions *in vitro* for 48 hrs and then analyzed by flow cytometry for the induction of GATA3. **(E and F)** Cecum LP $CD4^+$ T cells were isolated from WT or IL-4 deficient (KO) mice at D14 *T. muris* infection and analyzed for the expression of IL-4Rα. **(E)** Representative flow cytometric plots of the percentage of IL-$4R\alpha^+$ $CD4^+$ T cells and **(F)** quantification. Data were analyzed using linear mixed effects models and post-hoc pairwise comparisons between groups were made using **(A-C, F)** Tukey's HSD-multiple-comparison test or **(D)** unpaired student's t test. Mean ± SEM; ***, $P < 0.001$; ****, $P < 0.0001$. **(A)** Two independent experiments with technical replicates pooled together (T cells +RPMI, n = 6; T cells + basophils, n = 5; T cells + eosinophils, n = 6). **(B)** Two independent experiments with technical replicates pooled together (T cells alone, n = 5-6; T cells + O/N media, n = 6-7; T cells + O/N baso sup., n = 7). **(C)** Three independent experiments with technical replicates pooled together (IgG, n = 7; anti-MHC II, n = 7).**(D)** Two independent experiments with technical replicates pooled together (Th0, n = 6; Th2, n = 6). **(E and F)** Three independent experiments with biological replicates pooled together (WT N, n = 3); WT Tm, n = 8; KO Tm, n = 9).

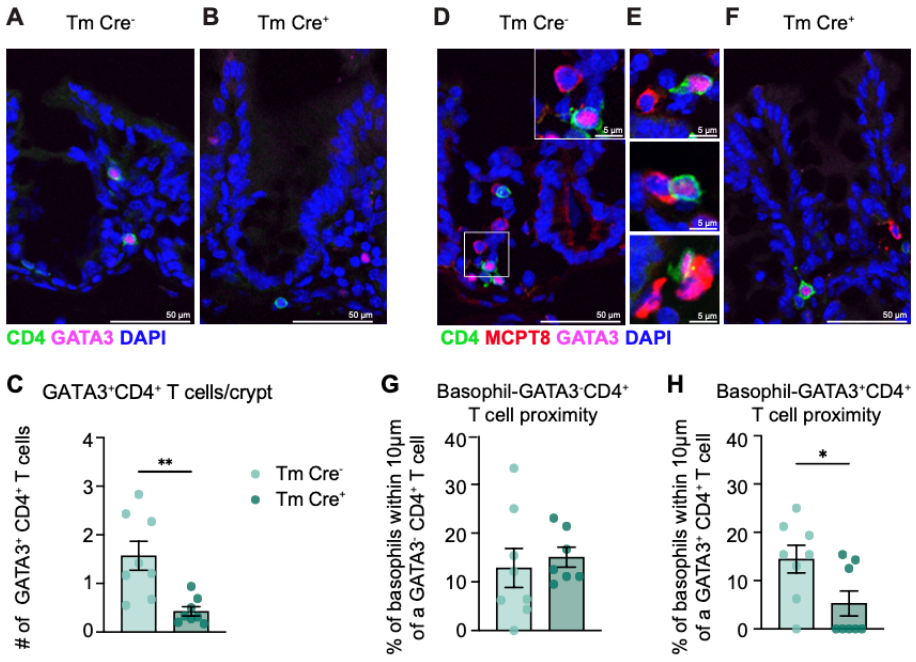

Figure 2.7. Basophil-intrinsic Notch signaling determines the expansion and spatial proximity of GATA3$^+$ Th2 cells to basophils in the cecum during *T. muris* infection.

(A-G) Immunofluorescent staining analysis of CD4$^+$ T cells and basophils in the cecum on D14 *T. muris* (Tm) infection. Representative images of staining of cecum crypt units of **(A)** Mcpt8-Cre$^-$ DNMAML F/F and **(B)** Mcp8t-Cre$^+$ DNMAML F/F mice for CD4 (green), GATA3 (magenta) and DAPI (blue). **(C)** Quantification of the number of GATA3$^+$CD4$^+$ Th2 cells (green $^+$ magenta) per cecum crypt unit in Mcpt8-Cre$^-$ DNMAML$^+$ (aqua) and Mcp8t-Cre$^+$ DNMAML (dark green) mice**.** Representative images of staining of cecum crypt units of **(D and E)** Mcpt8-Cre$^-$ DNMAML$^+$ and **(F)** Mcp8t-Cre$^+$ DNMAML mice for CD4 (green), GATA3 (magenta), MCPT (red), and DAPI (blue). Quantification of the percentage of basophils (MCPT, red) within 10 µm of **(G)** GATA3$^-$CD4$^+$ and **(H)** GATA3$^+$CD4$^+$ cells. Mean ± SEM; *, $P < 0.05$; **, $P < 0.01$**. (C, G, and H)** Data were analyzed using linear mixed effects models and post-hoc pairwise

comparisons were made using unpaired student's t-test. **(A, B, D, and F)** 20X objective lens; scale bar = 50 μm. **(E)** 20X objective lens, zoomed in X4; scale bar = 5 μm**. (A-H)** 3 independent experiments pooled together (Tm Cre^-, n = 7; Tm Cre^+, n = 7; n is total across all experiments).

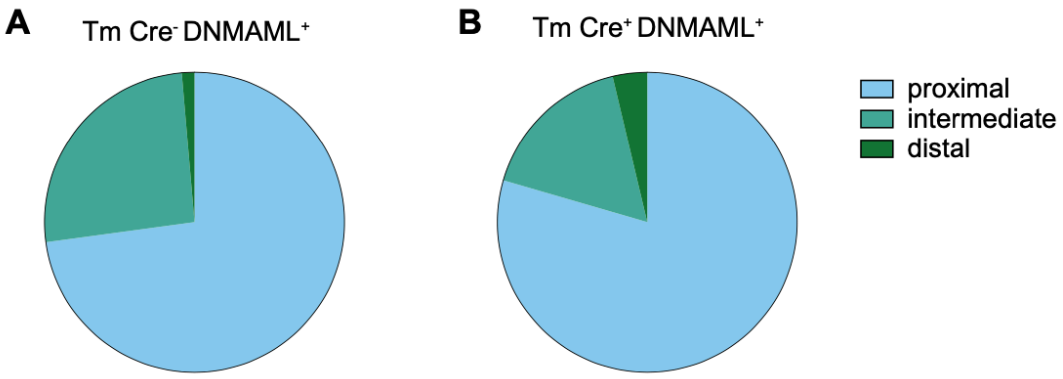

Supplementary Figure 2.7 (related to figure 2.7) Basophil organization in crypt units during *T. muris* infection.

Pie charts summarizing basophil location in cecum crypt units of at D14 post-*Trichuris muris* (Tm) infection. Crypt-unit distribution of basophils in proximal, intermediate, and distal areas of the crypt unit in relation to the cecum lamina propria in infected (A) Mcp8t-Cre- DNMAML$^+$ and (B) Mcpt8-Cre$^+$ DNMAML$^+$ mice. (A and B) Three independent experiments were pooled together (Tm Cre-, n = 7; Tm Cre$^+$, n = 7; n is total across all experiments).

Chapter 3. Conclusions.

3.1 Key findings

This thesis advances our understanding of the critical role Notch activated basophils play in supporting Th2 cell fate and function during *Trichuris muris* infection. Our findings show that Notch signaling in basophils is essential for the expansion of Th2 cells within the large intestinal environment, establishing Notch-activated basophils as key drivers of the Type 2 immune response to helminth infection. Our results demonstrate that Notch-activated basophils significantly enhance IL-4 and IL-13 production by Th2 cells, underscoring their importance in sustaining the cytokine milieu necessary for effective helminth immunity.

Additionally, this work uncovers a novel IL-4–producing TF^{-} $CD4^{+}$ T cell population that constitutes most IL-4 producers at steady state and during helminth infection. We show this population relies on Notch-activated basophils for optimal IL-4 production. This unique subset highlights a previously unrecognized pathway of IL-4 production within the large intestine, revealing new layers of complexity in the Type 2 immune response that go beyond classical GATA3-driven Th2 cells and what is known about Th2-associated functions in the lung.

Furthermore, we identified a contact-dependent mechanism between basophils and $CD4^{+}$ T cells, which is essential for maintaining GATA3 expression and IL-4 production in $CD4^{+}$ T cells *in vitro*. This interaction demonstrates the importance of direct basophil-$CD4^{+}$ T cell contact in sustaining Th2 polarization, suggesting that physical interactions facilitated by Notch signaling are vital for promoting robust Th2 responses. In agreement with this idea, our findings also reveal that basophil-intrinsic Notch signaling is required for optimal localization of basophils to GATA3-expressing Th2 cells in the cecum during helminth infection. This spatial organization appears critical for effective immune function, as it enables basophils to interact

closely with Th2 cells, further enhancing their cytokine production and supporting Type 2 immunity within the gut.

Looking forward, these findings open several promising avenues for future research. A key question is how Notch signaling in basophils is regulated within the unique intestinal microenvironment, where other tissue-specific signals may further modulate basophil function and positioning. Additionally, the mechanisms by which Notch-activated basophils influence TF^- IL-4–producing $CD4^+$ T cells warrant further exploration, as understanding these pathways could unveil new targets for modulating Type 2 immunity. Elucidating the molecular basis of the contact-dependent mechanism between basophils and Th2 cells could also provide deeper insights into how basophils maintain Th2 function over prolonged infection periods. While this body of work has advanced our understanding of basophil function and how they support $CD4^+$ T cell responses in the inflamed mucosa, several important questions remain. Future studies will be necessary to address these gaps in knowledge and build upon the findings presented here.

3.2 Regulation of Notch signaling in basophils within the intestinal microenvironment

The regulation of Notch signaling in basophils, particularly within the unique intestinal microenvironment, is one of the more intriguing questions that emerge from this work. While we have demonstrated that Notch signaling in basophils is essential for their role in supporting Th2 responses during *T. muris* infection, the precise cellular mechanisms by which Notch activation is triggered in basophils to promote their function during helminth infection remain unclear. Notch ligands are ubiquitously expressed by both hematopoietic and non-hematopoietic cells. Therefore, future research should focus on identifying the specific cellular sources of Notch

ligands that activate basophils during helminth infection[77]. Notch-ligand reporter mice would be a helpful tool in elucidating the cellular source of Notch ligands during *T. muris* infection.

Additionally, it will be important to ask how specific inflammatory niches induce canonical versus non-canonical Notch signaling in basophils. The molecular players of this signaling pathway are ubiquitously expressed and overlap with many other pathways, adding complexity to the transcriptional regulation of basophils. Notch-responding cells could potentially be integrating a multitude of signals from various cell types for their activation and function in local tissue microenvironments. This would be interesting to explore in the context of IL-3 elicited basophils versus TSLP-elicited basophils, as these basophils are developmentally, transcriptionally, and functionally distinct from each other in the context of helminth infection. Moreover, it will be crucial to understand the local cues, such as cytokines, metabolic signals, and interactions with microbiota, that influence Notch signaling in basophils. The gut is a highly specialized and sensitive environment, and the immune responses in the lamina propria are shaped by numerous factors, including the presence of commensal bacteria. Investigating how these factors contribute to Notch activation in basophils could provide valuable insights into how the immune system adapts to its local environment and may help tailor interventions that target specific immune pathways in the gut.

3.3 Basophils and TF^- IL-4-producing $CD4^+$ T cells

The identification of a TF^- IL-4 producing $CD4^+$ T cell population in the intestine during helminth infection was a surprising and exciting finding. This population challenges the current dogma where GATA3 expression is required for the expression of Type 2 cytokines by $CD4^+$ T cells, as our data show that IL-4 was produced primarily by TF^- $CD4^+$ T cells in the tissue during

helminth infection. Future work should aim to characterize these cells and determine whether GATA3 expression and/or STAT6 signaling is required for the development and activation of TF^- IL-4 producers.

This novel population of IL-4-producing T cells may represent an important source of Type 2 cytokines during *T. muris* infection that is also dependent on the presence of Notch-activated basophils, yet little is known about how they are regulated or how they interact with other immune cells. Are these TF^- IL-4-producing T cells derived from naïve $CD4^+$ T cells that are activated early in infection, or do they arise from more differentiated Th2 cells? These cells prompt the question: which came first, the chicken or the egg? Are $GATA3^+$ Th2 cells required to support a tissue wide IL-4 program across heterogenous TF^- $CD4^+$ T cells, or do TF^- $CD4^+$ cells, the major producers of IL-4 in the intestine, critically maintain Th2 cells in the tissue for robust Type 2 inflammation? This dynamic is further complicated by the fact that both $CD4^+$ T cell populations require Notch-activated basophils to expand and produce cytokines during *T. muris* infection. It will be crucial to perform fate mapping experiments to track intestinal $CD4^+$ T cell development throughout *T. muris* infection to identify key developmental differences between TF^- IL-4 producers and conventional Th2 cells.

Single-cell RNAseq analyses highlighted the heterogeneity among IL-4 producing $CD4^+$ T cells, including TF^- cells, in the inflamed cecum during helminth infection. Additionally, Notch signaling is required to drive basophil-Th2 proximity, but not basophil-$GATA3^-$ $CD4^+$ T cell proximity, suggesting IL-4 production by TF^- cells does not require the proximity-dependent effects of basophils. To validate the transcriptional findings, high parameter microscopy quantifying basophil proximity to various $CD4^+$ T cell subsets in the ceca of *T. muris* infected Mcpt8-Cre DNMAML F/F mice will highlight Notch-dependent proximity effects on basophil

positioning near heterogenous $CD4^+$ T cell subsets. In addition, mixed bone marrow chimera experiments utilizing Mcpt8-Cre DNMAML F/F and IL-4-IRES-eGFP (4Get) mice would importantly determine whether Notch signaling drives basophil proximity to *Il4* expressing $CD4^+$ T cells, including TF^- cells, in the cecum during infection. However, it is important to note that these experiments are limited to reporting *Il4* gene expression, not protein production, by $CD4^+$ T cells. Ideally, developing methods to specifically target and/or knock out IL-4 production in TF^- $CD4^+$ T cells without impacting Th2-dependet IL-4 would pinpoint the role of IL-4 production by these cells during helminth infection. In the future, it will be critical to develop better tools and methods to more precisely define these Basophil-Th2-TF^- dynamics in the intestine. Future studies will continue to elucidate how TF^- IL-4 $CD4^+$ T cells contribute to the inflammatory milieu for robust anti-helminth immunity and determine whether these cells are similarly impacted by Notch-activated basophils in other models of Type 2 inflammation.

3.4 Molecular basis of basophil-$CD4^+$ T cell interactions

In this thesis, we identified a contact-dependent mechanism through which basophils support Th2 cell fate and function *in vitro*. However, the specific molecular mechanism that governs this basophil-$CD4^+$ T cell interaction remains unknown. We did identify candidate molecules expressed by basophils that might mediate this interaction. We returned to our previous work[92] to examine RNA-seq data from splenic Mcpt8-Cre^- and Mcpt8-Cre^+ DNMAML F/F basophils isolated from *T. muris*-infected mice and selected candidates known to impact $CD4^+$ T cell function in a contact dependent manner and were differentially expressed between Notch-sufficient and -deficient basophils. To determine whether any of these candidate genes were required for the induction and/or maintenance of Th2 cells, additional basophil-$CD4^+$ T cell

coculture experiments were performed in the presence of blocking antibodies against these candidate molecules (anti-CD48, anti-CD155, anti-CTLA4, anti-TRAIL, and anti-ITGA4) (Fig. 3.1). Unfortunately, blocking these pathways *in vitro* did not result in significant decreases in GATA3 expression in $CD4^+$ T cells cocultured with basophils. Thus, despite efforts, the molecular mechanism by which basophils support Th2-associated fate and function remains unknown. Future studies should aim to identify the key receptor-ligand pairs involved in basophil-dependent support of GATA3 expression and IL-4 production by intestinal $CD4^+$ T cells. Defining how $CD4^+$ T cells cultured in contact with basophils are transcriptionally unique from $CD4^+$ T cells cocultured without basophil contact will be crucial to elucidating this cellular mechanism. For example, using our transwell coculture experiments to control basophil-$CD4^+$ T cell contact, we can perform low input RNA sequencing on recovered CD4s to identify basophil-contact-dependent gene expression patterns associated with Th2 identify in an unbiased fashion. Additionally, whether this basophil-dependent contact mechanism potentiates an IL-4 autocrine signaling module in $CD4^+$ T cells requires validation. For example, coculture experiments determining whether direct basophil interactions impact IL4Ra expression or phospho-STAT6 in $CD4^+$ T cells will be important next steps. Expanding these coculture studies to understand how basophil-$CD4^+$ T cells interaction influence Th2 fate and function during prolonged infection and in other models of helminth infection will further clarify how immune responses are sustained or resolved in the intestine. These future studies could lead to the identification of novel mechanisms modulating basophil-T cell interactions to enhance or suppress Type 2 immune responses.

3.5 Role of basophils in other tissue microenvironments

While this dissertation has focused on the role of basophils in the large intestinal microenvironment, it is likely that basophils also play important yet distinct roles in other tissues, particularly in the context of Type 2 inflammation. For example, basophils accumulate in tissues such as the lungs during allergic reactions, but whether Notch-activated basophils shape immune responses in the lungs, skin, small intestine, or other barrier tissues remains to be explored. Additionally, the immune response generated against *T. muris* is highly dependent on basophil activation in the tissue compared to other models of helminth infection, like *Nippostrongylus brasiliensis*. While both are both models of gastrointestinal helminth infection, *T. muris* infects the large intestine while *N. brasiliensis* primarily infects the duodenum and jejunum of the small intestine. The recruitment and activation of Notch-dependent basophils likely depends on tissue specific cues in the large intestine that are absent in other models of helminth infection. While extending these studies into other models of helminth infection, and more broadly Type 2 immunity, are of utmost interest, the role of Notch-activated basophils cannot be generalized across Type 2 inflammation. Future studies will investigate whether basophils interact with Th2 cells in these other tissues and determine whether basophil-intrinsic Notch signaling governs GATA3 and IL-4 signaling modules in $CD4^+$ T cells across other tissues and models of Type 2 inflammation. Improving our understanding of the tissue-specific roles basophils play in shaping local inflammation could provide new insights into the regulation of immune responses in different tissue microenvironment and help develop therapies that target distinct tissue sites.

3.6 Therapeutic implications and closing remarks

The insights garnered from this work could have significant impacts on the development of therapies and vaccines for a range of Type 2 inflammatory diseases, including helminthiasis, asthma, allergies, and other conditions characterized by excessive or maladaptive Th2 responses. These diseases often share a common feature: an overactive Type 2 immune response that leads to chronic inflammation and tissue damage. For example, asthma is associated with elevated levels of IL-4, IL-5, and IL-13, all key cytokines produced by Th2 cells. Allergic reactions, including those to pollen, food, and insect stings, also involve inappropriate activation of the Th2 cells and their associated inflammatory mediators[23].

By identifying Notch-activated basophils as key players in the expansion and maintenance of Th2 cells, our study suggests that targeting the Notch signaling pathway in basophils may offer a novel route for therapeutic intervention in treating a variety of Type 2 mediated diseases. Blocking the Notch signaling cascade specifically in basophils has the potential to reduce the exacerbated Type 2 pathologies seen in conditions like asthma. On the other hand, enhancing Notch signaling in basophils may be beneficial in enhancing immune responses against helminths, where a robust Type 2 immune response is required for effective worm expulsion.

Moreover, vaccines aimed at enhancing the immune system's ability to mount a strong and effective Th2 response could benefit from targeting Notch signaling in basophils. During helminth infection, the immune system must generate a tightly regulated Type 2 immune response to clear the infection without causing excessive tissue damage. By leveraging Notch-signaling in basophils, vaccines could be designed to boost local immune responses within the intestinal mucosa, thereby enhancing the body’s ability to recognize and expel parasitic threats.

This approach offers flexibility in treatment as well, as basophils are relatively short-lived cells and can be targeting transiently. Such strategies could lead to more effective vaccines not only against helminths but also against other parasitic diseases that rely on Type 2 immune responses.

Additionally, the identification of the novel TF^- IL-4-producing $CD4^+$ T cell population opens new possibilities for therapeutic manipulation of these cells in Type 2 inflammatory diseases. In diseases like asthma, where IL-4 production is pivotal in driving inflammation, strategies that target these TF^- IL-4-producing T cells, which during *T. muris* infection are the major source of IL-4 in the tissue, could help restore balance in the immune system. Understanding how Notch-activated basophils influence these cells and promote IL-4 production could pave the way for therapies that specifically modulate a larger pool of $CD4^+$ T cell subsets in the tissue.

Together, these findings expand our knowledge of the roles basophils play in Type 2 immunology by elucidating Notch-dependent mechanisms that govern cytokine production, cellular interaction, and spatial organization (Fig. 3.2). Importantly, these studies emphasize that basophils are unique cellular players that, apart from their canonical role as short-lived cells that deliver inflammatory mediators and then die, can fine tune the adaptive Type 2 immune response. By highlighting the significance of Notch signaling in shaping basophil-mediated support of Th2 responses, this work establishes a foundation for further exploration into the therapeutic potential of targeting basophil-Notch interactions in Type 2 inflammatory diseases and parasitic infections and expands upon our knowledge of the tissue specific cue that optimize intestinal $CD4^+$ T cell function in these settings. Through these insights, this research contributes to the broader field of Type 2 immunity, opening new avenues for targeted modulation of immune responses in helminth infections and related conditions.

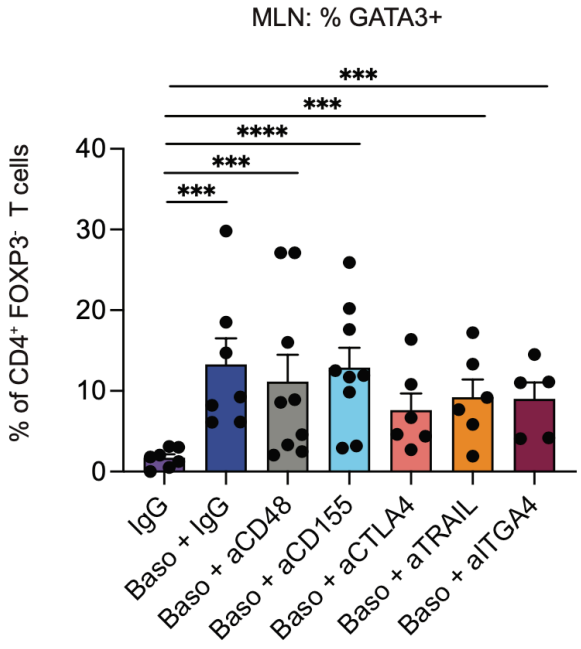

Figure 3.1 Basophil-CD4$^+$ T cell target validation.

Splenic basophils were sort-purified from C57BL/6 mice and co-cultured with mesenteric lymph node (MLN)-derived CD4$^+$ T cells sort-purified from C57BL/66 mice at D14 p.i. with *T. muris* for 72 hours under the indicated conditions. % of GATA3$^+$ of MLN CD4$^+$ T cells co-cultured alone with isotype control (IgG; purple), or with basophils and isotype control (dark blue), basophils and anti-CD48 (gray), basophils and anti-CD155 (aqua), basophils and anti-CTLA4 (salmon), basophils and anti-TRAIL (gold), or basophils and anti-ITGA4 (fuchsia). Mean ± SEM; ***, $P < 0.001$; ****, $P < 0.0001$. Data were analyzed using linear mixed effects models and post-hoc pairwise comparisons between groups were made using Tukey's HSD-multiple-comparison test. Three to four independent experiments with technical replicates pooled together (T cells + IgG, n = 6; T cells + basophils + IgG, n = 7; T cells + basophils + anti-CD48, n = 9; T cells + basophils + anti-CD155, n = 9; T cells + basophils + anti-CTLA4, n = 6; T cells + basophils + anti-TRAIL, n = 6; T cells + basophils + anti-ITGA4, n = 5).

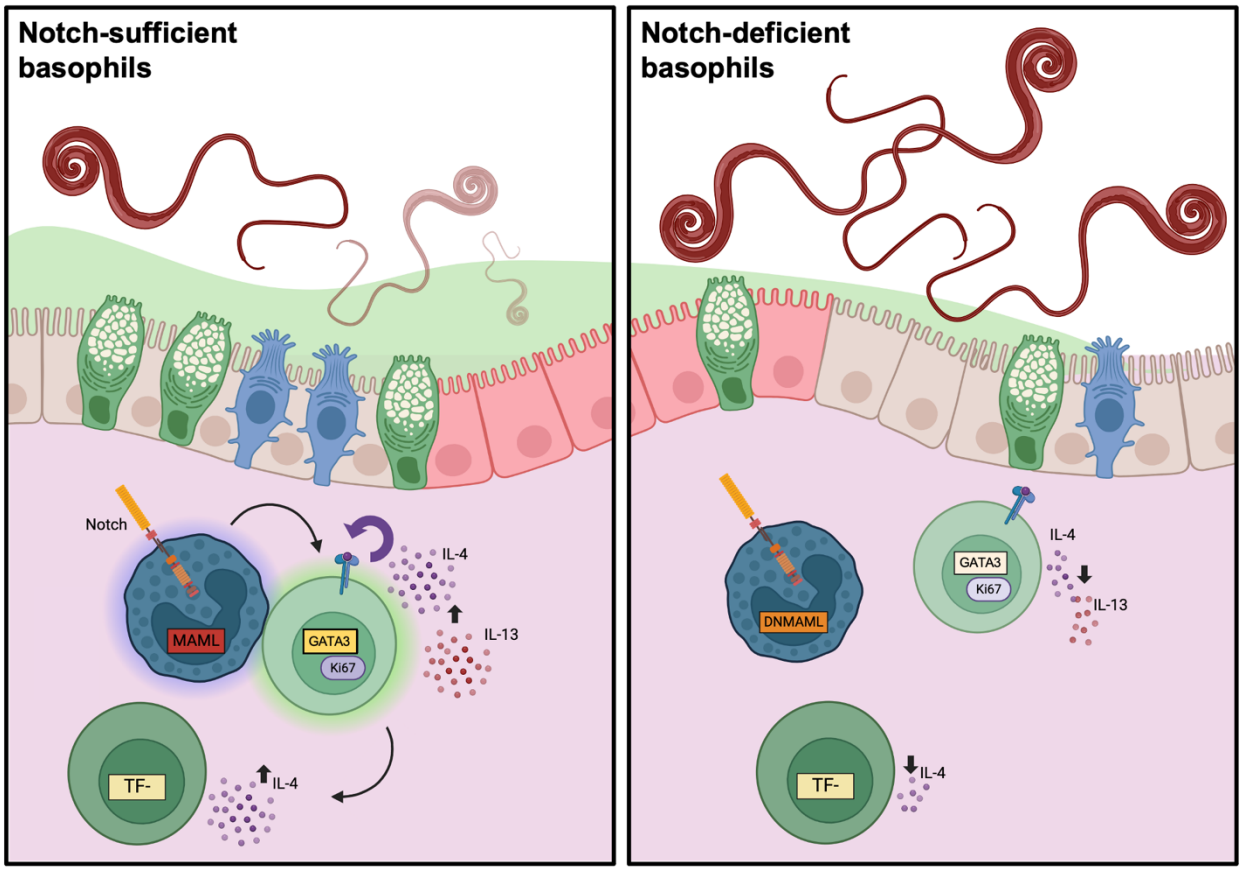

Figure 3.2 Working model.

Basophil-intrinsic Notch drives appropriate positioning for basophil-Th2 cell interactions in the cecum lamina propria via a cell contact-dependent mechanism to promote Th2 cells and a broader IL-4 producing TF^{-} $CD4^{+}$ T cell population, potentially via T cell-intrinsic autocrine IL-4 signaling, to promote parasite clearance (left). Loss of Notch-activated basophils results in their failure to colocalize to Th2 cells, leading to diminished Th2 cell expansion, IL-4 production, and inability to clear parasites from the tissue (right).

Bibliography

1. Zawawi, A. & Else, K. J. Soil-Transmitted Helminth Vaccines: Are We Getting Closer? *Frontiers in Immunology* **11**, (2020).
2. Gebreyesus, T. D. *et al.* Prevalence, intensity, and correlates of schistosomiasis and soil-transmitted helminth infections after five rounds of preventive chemotherapy among school children in southern Ethiopia. *Pathogens* **9**, (2020).
3. Bethony, J. *et al.* Soil-transmitted helminth infections: ascariasis, trichuriasis, and hookworm. *Lancet* **367**, (2006).
4. Vaz Nery, S. *et al.* The role of water, sanitation and hygiene interventions in reducing soil-transmitted helminths: Interpreting the evidence and identifying next steps. *Parasites and Vectors* **12**, (2019).
5. Bogoch, I. I. *et al.* Clinical evaluation for morbidity associated with soil-transmitted helminth infection in school-age children on Pemba Island, Tanzania. *PLoS Negl Trop Dis* **13**, (2019).
6. Lustigman, S. *et al.* A research agenda for helminth diseases of humans: The problem of helminthiases. *PLoS Neglected Tropical Diseases* **6**, (2012).
7. Olds, G. R. Deworming the world. *Trans Am Clin Climatol Assoc* **124**, (2013).
8. Gause, W. C., Wynn, T. A. & Allen, J. E. Type 2 immunity and wound healing: Evolutionary refinement of adaptive immunity by helminths. *Nature Reviews Immunology* vol. **13**, (2013).
9. McSorley, H. J. & Maizels, R. M. Helminth infections and host immune regulation. *Clin Microbiol Rev* **25**, (2012).

10. Harris, N. L. & Loke, P. Recent Advances in Type-2-Cell-Mediated Immunity: Insights from Helminth Infection. *Immunity* **47**, (2017).

11. Van Dyken, S. J. *et al.* A tissue checkpoint regulates type 2 immunity. *Nat Immunol* **17**, (2016).

12. Gause, W. C., Rothlin, C. & Loke, P. Heterogeneity in the initiation, development and function of type 2 immunity. *Nature Reviews Immunology* vol. **20**, (2020).

13. Webb, L. M. & Wojno, E. D. T. The role of rare innate immune cells in Type 2 immune activation against parasitic helminths. *Parasitology* vol. **144**, (2017).

14. Allen, J. E. & Sutherland, T. E. Host protective roles of type 2 immunity: Parasite killing and tissue repair, flip sides of the same coin. *Seminars in Immunology* vol. **26**, (2014).

15. Divekar, R. & Kita, H. Recent advances in epithelium-derived cytokines (IL-33, IL-25, and thymic stromal lymphopoietin) and allergic inflammation. *Current Opinion in Allergy and Clinical Immunology* vol. **15**, (2015).

16. Schneider, C., O'Leary, C. E. & Locksley, R. M. Regulation of immune responses by tuft cells. *Nature Reviews Immunology* vol. **19**, (2019).

17. Ting, H.-A. & von Moltke, J. The Immune Function of Tuft Cells at Gut Mucosal Surfaces and Beyond. *The Journal of Immunology* **202**, (2019).

18. Von Moltke, J., Ji, M., Liang, H. E. & Locksley, R. M. Tuft-cell-derived IL-25 regulates an intestinal ILC2-epithelial response circuit. *Nature* **529**, (2016).

19. Schneider, C. *et al.* A Metabolite-Triggered Tuft Cell-ILC2 Circuit Drives Small Intestinal Remodeling. *Cell* **174**, (2018).

20. Bancroft, A. J., McKenzie, A. N. J. & Grencis, R. K. A Critical Role for IL-13 in Resistance to Intestinal Nematode Infection. *The Journal of Immunology* **160**, (1998).

21. Bancroft, A. J., Artis, D., Donaldson, D. D., Sypek, J. P. & Grencis, R. K. Gastrointestinal nematode expulsion in IL-4 knockout mice is IL-13 dependent. *Eur J Immunol* **30**, (2000).

22. Paul, W. E. & Zhu, J. How are TH2-type immune responses initiated and amplified? *Nature Reviews Immunology* vol. **10**, (2010).

23. Nakayama, T. *et al.* Th2 cells in health and disease. *Annual Review of Immunology* vol. **35**, at (2017).

24. McKenzie, G. J., Bancroft, A., Grencis, R. K. & McKenzie, A. N. J. A distinct role for interleukin-13 in Th2-cell-mediated immune responses. *Current Biology* **8**, (1998).

25. Westermann, S. *et al.* Th2-dependent STAT6-regulated genes in intestinal epithelial cells mediate larval trapping during secondary Heligmosomoides polygyrus bakeri infection. *PLoS Pathog* **19**, (2023).

26. Walker, J. A. & McKenzie, A. N. J. TH2 cell development and function. *Nature Reviews Immunology* vol. **18**, (2018).

27. Jang, S. W. & Lee, G. R. GATA3, SATB1, IRF4 complex binds to the Th2 cytokine locus through cis -acting element RHS6, regulating allergic airway inflammation. *The Journal of Immunology* **200**, (2018).

28. Zhu, J., Guo, L., Watson, C. J., Hu-Li, J. & Paul, W. E. Stat6 Is Necessary and Sufficient for IL-4's Role in Th2 Differentiation and Cell Expansion. *The Journal of Immunology* **166**, (2001).

29. Zheng, W. P. & Flavell, R. A. The transcription factor GATA-3 is necessary and sufficient for Th2 cytokine gene expression in CD4 T cells. *Cell* **89**, (1997).

30. McKenzie, G. J., Fallon, P. G., Emson, C. L., Grencis, R. K. & McKenzie, A. N. J. Simultaneous disruption of interleukin (IL)-4 and IL-13 defines individual roles in T helper cell type 2-mediated responses. *Journal of Experimental Medicine* **189**, (1999).

31. Pearce, E. J. Th2 cell responses in immunity and inflammation following helminth infection. in *The Th2 Type Immune Response in Health and Disease: From Host Defense and Allergy to Metabolic Homeostasis and Beyond* (2015). doi:10.1007/978-1-4939-2911-5_4.

32. Jenkins, S. J., Perona-Wright, G., Worsley, A. G. F., Ishii, N. & MacDonald, A. S. Dendritic Cell Expression of OX40 Ligand Acts as a Costimulatory, Not Polarizing, Signal for Optimal Th2 Priming and Memory Induction In Vivo. *The Journal of Immunology* **179**, (2007).

33. Rulifson, I. C., Sperling, A. I., Fields, P. E., Fitch, F. W. & Bluestone, J. A. CD28 costimulation promotes the production of Th2 cytokines. *The Journal of Immunology* **158**, (1997).

34. Webb, G. J., Hirschfield, G. M. & Lane, P. J. L. OX40, OX40L and Autoimmunity: a Comprehensive Review. *Clinical Reviews in Allergy and Immunology* vol. **50**, (2016).

35. Barrett, N. A., Maekawa, A., Rahman, O. M., Austen, K. F. & Kanaoka, Y. Dectin-2 Recognition of House Dust Mite Triggers Cysteinyl Leukotriene Generation by Dendritic Cells. *The Journal of Immunology* **182**, (2009).

36. Everts, B. *et al.* Schistosome-derived omega-1 drives Th2 polarization by suppressing protein synthesis following internalization by the mannose receptor. *Journal of Experimental Medicine* **209**, (2012).

37. Pulendran, B. *et al.* Lipopolysaccharides from Distinct Pathogens Induce Different Classes of Immune Responses In Vivo. *The Journal of Immunology* **167**, (2001).

38. Ito, T. *et al.* TSLP-activated dendritic cells induce an inflammatory T helper type 2 cell response through OX40 ligand. *Journal of Experimental Medicine* **202**, (2005).

39. Connor, L. M., Tang, S.-C., Camberis, M., Le Gros, G. & Ronchese, F. Helminth-Conditioned Dendritic Cells Prime CD4+ T Cells to IL-4 Production In Vivo. *The Journal of Immunology* **193**, (2014).

40. Kumamoto, Y. *et al.* CD301b+ dermal dendritic cells drive T helper 2 cell-mediated immunity. *Immunity* **39**, (2013).

41. Williams, J. W. *et al.* Transcription factor IRF4 drives dendritic cells to promote Th2 differentiation. *Nat Commun* **4**, (2013).

42. Halim, T. Y. F. *et al.* Group 2 innate lymphoid cells license dendritic cells to potentiate memory TH2 cell responses. *Nat Immunol* **17**, (2016).

43. Nair, M. G. & Herbert, D. R. Immune polarization by hookworms: Taking cues from T helper type 2, type 2 innate lymphoid cells and alternatively activated macrophages. *Immunology* **148**, (2016).

44. Hammad, H. & Lambrecht, B. N. Barrier Epithelial Cells and the Control of Type 2 Immunity. *Immunity* vol. **43**, (2015).

45. McSorley, H. J. & Smyth, D. J. IL-33: A central cytokine in helminth infections. *Seminars in Immunology* vol. **53**, (2021).

46. Hammad, H. *et al.* House dust mite allergen induces asthma via Toll-like receptor 4 triggering of airway structural cells. *Nat Med* **15**, (2009).

47. Oliphant, C. J. *et al.* MHCII-mediated dialog between group 2 innate lymphoid cells and CD4+ T cells potentiates type 2 immunity and promotes parasitic helminth expulsion. *Immunity* **41**, (2014).

48. Mirchandani, A. S. *et al.* Type 2 Innate Lymphoid Cells Drive CD4+ Th2 Cell Responses. *The Journal of Immunology* **192**, (2014).

49. Pelly, V. S. *et al.* IL-4-producing ILC2s are required for the differentiation of TH2 cells following Heligmosomoides polygyrus infection. *Mucosal Immunol* **9**, (2016).

50. Varricchi, G., Raap, U., Rivellese, F., Marone, G. & Gibbs, B. F. Human mast cells and basophils—How are they similar how are they different? *Immunological Reviews* vol. **282**, (2018).

51. Radtke, D. & Voehringer, D. Granulocyte development, tissue recruitment, and function during allergic inflammation. *European Journal of Immunology* vol. **53**, (2023).

52. Voehringer, D. Protective and pathological roles of mast cells and basophils. *Nature Reviews Immunology* vol. **13**, (2013).

53. Kabashima, K. *et al.* Biomarkers for evaluation of mast cell and basophil activation. *Immunological Reviews* vol. **282**, (2018).

54. Arinobu, Y. *et al.* Developmental checkpoints of the basophil/mast cell lineages in adult murine hematopoiesis. *Proc Natl Acad Sci U S A* **102**, (2005).

55. Reber, L. L., Marichal, T. & Galli, S. J. New models for analyzing mast cell functions in vivo. *Trends in Immunology* vol. **33**, (2012).

56. Siracusa, M. C. *et al.* Thymic Stromal Lymphopoietin-Mediated Extramedullary Hematopoiesis Promotes Allergic Inflammation. *Immunity* **39**, (2013).

57. Saenz, S. A. *et al.* IL25 elicits a multipotent progenitor cell population that promotes T H 2 cytokine responses. *Nature* **464**, (2010).

58. Peng, J. & Siracusa, M. C. Basophils in antihelminth immunity. *Seminars in Immunology* vol. **53**, (2021).

59. Schneider, E., Thieblemont, N., De Moraes, M. L. & Dy, M. Basophils: New players in the cytokine network. *European Cytokine Network* vol. **21**, (2010).

60. Stone, K. D., Prussin, C. & Metcalfe, D. D. IgE, mast cells, basophils, and eosinophils. *Journal of Allergy and Clinical Immunology* **125**, (2010).

61. Katona, I. M., Urban, J. F. & Finkelman, F. D. The role of L3T4+ and Lyt-2+ T cells in the IgE response and immunity to Nippostrongylus brasiliensis. *The Journal of Immunology* **140**, (1988).

62. Ohnmacht, C. *et al.* Basophils Orchestrate Chronic Allergic Dermatitis and Protective Immunity against Helminths. *Immunity* **33**, 364–374 (2010).

63. Siracusa, M. C. *et al.* TSLP promotes interleukin-3-independent basophil haematopoiesis and type 2 inflammation. *Nature* **477**, (2011).

64. Taylor, B. C. *et al.* TSLP regulates intestinal immunity and inflammation in mouse models of helminth infection and colitis. *Journal of Experimental Medicine* **206**, (2009).

65. van Panhuys, N. *et al.* Basophils Are the Major Producers of IL-4 during Primary Helminth Infection. *The Journal of Immunology* **186**, (2011).

66. Min, B. *et al.* Basophils produce IL-4 and accumulate in tissues after infection with a Th2-inducing parasite. *Journal of Experimental Medicine* **200**, (2004).

67. Sokol, C. L. *et al.* Basophils function as antigen-presenting cells for an allergen-induced T helper type 2 response. *Nat Immunol* **10**, (2009).

68. Hammad, H. *et al.* Inflammatory dendritic cells - not basophils - are necessary and sufficient for induction of Th2 immunity to inhaled house dust mite allergen. *Journal of Experimental Medicine* **207**, (2010).

69. Sullivan, B. M. *et al.* Genetic analysis of basophil function in vivo. *Nat Immunol* **12**, (2011).

70. Crowle, P. K. Mucosal mast cell reconstitution and Nippostrongylus brasiliensis rejection by W/Wv mice. *J Parasitol* **69**, (1983).

71. Ohnmacht, C. & Voehringer, D. Basophils Protect against Reinfection with Hookworms Independently of Mast Cells and Memory Th2 Cells. *The Journal of Immunology* **184**, (2010).

72. Perrigoue, J. G. *et al.* Major histocompatibility complex class II-dependent basophil-CD4 + T cell interactions promote T H 2 cytokine-dependent immunity HHS Public Access. *Nat Immunol* **10**, (2009).

73. Hurst, R. J. M. & Else, K. J. Trichuris muris research revisited: A journey through time. *Parasitology* vol. **140**, (2013).

74. Webb, L. M. & Tait Wojno, E. D. Notch Signaling Orchestrates Helminth-Induced Type 2 Inflammation. *Trends in Immunology* vol. **40**, 2019).

75. Sakata-Yanagimoto, M. *et al.* Notch2 signaling is required for proper mast cell distribution and mucosal immunity in the intestine. *Blood* **117**, (2011).

76. Tu, L. L. *et al.* Notch signaling is an important regulator of type 2 immunity. *Journal of Experimental Medicine* **202**, (2005).

77. Zhou, B. *et al.* Notch signaling pathway: architecture, disease, and therapeutics. *Signal Transduction and Targeted Therapy* vol. **7**, (2022).

78. Kopan, R. & Ilagan, M. X. G. The Canonical Notch Signaling Pathway: Unfolding the Activation Mechanism. *Cell* vol. 137 Preprint at https://doi.org/10.1016/j.cell.2009.03.045 (2009).

79. Gazave, E. *et al.* Origin and evolution of the Notch signaling pathway: An overview from eukaryotic genomes. *BMC Evolutionary Biology* vol. **9**, (2009).

80. Li, Y. M. *et al.* Presenilin 1 is linked with γ-secretase activity in the detergent solubilized state. *Proc Natl Acad Sci U S A* **97**, (2000).

81. Li, Y. M. *et al.* Photoactivated γ-secretase inhibitors directed to the active site covalently label presenilin 1. *Nature* **405**, (2000).

82. Seegar, T. C. M. *et al.* Structural Basis for Regulated Proteolysis by the α-Secretase ADAM10. *Cell* **171**, (2017).

83. Bray, S. J. Notch signalling in context. *Nature Reviews Molecular Cell Biology* vol. 17 Preprint at https://doi.org/10.1038/nrm.2016.94 (2016).

84. Polacheck, W. J. *et al.* A non-canonical Notch complex regulates adherens junctions and vascular barrier function. *Nature* **552**, (2017).

85. Mangolini, M. *et al.* Notch2 controls non-autonomous Wnt-signalling in chronic lymphocytic leukaemia. *Nat Commun* **9**, (2018).

86. Luo, K. Signaling cross talk between TGF-β/Smad and other signaling pathways. *Cold Spring Harbor Perspectives in Biology* vol. **9**, (2017).

87. Helbig, C. *et al.* Notch controls the magnitude of T helper cell responses by promoting cellular longevity. *Proc Natl Acad Sci U S A* **109**, (2012).

88. Vanderbeck, A. & Maillard, I. Notch signaling at the crossroads of innate and adaptive immunity. *Journal of Leukocyte Biology* vol. **109**, (2021).

89. Radtke, F., MacDonald, H. R. & Tacchini-Cottier, F. Regulation of innate and adaptive immunity by Notch. *Nature Reviews Immunology* vol. **13**, (2013).

90. Qu, S. yao *et al.* Notch signaling pathway regulates the growth and the expression of inflammatory cytokines in mouse basophils. *Cell Immunol* **318**, (2017).

91. Qu, S. Y., He, Y. L., Zhang, J. & Wu, C. G. Transcription factor RBP-J-mediated signalling regulates basophil immunoregulatory function in mouse asthma model. *Immunology* **152**, (2017).

92. Webb, L. M. *et al.* The Notch signaling pathway promotes basophil responses during helminth-induced type 2 inflammation. *Journal of Experimental Medicine* **216**, (2019).

93. Allen, J. E. & Maizels, R. M. Diversity and dialogue in immunity to helminths. *Nat Rev Immunol* **11**, (2011).

94. Karasuyama, H., Mukai, K., Obata, K., Tsujimura, Y. & Wada, T. Nonredundant roles of basophils in immunity. *Annu Rev Immunol* **29**, (2011).

95. Yoichi, I. The absence of resistance in congenitally athymic nude mice toward infection with the intestinal nematode, Trichuris muris: Resistance restored by lymphoid cell transfer. *Int J Parasitol* **21**, (1991).

96. Else, K. J. & Grencis, R. K. Antibody-independent effector mechanisms in resistance to the intestinal nematode parasite Trichuris muris. *Infect Immun* **64**, (1996).

97. Oyesola, O. O., Früh, S. P., Webb, L. M. & Tait Wojno, E. D. Cytokines and beyond: Regulation of innate immune responses during helminth infection. *Cytokine* vol. **133**, (2020).

98. Cliffe, L. J. & Grencis, R. K. The Trichuris muris system: A paradigm of resistance and susceptibility to intestinal nematode infection. *Advances in Parasitology* vol. **57**, (2004).

99. Else, K. J. & Grencis, R. K. Cellular immune responses to the murine nematode parasite Trichuris muris. I. Differential cytokine production during acute or chronic infection. *Immunology* **72**, (1991).

100. Else, K. J. & Finkelman, F. D. Intestinal nematode parasites, cytokines and effector mechanisms. *Int J Parasitol* **28**, (1998).

101. Halim, T. Y. F. *et al.* Group 2 innate lymphoid cells are critical for the initiation of adaptive T helper 2 cell-mediated allergic lung inflammation. *Immunity* **40**, (2014).

102. Mohrs, K., Wakil, A. E., Killeen, N., Locksley, R. M. & Mohrs, M. A two-step process for cytokine production revealed by IL-4 dual-reporter mice. *Immunity* **23**, (2005).

103. Liang, H. E. *et al.* Divergent expression patterns of IL-4 and IL-13 define unique functions in allergic immunity. *Nat Immunol* **13**, (2012).

104. Michieletto, M. F. *et al.* Multiscale 3D genome organization underlies ILC2 ontogenesis and allergic airway inflammation. *Nat Immunol* **24**, (2023).

105. Zaretsky, A. G. *et al.* T follicular helper cells differentiate from Th2 cells in response to helminth antigens. *Journal of Experimental Medicine* **206**, (2009).

106. Gowthaman, U. *et al.* Identification of a T follicular helper cell subset that drives anaphylactic IgE. *Science (1979)* **365**, (2019).

107. Liu, Q. *et al.* IL-33–mediated IL-13 secretion by ST2+ Tregs controls inflammation after lung injury. *JCI Insight* **4**, (2019).

108. King, I. L. & Mohrs, M. IL-4-producing CD4+ T cells in reactive lymph nodes during helminth infection are T follicular helper cells. *Journal of Experimental Medicine* **206**, (2009).

109. Tibbitt, C. A. *et al.* Single-Cell RNA Sequencing of the T Helper Cell Response to House Dust Mites Defines a Distinct Gene Expression Signature in Airway Th2 Cells. *Immunity* **51**, (2019).

110. Klementowicz, J. E., Travis, M. A. & Grencis, R. K. Trichuris muris: A model of gastrointestinal parasite infection. *Seminars in Immunopathology* vol. **34**, (2012).

111. Phillips, C., Coward, W. R., Pritchard, D. I. & Hewitt, C. R. A. Basophils express a type 2 cytokine profile on exposure to proteases from helminths and house dust mites. *J Leukoc Biol* **73**, (2003).

112. Even, Z., Meli, A. P. & Rothlin, C. V. The amalgam of naive CD4+ T cell transcriptional states is reconfigured by helminth infection to dampen the amplitude of the immune response. *Immunity* **57**, 1893–1907 (2024).

113. Keegan, A. D., Leonard, W. J. & Zhu, J. Recent advances in understanding the role of IL-4 signaling. *Fac Rev* **10**, (2021).

114. Kuwahara, M. *et al.* Bach2-Batf interactions control Th2-type immune response by regulating the IL-4 amplification loop. *Nat Commun* **7**, (2016).

115. Otsuka, A. *et al.* Basophils are required for the induction of Th2 immunity to haptens and peptide antigens. *Nat Commun* **4**, (2013).

116. Yamanishi, Y., Miyake, K., Iki, M., Tsutsui, H. & Karasuyama, H. Recent advances in understanding basophil-mediated Th2 immune responses. *Immunological Reviews* vol. **278**, (2017).

117. Yang, L. *et al.* Intraepithelial mast cells drive gasdermin C-mediated type 2 immunity. *Immunity* **5**, 1056–1070 (2024).

118. Else, K. J., Finkelman, F. D., Maliszewski, C. R. & Grencis, R. K. Cytokine-mediated regulation of chronic intestinal helminth infection. *Journal of Experimental Medicine* **179**, (1994).

119. Kim, S. *et al.* Cutting Edge: Basophils Are Transiently Recruited into the Draining Lymph Nodes during Helminth Infection via IL-3, but Infection-Induced Th2 Immunity Can Develop without Basophil Lymph Node Recruitment or IL-3. *The Journal of Immunology* **184**, (2010).

120. Vacca, F. & Le Gros, G. Tissue-specific immunity in helminth infections. *Mucosal Immunology* vol. **15**, (2022).

121. Mayer, J. U., Brown, S. L., MacDonald, A. S. & Milling, S. W. Defined Intestinal Regions Are Drained by Specific Lymph Nodes That Mount Distinct Th1 and Th2 Responses Against Schistosoma mansoni Eggs. *Front Immunol* **11**, (2020).

122. Lyons-Cohen, M. R., Shamskhou, E. A. & Gerner, M. Y. Site-specific regulation of Th2 differentiation within lymph node microenvironments. *Journal of Experimental Medicine* **221**, (2024).

123. Giacomin, P. R. *et al.* Thymic Stromal Lymphopoietin-Dependent Basophils Promote Th2 Cytokine Responses following Intestinal Helminth Infection. *The Journal of Immunology* **189**, (2012).

124. Wang, F. *et al.* A basophil-neuronal axis promotes itch. *Cell* **184**, (2021).